Influence of matrix structures in spin systems

Dissertation

zur Erlangung des akademischen Grades eines
Doktors der Naturwissenschaften (Dr. rer. nat.)

dem Fachbereich Mathematik/Informatik/Physik
der Universität Osnabrück
vorgelegt von

Mats H. Lamann

Osnabrück, September 2023

Betreuender Professor : Prof. Dr. Jochen Gemmer

Influence of matrix structures in spin systems

Mats H. Lamann

School of Mathematics/Computer Science/Physics
University of Osnabrück,
BarbarastraSSe 7,
D-49076 Osnabrück,
Germany

Abstract

Within this thesis the effect of structures of quantum systems and their impact on the dynamics of these systems are investigated. At first, the focus will be on the properties of elements of specific observables in the energy eigenbasis. In this approach, a framework already exists with the Eigenstate Thermalization Hypothesis (ETH), which makes certain assumptions about those elements. The assumptions were investigated within the work for different spin-1/2 models. These results have been published in Ref. [P1] and contradict assumptions made by ETH in a strict sense. Furthermore, the results from Ref. [P2] will be presented, which investigates a new type of perturbation theory based on similar assumptions to those of ETH. It is shown that the perturbation theory can yield good results in spite of non-satisfied assumptions, but those cases can either be explained otherwise and/or it is questionable whether these results are transferable to mesoscopic systems. Cases in which all assumptions are strictly fulfilled were not found. In addition, further investigations were carried out based on the fact that autocorrelation functions can be described as 1-dimensional transport dynamics. Thereby possibilities were investigated, which allow a substantial reduction of the complicity of the transport.

Contents

1 Introduction

This thesis is based on the fundamentals of quantum thermodynamics, which is the interface between thermodynamics and quantum mechanics. Thus, this topic connects two very different branches of physics, both of which have shown their validity and significance in various experiments. The diametrical behavior of both individual theories becomes especially clear in the area of their application: While the quantum mechanical properties of physical systems are mostly only visible at very small system sizes, the focus of thermodynamics is on meso- and macroscopic systems. Thus, for sufficiently large systems, quantum mechanics is expected to merge into classical theory. On the other hand, due to its statistical nature, thermodynamics loses more and more accuracy and explanatory power as the size of the system decreases.
Another difference is also the way of describing the state of a physical system: While thermodynamics usually uses a few macroscopic quantities (e.g. pressure, volume and temperature) to describe a system and can make statements about it, a quantum mechanical description requires exponentially many parameters to describe a system (e.g. to describe a spin 1/2 system with N-particles 2^N parameters are needed). In connection with the fact that thermodynamics can describe meso- and macroscopic, the problem becomes apparent when comparing both theories, since a quantum mechanical description of such system sizes is hardly feasible. Moreover, everyday observations seem to contradict those statements of quantum mechanics, since mesoscopic systems rarely depend on the exact state of a system. As an example, consider a cup of tea which, when left open in a room, cools to room temperature. How exactly the molecules are distributed in the cup (or in the room) are not relevant for the equilibrium values of the system.
Despite the huge successes of thermodynamics, this branch of physics is based on assumptions that are difficult to verify and still not really proven, even if there are many good reasons for them [1]. The combination with quantum mechanics could help to further understand those assumptions and under which conditions thermodynamics is applicable.
Vice versa, quantum mechanics itself could also benefit from thermodynamics; for example, the former does not show a clear direction of time compared to the latter. Processes are possible in both directions, respectively. This contradicts everyday experience. Imagine a plate falling down and shattering on the ground. The reverse case (the broken pieces assemble to a plate) is not to be observed in everyday life, although this would be completely legitimate in the sense of classical mechanics. Even if that case satisfies a classical description, similar kinds of situations are also possible in quantum mechanical descriptions[1]. Thermodynamics, on the other hand, assigns a direction to time by the second law; thus, time always proceeds in the direction in which entropy does not decrease. A combined consideration of both topics could therefore provide improvements for both areas and lead to a better understanding.
This thesis is to be considered in four parts. In the first part (Section 2), basic background will be explained, which is needed for the understanding and interpretation of the results. Thereby already established concepts are described with the focus on understanding the results of the thesis. Therefore, many derivations are omitted, whereby always care was taken to provide sources for further deepening.
The Section 3 will address statements of the Eigenstate Thermalization Hypothesis (ETH), which is also described in Subsection 2.5. This hypothesis is an explanation for the independence of the long-time value from the exact initial state[2]. In Section 4, a novel perturbation theory, in which perturbations are described by only a few parameters, is examined for its applicability and the va-

[1] In addition, quantum mechanics merges into classical mechanics for sufficiently large systems.
[2] Some dependence is nevertheless given, so the long-time value of macroscopic observables depends on the energy and other conservation variables.

lidity of the basic assumptions.
A strong focus in Sections 3 and 4 is on the randomness of elements. Although it may seem counter-intuitive at first glance, the randomness of elements is also a structure that allows various statements about systems. Thus, randomness here is not to be understood as the absence, but rather as a particular (possibly unusual) kind of structure.
In Section 5, physical systems are approached in a way that is very different from the previous sections. It treats physical systems as 1-dimensional transport problems of a semi-infinite chain. On the basis of a new estimation of the transport coefficients, further investigations are carried out. A truncation of the chain is performed, where the dynamics should give the same results as the complete chain, if possible. This can be interpreted in the sense of thermodynamic reduction of parameters. Also, it forms a potential point of attack to understand why some dynamics occur more often than others in macroscopic systems [2].
Furthermore, the breaking of the chain was used to estimate the time integral of these dynamics from $t = 0$ to ∞.
All these investigations of Section 5 are not yet finished and still part of intensive research, so that a complete interpretation of the situation there is not possible and instead potential continuations of the investigations will be highlighted.
A summary and potential continuations of the findings of the thesis can be found in Section 6.
This work does not claim to be a complete overview of the above mentioned topics. The aim of the thesis is to enable the reader to understand, interpret and, if necessary, reproduce the results herein. Thereby, extensive derivations shall be avoided, if they are not part of the results of this thesis. For further deepening, sources shall always be given.

2 Theoretical Background

In order to be able to understand and interpret the results of the thesis presented latter, it is first necessary to illuminate the background and basics of the subject area treated. The following fundamentals are far from complete, as this would go beyond the scope of the thesis.
There will be a focus on enabling an understanding of the results and a reproduction of theses without further sources. In doing so, some phenomena and facts are mentioned without derivation, although sources are always given to the interested reader.
First in Subsection 2.1 shall be explained how quantum systems and their time evolutions can be described. Since within this thesis the dynamics of quantum systems are often considered from the point of view of autocorrelation functions, those are briefly described in Subsection 2.2. A justification why the systems in this thesis can often be described by pure states is given in Subsection 2.3. The notions of equilibration and thermalization are introduced in Subsection 2.4. In Subsection 2.5 the ETH is presented as a possible explanation for the thermalization of many quantum systems. The connection of this hypothesis with the Random Matrix Theory (RMT) is explained in Subsection 2.6. There are also several common properties of those random matrices to be pointed out.
In addition to these established methods, the Subsection 2.7 describes a recently developed perturbation theory whose effectiveness is examined in this thesis.
With the Recursion Method, another approach to autocorrelation functions will be explained in Subsection 2.8. The models, which are used within this thesis, will be described in Subsection 2.9. Since the main results of this work are based on numerical investigations, Subsection 2.10 explains the numerical methods necessary to reproduce the data of this thesis.

2.1 Dynamics in Quantum Systems

The state of a quantum (sub)system is described in general by a density operator $\hat{\rho}$, which has the following properties

$$\hat{\rho} = \hat{\rho}^\dagger \qquad \mathrm{Tr}\left\{\hat{\rho}\right\} = 1 \tag{2.1.1}$$

$$p_n \geq 0 \qquad \mathrm{Tr}\left\{\hat{\rho}^2\right\} \leq 1 \tag{2.1.2}$$

where ρ_n are the eigenvalues of the density operator, which satisfy $\hat{\rho}\left|\phi_n\right\rangle = p_n \left|\phi_n\right\rangle$, where $\left|\phi_n\right\rangle$ is an eigenstate of $\hat{\rho}$. $\bullet^\dagger$ represents the hermitian conjugate and $\mathrm{Tr}\left\{\right\}$ denotes the trace.
Every density operator can be written in the form

$$\hat{\rho} = \sum_n p_n \left|\phi_n\right\rangle \left\langle\phi_n\right| \phi_n. \tag{2.1.3}$$

The dynamical evolution of such a state is given by the von Neumann equation

$$\frac{\partial \hat{\rho}}{\partial t} = \frac{\mathrm{i}}{\hbar}\left[\hat{\rho}, \hat{H}(t)\right] \tag{2.1.4}$$

with the (possible time dependent) Hamiltonian $\hat{H}$ and the reduced Planck constant $\hbar$.
For the case of a time independent Hamiltonian, this equation has the formal solution

$$\hat{\rho}_S(t) = \hat{U}(t-t_0)\hat{\rho}(t_0)\hat{U}^\dagger(t-t_0) \tag{2.1.5}$$

with

$$\hat{U}(t) = \mathrm{e}^{-\frac{\mathrm{i}}{\hbar}\hat{H}t}. \tag{2.1.6}$$

Since the Hamiltonian is a hermitian operator (as all observables) the time-evolution-operator $\hat{U}(t)$ is a unitary operator such that

$$\hat{U}(t) \cdot \hat{U}^{\dagger}(t) = \hat{1} \tag{2.1.7}$$

The expectation value $A(t)$ at a given time t for a state $\hat{\rho}$ is given by

$$A(t) = \mathrm{Tr}\left\{\hat{\rho}_S(t)\hat{A}\right\} \tag{2.1.8}$$

where $\hat{A}$ is the corresponding observable to the expectation value.
If the special case of a pure state ($\mathrm{Tr}\left\{\hat{\rho}^2\right\} = 1$) is considered, it is easy to see that the density operator can be reduced to

$$\hat{\rho} = |\phi_n\rangle \langle\phi_n| \, \phi_n \tag{2.1.9}$$

such that the expectation value has now the following form

$$A(t) = \mathrm{Tr}\left\{\hat{A}\hat{U}(t) \, |\phi_n\rangle \langle\phi_n| \, \hat{U}^{\dagger}(t)\right\} \tag{2.1.10}$$

$$= \mathrm{Tr}\left\{\langle\phi_n|\hat{U}^{\dagger}(t)\hat{A}\hat{U}(t)|\phi_n\rangle\right\} \tag{2.1.11}$$

$$= \langle\phi_n|\hat{U}^{\dagger}(t)\hat{A}\hat{U}(t)|\phi_n\rangle \tag{2.1.12}$$

where the cyclic invariance of the trace operator and that the trace of a scalar is the scalar itself is used.
To calculate the time dependent expectation value, it is not necessary to evolve the density operator in time, it is sufficient to calculate

$$|\phi_n(t)\rangle_S = \hat{U}(t) \, |\phi_n\rangle \, , \tag{2.1.13}$$

since ${}_S\langle\phi_n(t)| = (|\phi_n(t)\rangle_S)^{\dagger}$.
With Eq. (2.1.6) it follows that

$$\frac{\partial}{\partial t} |\phi_n(t)\rangle_S = -\frac{\mathrm{i}}{\hbar}\hat{H} \, |\phi_n(t)\rangle_S \tag{2.1.14}$$

which is exactly the Schrödinger equation.
Until now the whole dynamic only takes place only in the state, the observable itself does not change at all. The kind of view on the dynamic is called Schrödinger picture (therefore the index S).
Another perspective is the so-called Heisenberg picture. A closer look at Eq. (2.1.8) reveal

$$A(t) = \mathrm{Tr}\left\{\hat{U}(t)\hat{\rho}\hat{U}^{\dagger}(t)\hat{A}\right\} \tag{2.1.15}$$

$$= \mathrm{Tr}\left\{\hat{\rho}\hat{A}_H(t)\right\} \tag{2.1.16}$$

with

$$\hat{A}_H(t) = \hat{U}^{\dagger}(t)\hat{A}\hat{U}(t). \tag{2.1.17}$$

which is the solution of the corresponding differential equation

$$\frac{d}{dt}\hat{A}(t) = \frac{\mathrm{i}}{\hbar}\left[\hat{H}, \hat{A}(t)\right], \tag{2.1.18}$$

this is known as the Heisenberg equation. In this picture, the state of the system is constant in time, while the observable evolves in time.
A hybrid between these two approaches is also possible and is called Interaction picture. Thereby the Hamiltonian H is split in two parts

$$\hat{H} = \hat{H}_0 + \hat{H}_1 \tag{2.1.19}$$

whereby one part of the time evolution happen in the observable while the other one effects the state:

$$\hat{\rho}_I(t) = \mathrm{e}^{\mathrm{i}\hat{H}_0 \frac{t}{\hbar}} \mathrm{e}^{-\mathrm{i}\hat{H} \frac{t}{\hbar}} \hat{\rho} \mathrm{e}^{\mathrm{i}\hat{H} \frac{t}{\hbar}} \mathrm{e}^{\mathrm{i}\hat{H}_0 \frac{t}{\hbar}} \tag{2.1.20}$$

$$\hat{A}_I(t) = \mathrm{e}^{-\mathrm{i}\hat{H}_0 \frac{t}{\hbar}} \hat{A} \mathrm{e}^{\mathrm{i}\hat{H}_0 \frac{t}{\hbar}}. \tag{2.1.21}$$

Although this representation may seem unnecessarily complicated at first glance, it has proved useful in time-dependent perturbation theory and is thus a central component for the derivation of, for example, Fermi's Golden Rule [3].
For the sake of simplicity, the indices of the time evolutions (S, H & I) are omitted within this work. An operator $\hat{A}(t)$ therefore describes the Heisenberg picture while a state $|\phi(t)\rangle$ always implies the Schrödinger picture.
Also $\hbar = 1$ is always used outside this section for time evolutions.

2.2 Correlation functions

Since the dynamics of the systems considered in this thesis are mostly viewed through the lenses of autocorrelation functions, this subsection will briefly explain how those functions are defined.
First consider the most general case of a correlation function

$$C^{\hat{\rho}}_{\hat{A}\hat{B}}(t) = \mathrm{Tr}\left\{\hat{A}(t)\hat{B}\hat{\rho}\right\}. \tag{2.2.1}$$

where $\hat{\rho}$ is the density operator of a system and $\hat{B}$ is an operator at the time $t = 0$ while $\hat{A}(t)$ is an operator at time t in the Heisenberg picture. In most cases $\hat{A}$ and $\hat{B}$ are observables and as such hermitian $\hat{A} = \hat{A}^\dagger$.
Within this thesis only the case $\hat{\rho} = \frac{1}{\mathcal{D}}\hat{1}$[3] is considered, for which the correlation function is real for all t.
Another common reduction is the case of autocorrelation, in which $\hat{A} = \hat{B}$. These autocorrelation functions are time symmetric $C_{\hat{A}}(t) = C_{\hat{A}}(-t)$ and real.
In viewing of the Recursion Method (Subsection 2.8), such autocorrelation functions are often represented in normalized form such that

$$\tilde{C}_{\hat{A}}(t) = \frac{C_{\hat{A}}(t)}{C_{\hat{A}}(0)}. \tag{2.2.2}$$

In addition, if one is only interested in the shape of the function and nether long-time values nor prefactors are important, one can also use

$$\tilde{\mathcal{C}}_{\hat{A}}(t) = \frac{C_{\hat{A}}(t) - C_{\hat{A}}(t \to \infty)}{C_{\hat{A}}(0) - C_{\hat{A}}(t \to \infty)}. \tag{2.2.3}$$

[3]This corresponds to the canonical ensemble for infinitely high temperatures (see Subsection 2.4).

For instance this is used for determining the timescales of autocorrelation functions[4]. Moreover, the autocorrelation functions can also be described by using the dynamics of a density operator

$$\hat{\rho}_{\hat{A}} = \frac{\hat{A} - A_{\min}\hat{1}}{A_{\max} - A_{\min}} \tag{2.2.4}$$

so that

$$\mathrm{Tr}\left\{\hat{\rho}_{\hat{A}}(t)\hat{A}\right\} = \frac{C_{\hat{A}}(t) - A_{\min}\mathrm{Tr}\left\{\hat{A}\right\}}{\hat{A}_{\max} - \hat{A}_{\min}} \tag{2.2.5}$$

where $A_{\min}$ ($A_{\max}$) is the smallest (largest) eigenvalue of $\hat{A}$. In this case, the dynamics are merely shifted and scaled by an offset; the basic shape of the dynamics remains unchanged.
This connection also allows theories dealing with the dynamics of a density operator to be applied to autocorrelation functions (e.g. the theory in Subsection 2.7).
Besides the direct interpretation, correlation functions can also be used in the framework of linear response theory [4], for example, to study transport properties of systems.

2.3 Dynamical Quantum Typicality

Even though the state of a quantum (sub)system is generally described by a density matrix $\hat{\rho}$, the dynamics of such a system can be approximately developed by a pure state $|\phi\rangle$.
This approximation is called Dynamical Quantum Typicality (DQT) and has the advantage that the amount of elements to be time evolved decreases drastically. In a finite system, the density operator corresponds to a hermitian $\mathcal{D} \times \mathcal{D}$ matrix with complex entries, where $\mathcal{D}$ is the dimension of the associated Hilbert $\mathscr{H}$ space. Thus, for a time evolution, $\mathcal{D}^2$ elements have to be considered. The evolution of a pure state $|\phi\rangle$, on the other hand, requires only the evolution of $2\mathcal{D}$ real elements, since those states correspond to a complex vector (in a dual space). Since the dimension of the Hilbert space grows exponentially with the number of particles (and the number of degrees of freedom), the reduction to a pure state is reasonable.
This possibility of reduction to dynamics of pure states has been first shown in Ref. [5] and has become a standard tool for quantum mechanical simulations in recent years. There are several derivations for this approximation [6, 7, 8]. In this subsection, the derivation from Ref. [6] will be summarized succinctly. Let $\hat{\rho}$ be a density operator whose dynamics is to be discussed. Moreover, let $\hat{R}$ be an operator satisfying

$$\hat{\rho} = \hat{R}\hat{R}^\dagger \tag{2.3.1}$$

which is always possible for density operators, since their eigenvalues are semi positive. In addition, also a pure state

$$|\Phi\rangle = \sum_n c_n |n\rangle \tag{2.3.2}$$

is defined. c_n are independent random Gaussian numbers with mean $\overline{c} = 0$ and variance $\overline{(c - \overline{c})^2} = 1$, where the bar denotes the mean over all possible realizations of $|\Phi\rangle$. $\{|n\rangle\}$ is an arbitrary orthonormal

[4] Of course this is only useful if a long-time value exists at all.

basis. The precise basis is not important, since a random vector transforms into a random vector under unitary transformation. Let $\hat{A}$ be the observable of interest, it can be concluded that

$$\overline{\langle\Phi|\hat{R}\hat{A}\hat{R}^\dagger|\Phi\rangle} = \overline{\sum_{n,m}(c_n \cdot c_m)\,\langle n|\hat{R}\hat{A}\hat{R}^\dagger|m\rangle} \tag{2.3.3}$$

$$= \sum_{n,m}\underbrace{\overline{(c_n \cdot c_m^*)}}_{\approx\delta_{nm}}\langle n|\hat{R}\hat{A}\hat{R}^\dagger|m\rangle \tag{2.3.4}$$

$$\approx \sum_n \langle n|\hat{R}\hat{A}\hat{R}^\dagger|n\rangle \tag{2.3.5}$$

$$= \mathrm{Tr}\left\{\hat{R}\hat{A}\hat{R}^\dagger\right\} \tag{2.3.6}$$

$$= \mathrm{Tr}\left\{\hat{\rho}\hat{A}\right\}. \tag{2.3.7}$$

holds. It can be seen that the expected value of a mixed state is obtained as the mean value of modified pure states.
A possible problem that might arise is that one needs a great many realizations of $|\Phi\rangle$ to determine this mean. To investigate this problem, the variance of the ensemble of random states are considered:

$$\sigma^2_{DQT} = \overline{\left(\langle\Phi|\hat{R}\hat{A}\hat{R}^\dagger|\Phi\rangle - \overline{\langle\Phi|\hat{R}\hat{A}\hat{R}^\dagger|\Phi\rangle}\right)^2} \tag{2.3.8}$$

$$\leq \mathrm{Tr}\left\{\hat{\rho}^2\right\}||\hat{A}||^2 \tag{2.3.9}$$

Here $||\hat{A}||$ is the largest eigenvalue of the operator $\hat{A}$ in absolute value. The complete derivation can be found in Ref. [6]. Since in many cases $\mathrm{Tr}\left\{\hat{\rho}^2\right\} \ll 1$, the most realizations of $|\Phi\rangle$ are already very close to the expectation value of the mixed state[5]. $\mathrm{Tr}\left\{\hat{\rho}^2\right\}$ is also called the purity of a state; the reciprocal of this purity is also known as the effective dimension d_{eff} [9].
An expansion to time evolution is easily seen in terms of the Heisenberg picture. Thus, the derivation shown above only needs to be performed with $\hat{A}(t)$.
It is trivial that some information of the density operator is still lost by the reduction to pure states. A trivial example is the purity of the density operator: Every pure state $|\Phi\rangle$ has by definition a purity of 1, while the density operator $\hat{\rho}$ itself can also take smaller values for the purity.
Note that the method of DQT can be used in numerous ways for numerical simulations [7] and can also be combined with other methods [10].
Before a possible application of the DQT is explained, it should be pointed out that even if the DQT is used here mostly as a means to an end, the typicality already makes statements about quantum systems itself. Thus, it shows that for sufficiently large systems the majority of all possible states are similar in their properties, which hereby are to be understood as the expectation values of observables and their dynamics. This fact reflects the principle often used in thermodynamics, according to which a system can be described independently of the exact state[6].

[5] For example, an often considered case is the thermal equilibrium by infinite temperature, for which $\mathrm{Tr}\left\{\rho^2\right\} = \frac{1}{\mathcal{D}}$, where $\mathcal{D}$ is the dimension of the system.

[6] In classical systems the exact position and velocity of every particle is not important for macroscopic behavior.

2.3.1 Determination of the (local) density of states by means of dynamic quantum typicality

An actual application of the DQT, which is used within the thesis, will be described in the following subsection. The local density of states (LDOS) is determined by means of DQT and the Fourier transform. LDOS of a (mixed) state $\hat{\rho}$ is defined as

$$\Omega_{\mathrm{loc}}(E) = \sum_n \langle E_n|\hat{\rho}|E_n\rangle \,\mathrm{rect}\left(\frac{E-E_n}{\delta E}\right) \tag{2.3.10}$$

where

$$\mathrm{rect}\,(x) = \begin{cases} 1 & \text{for } |x| < \frac{1}{2} \\ 0 & \text{else} \end{cases} \tag{2.3.11}$$

denotes the rectangle-function and δE is the width of an energy shell. The latter is chosen to be macroscopically small, but still contains exponentially many states. In the spirit of DQT the density matrix $\hat{\rho}$ is replaced by a pure, random state $|\Phi\rangle$, which results to

$$\Omega_{\mathrm{loc}}(E) \propto \sum_n \langle E_n|\hat{R}^\dagger|\Phi\rangle \,\langle\Phi|\hat{R}|E_n\rangle \,\mathrm{rect}\left(\frac{E-E_n}{\delta E}\right) \tag{2.3.12}$$

$$\propto \sum_n \underbrace{|\,\langle\Phi|\hat{R}|E_n\rangle\,|^2}_{c_n^2} \cdot \mathrm{rect}\left(\frac{E-E_n}{\delta E}\right). \tag{2.3.13}$$

To calculate c_n^2 now consider the dynamics

$$\langle\Phi|\hat{R}^\dagger\hat{U}^\dagger(t)\hat{R}|\Phi\rangle = \sum_n \langle\Phi|\hat{R}^\dagger|E_n\rangle \,\langle E_n|\hat{R}|\Phi\rangle \,\mathrm{e}^{\mathrm{i}E_n t} \tag{2.3.14}$$

$$= \sum_n |c_n|^2 \mathrm{e}^{\mathrm{i}E_n t}. \tag{2.3.15}$$

It is easy to see that the Fourier transforms $\mathcal{F}\{\bullet\}(\omega)$ results in

$$\mathcal{F}\left\{\langle\Phi|\hat{R}^\dagger\hat{U}^\dagger(t)\hat{R}|\Phi\rangle\right\}(\omega) = \frac{1}{\sqrt{2\pi}} \int_{-\infty}^{\infty} \langle\Phi|\hat{R}^\dagger\hat{U}^\dagger(t)\hat{R}|\Phi\rangle \,\mathrm{e}^{-\mathrm{i}\omega t} dt \tag{2.3.16}$$

$$= \sum_n \delta(E_n-\omega)|c_n|^2. \tag{2.3.17}$$

In practice, the integral is determined only over finite times, resulting in a limited resolution of the δ-distributions. However, since LDOS itself is defined over a (small) energy range, that lack of resolution is not only not a problem, but even a wanted result.
For the choice of $\hat{R} = \hat{1}$, the result corresponds to the density of states (DOS), which is the LDOS for $\hat{\rho} \propto \hat{1}$, i.e., the canonical density of states at infinitely high temperature (see Subsection 2.4).

2.4 Equilibration & thermalization in isolated Quantum Systems

Nearly all systems that one can observe tend to equilibrate in such a sense, that after a given time[7], the macroscopic properties of the system do not change much. For the sake of clarity, the example

[7] The timescale on which this equilibration occurs depends on the system and can differ a lot. E.g. a hot cup of tea equilibrates in a normal room on a timescale of minutes to hours, the pitch drop experiment is running since 1930 [11] and is still not over (December 4, 2023).

of a box shall be used for illustration, in which a large number of gas particles are located in one corner at the time $t = 0$. The box is completely isolated from the outside world (neither energy nor particles can be exchanged). After a certain time, the gas particles will be evenly distributed in the box. This state will hardly change (in realistic timescales[8]). This example is in so far well suited to describe the equilibration since here it is easy to recognize that the position of individual gas particles changes naturally over the time anyway and does not take an equilibrium value. Nevertheless, no change can be seen from the outside.
From this picture, two properties of an equilibrium state are to be expected. Firstly, a long term average exists, thus

$$\overline{A} = \lim_{\tau\to\infty} \frac{1}{\tau} \int_0^\tau A(t)\mathrm{d}t \tag{2.4.1}$$

converges.
Secondly, the deviations

$$\sigma_A^2 = \lim_{\tau\to\infty} \frac{1}{\tau} \int_0^\tau \left(A(t) - \overline{A}\right)^2 \mathrm{d}t \tag{2.4.2}$$

from this mean value should also remain small. Note that this does not describe the deviation of individual measurements, but the deviations of the mean value of the measurements to the long term value of those expectation values.
These two conditions, which are necessary for equilibrium, nevertheless allow large deviations from the long-term mean as long as they do not occur too frequently and/or last for a long time.
Even if this contradicts the everyday expectation of an equilibrium (think of a cold cup of tea which would start boiling again for a short time), this would be acceptable in the sense of the definition of equilibrium mentioned above.
Assuming a pure[9] state $|\phi\rangle$ as the initial state and using the time evolution from Eq. (2.1.13), the long term value can be determined as

$$\begin{aligned}
\overline{A} &= \lim_{\tau\to\infty} \frac{1}{\tau} \int_0^\tau A(t)\mathrm{d}t && (2.4.3)\\
&= \lim_{\tau\to\infty} \frac{1}{\tau} \int_0^\tau \sum_{n,m} \underbrace{\langle\phi|E_n\rangle}_{c_n^*} \mathrm{e}^{-\mathrm{i}E_n t} \underbrace{\langle E_n|\hat{A}|E_m\rangle}_{A_{nm}} \underbrace{\langle E_m|\phi\rangle}_{c_m} \mathrm{e}^{\mathrm{i}E_m t}\mathrm{d}t && (2.4.4)\\
&= \lim_{\tau\to\infty} \frac{1}{\tau} \int_0^\tau \left(\sum_n |c_n|^2 A_{nn}\right) + \left(\sum_{n\neq m} \mathrm{e}^{\mathrm{i}(E_m-E_n)t} c_n^* c_m A_{nm}\right) \mathrm{d}t && (2.4.5)\\
&= \sum_n |c_n|^2 A_{nn} && (2.4.6)
\end{aligned}$$

[8] In both classical mechanics and quantum mechanics, it is known that any closed system approaches infinitely close to its initial state. This phenomenon is called Poincaré recurrence [12]. However, the time the system needs for this is far beyond the human timescale.

[9] The derivation is very similar for mixed states. With the results on Subsection 2.3, however, it is evident that the case of pure states also has an impact on the case of mixed states.

where it was assumed that there is a minimum distance between two energy states $|E_n - E_m| > \epsilon$[10]. For the deviation from the long-term value can be shown in a similar manner:

$$\sigma_A^2 = \lim_{\tau\to\infty} \frac{1}{\tau}\int_0^\tau \left(A(t) - \overline{A}\right)^2 \mathrm{d}t \tag{2.4.7}$$

$$= \lim_{\tau\to\infty} \frac{1}{\tau}\int_0^\tau A(t)^2 - 2\overline{A}A(t) + \overline{A}^2 \mathrm{d}t \tag{2.4.8}$$

$$= -\overline{A}^2 + \lim_{\tau\to\infty} \frac{1}{\tau}\int_0^\tau A(t)^2 \mathrm{d}t \tag{2.4.9}$$

$$= -\overline{A}^2 + \lim_{\tau\to\infty} \frac{1}{\tau}\int_0^\tau \sum_{n,m,k,l} \mathrm{e}^{\mathrm{i}(E_m - E_n + E_l - E_k)t} c_n^* c_m c_k^* c_l A_{nm} A_{kl} \mathrm{d}t \tag{2.4.10}$$

$$= -\overline{A}^2 + \sum_{n,l} \left(|c_n|^2 A_{nn} |c_l|^2 A_{ll} + |c_n|^2 |c_l|^2 |A_{nl}|^2\right) - \sum_n |c_n|^4 |A_{nn}|^2 \tag{2.4.11}$$

$$= -\overline{A}^2 + \left(\sum_n |c_n|^2 A_{nn}\right)^2 + \sum_{n\neq l} |c_n|^2 |c_l|^2 |A_{nl}|^2 \tag{2.4.12}$$

$$= \sum_{n\neq l} |c_n|^2 |c_l|^2 |A_{nl}|^2 \tag{2.4.13}$$

Here the non-resonance condition was assumed, which states that $E_n - E_m \neq E_k - E_l$ is valid as long as $k \neq m$ and $l \neq n$.
It is easy to see that in any system it is possible to define an observable which does not equilibrate e.g. $\hat{A} = |E_n\rangle \langle E_n| E_m + |E_m\rangle \langle E_m| E_n$. As long as $E_m \neq E_n$ and $c_n \neq 0 \neq c_m$ this observable will never arrive at equilibrium but will always oscillate. In Ref. [13] von Neumann already emphasizes that it is important to focus on physically relevant observables rather than equilibration of states or on more artificial observables[11] .
As a special case of equilibration, these properties are also necessary for thermalization. In the case of the latter, another everyday experience of equilibrium is added: The equilibrium state does not depend on the exact initial state. In the image of the box, even if all gas particles are shifted randomly at the beginning, the equilibrium state will still be the one in which the gas particles fill the volume evenly.
For the case of an isolated system, the long-time value is assumed to correspond to the value of the microcanonical ensemble [14]. Thus,

$$\overline{A} \approx A_{\mathrm{mc}} = \mathrm{Tr}\left\{\hat{\rho}_{\mathrm{mc}} \hat{A}\right\} \tag{2.4.14}$$

with

$$\hat{\rho}_{\mathrm{mc}} = \frac{\sum_n |E_n\rangle \langle E_n| E_n \mathrm{rect}\left(\frac{E-E_n}{\delta E}\right)}{\sum_n \mathrm{rect}\left(\frac{E-E_n}{\delta E}\right)}. \tag{2.4.15}$$

E is the mean energy of the microcanonical ensemble and δE denotes a narrow energy shell around this mean energy. The word "narrow" refers to the fact that this shell is macroscopic small, but still

[10] This expression is also applicable in the case of degeneracies, but then a base change must be made so that $A_{nm} = 0$ holds for all mutually degenerate states $\{|n\rangle |m\rangle\}$.
[11] Note that this is also the case in classical thermodynamics; it is always possible to find an observable which does not equilibrate.

contains exponentially many states. The physical properties of the system should not be sensitive to a change of the width.
Note that this is the case for an isolated quantum system. If the system is weakly coupled to a heat bath with temperature T, the expected long term value corresponds to

$$\overline{A} \approx A_\beta = \mathrm{Tr}\left\{\hat{\rho}_\beta \hat{A}\right\} \tag{2.4.16}$$

with

$$\hat{\rho}_\beta = \frac{\mathrm{e}^{-\beta \hat{H}}}{\mathrm{Tr}\left\{\mathrm{e}^{-\beta \hat{H}}\right\}} \tag{2.4.17}$$

and

$$\beta = \frac{1}{k_B T}. \tag{2.4.18}$$

$\hat{\rho}_\beta$ is the density operator of a canonical ensemble [15] and k_B denotes the Boltzmann constant[12]. For other types of open systems (e.g. with particle exchange), there are corresponding ensembles in each case [15].

2.5 Eigenstate Thermalization Hypothesis

One explanation for the thermalization of an isolated quantum system is the Eigenstate Thermalization Hypothesis (ETH) [16, 17]. It states that few-body observables $\hat{A}$ in non-integrable quantum systems can be represented as follows:

$$\langle E_n|\hat{A}|E_m\rangle = \mathcal{A}(\bar{E})\delta_{nm} + \Omega\left(\bar{E}\right)^{-\frac{1}{2}} f\left(\bar{E},\omega\right) r_{nm} \tag{2.5.1}$$

with

$$\omega = E_n - E_m \qquad \bar{E} = \frac{E_m + E_n}{2} \tag{2.5.2}$$

where $A(\bar{E})$ and $f\left(\bar{E},\omega\right)$ are smooth functions of their arguments and $\Omega\left(\bar{E}\right)$ is the DOS [18]. The latter is defined as

$$\Omega(E) = \frac{1}{\mathcal{D}} \sum_n \mathrm{rect}\left(\frac{E - E_n}{\delta E}\right) \tag{2.5.3}$$

where δE is the width of an energy shell chosen to be macroscopically small but to include exponentially many states.
The fact that r_{nm} are considered to be (complex) Gaussian independent[13] random numbers shows the connection of ETH with Random Matrix Theory (RMT). These random numbers have a mean of 0 and a unit variance[14].
It should be noted that this structure applies to symmetry-free subspaces, since otherwise the observable has a structured sparseness, which trivially contradicts the randomness of the matrix elements.

[12] Note that $k_B = 1$ is chosen within this work, if not mentioned otherwise.
[13] To preserve hermicity, $r_{nm} = r^*_{mn}$ is needed.
[14] For observables with time-reversal symmetry, the variance of the diagonal elements is $\overline{R^2_{mm}} = 2$ and the numbers are all real.

Substituting the ETH-structure into Eq. (2.4.3), one obtains for the long-term value

$$\bar{A} = \sum_n |c_n|^2 \mathcal{A}(E_n). \tag{2.5.4}$$

Under the assumption that the c_n are concentrated within a narrow energy shell, it follows by the smoothness of $\mathcal{A}(E)$ that $A_{\mathrm{mc}} \approx \bar{A}$.
To show that the deviations from this mean value are small on average, the ETH structure is inserted in Eq. (2.4.7):

$$\sigma_A^2 = \sum_{n \neq l} |c_n|^2 |c_l|^2 \Omega^{-1}(\bar{E}) \cdot \left| f(\omega, \bar{E}) \right|^2 |r_{nl}|^2 \tag{2.5.5}$$

$$\leq \max |A_{nl}|^2 \propto \Omega^{-1}(\bar{E}) \tag{2.5.6}$$

Since the DOS increases exponentially with system size, this deviation becomes very small even for medium sized systems[15].
Even though the independent randomness of the matrix elements is not necessary for the above statements, it is a common assumption. Moreover, the Gaussian distribution has been established in various numerical investigations[16][19, 20, 21, 22].
Of course, observables can be generated which trivially do not fulfill the ETH structure. The statement of the ETH is to be understood much more in such a way that physically relevant observables in non-integrable systems show this structure[17]. It should also be mentioned that even such observables must show deviations from that structure. For example, if one considers as an observable the magnetization of a spin 1/2 particle in z-direction, then the observable must have $-1/2$ and $1/2$ as eigenvalues. This would not be possible without correlations. In addition, matrix-element correlations (MEC) are necessary to fulfill properties of chaotic systems, such as the information scrambling [23].
However, these correlations between elements are assumed to be long-range and therefore observables in sufficiently small energy windows should be free of correlations [14, 24]. The size of those energy windows is often associated with the Thouless Energy $\Delta E_{Th} = 2\pi/\tau_{Th}$, where τ_{Th} is the so-called Thouless time. The original definition of τ_{Th} as a timescale in which a single particle diffuses through the complete system [25] shows the connection with the relaxation time $\tau_{\mathrm{rel.}}$ [26]. Within this work, $\tau_{\mathrm{rel.}}$ is defined as the time after which the autocorrelation function deviates only marginally from the long-term value

$$\tilde{\mathcal{C}}(t) = \frac{C(t) - C(\infty)}{C(0) - C(\infty)} \leq \epsilon \qquad \text{for } t \geq \tau_{\mathrm{rel.}}. \tag{2.5.7}$$

In this work, $\epsilon = 0.01$ is chosen. The relaxation time depends on the considered observable and is only usefully defined for systems which reach a long time value at all. From that definition of the relaxation time, it can be seen that $f(\bar{E}, \omega) \approx$ const. holds for a corresponding energy window $\Delta E_{rel} = \frac{2\pi}{\tau_{\mathrm{rel.}}}$.

[15] The assumption was made that $|f(\omega, \bar{E})|^2$ does not grow exponentially with system size. For common observables, this function grows at most linearly with system size.

[16] Note that this does not make any statement about the independence of the matrix elements.

[17] The question of which observables fulfill the ETH and which do not is still an open question. However, it is assumed that at least few-body observables in non-integrable systems fulfill the ETH [14].

2.6 Random Matrix Theory and indicators

In this subsection, some properties of specific random matrices are explained. This is motivated by the fact that the ETH for small energy windows transition to the RMT, since

$$f(\bar{E},\omega) \approx \text{const.} \qquad \mathcal{A}(\bar{E}) \approx \text{const.} \tag{2.6.1}$$

holds in this limiting case. For simplicity, it is assumed here that $\mathrm{Tr}\left\{\hat{A}\right\} = 0$; this can be realized by subtraction with a suitably scaled identity matrix.
What kind of random matrix this limiting case yields depends on the system and the observable: If there is a basis in which both the Hamiltonian and the observable are real, the associated ensemble of random matrices is called a Gaussian Orthogonal Ensemble (GOE)[18].
If, on the other hand, there is no such basis, so that either the Hamiltonian or the observable always has complex components[19], the associated ensemble is called a Gaussian Unitary Ensemble (GUE)[20].
The elements of such matrices can be described by

$$r_{mn}^{\mathrm{GOE}} = \begin{cases} X & \text{for } m \neq n \\ \sqrt{2}\cdot X & \text{for } m = n \end{cases} \tag{2.6.2}$$

and

$$r_{mn}^{\mathrm{GUE}} = \begin{cases} X + \mathrm{i}Y & \text{for } m \neq n \\ \sqrt{2}\cdot X & \text{for } m = n \end{cases} \tag{2.6.3}$$

for the GOE and GUE. X and Y denote independently drawn gaussian numbers[21].
In the following part of this subsection some properties of these random matrices shall be explained, which are already established as indicators of the randomness of the matrix elements of the observables used. The first indicator is Wigner's semicircle law (WSC), which states that for distribution of eigenvalues λ of a random matrix from GOE or GUE

$$P(\lambda) = \begin{cases} \frac{2}{\pi R^2}\sqrt{R^2-\lambda^2} & \text{for } |\lambda| \leq R \\ 0 & \text{else} \end{cases} \tag{2.6.4}$$

is valid, where R is the absolute largest eigenvalue[22]. The example of the already mentioned magnetization in z-direction of a single spin shows that at least this observable trivially does not fulfill WSC. As an example, Fig. 1 shows the eigenvalue distribution of $2^4 \times 2^4$ GOE matrices, averaged over 5000 realizations.

[18] This corresponds to systems with Time Reversal Symmetry.
[19] Nevertheless, the matrices are hermitian.
[20] There is also the Gaussian Symplectic Ensemble, which should be mentioned for completeness, but is not discussed further.
[21] The only dependence between the elements is given by the hermiticity $r_{mn} = r_{nm}^*$.
[22] This is also often used as a norm of a matrix.

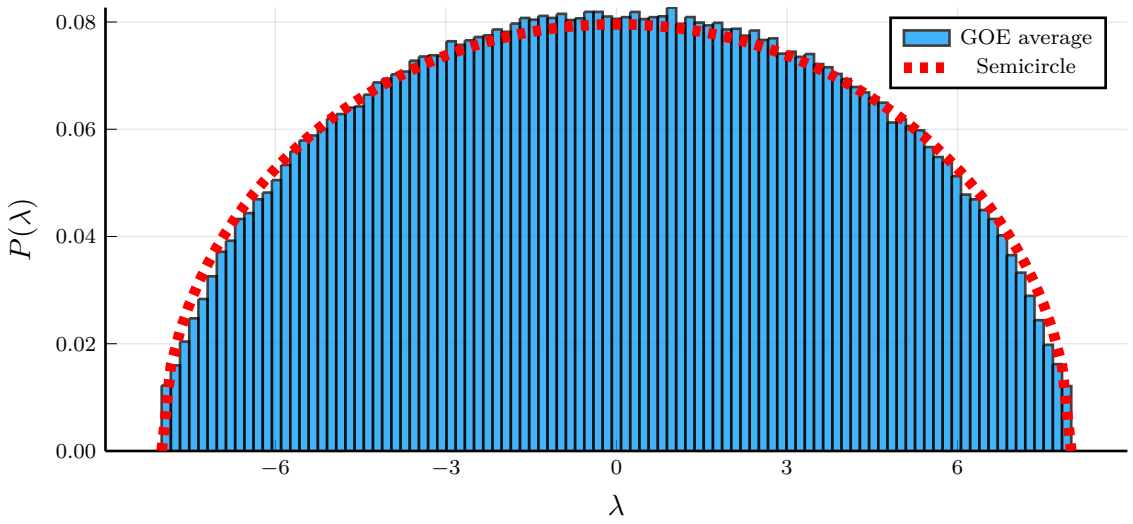

Fig. 1: Eigenvalue distribution of $2^4 \times 2^4$ GOE matrices as well as Wigner's semicircle law with $R = 2^3$ average over 5000 realizations. On average $\bar{r} = 0.529$ holds.

Thus, the deviation of the distribution of eigenvalues from the WSC is an indicator of randomness. Here R must always be adapted to the operator, since a prefactor does not change the randomness of the matrix elements. It should be noted that non-random matrices can also satisfy the indicators, for example a diagonal matrix with eigenvalues obeying the WSC would still be far from being a random matrix even if this indicator cannot distinguish it from such a matrix.
Another indicator can be examined by level spacing. For this, one considers

$$\bar{r} = \frac{1}{\mathtt{N}-1} \sum_{n=1}^{\mathtt{N}-1} \frac{\min\{\Delta_n, \Delta_{n+1}\}}{\max\{\Delta_n, \Delta_{n+1}\}} \tag{2.6.5}$$

with

$$\Delta_n = \lambda_{n+1} - \lambda_n \tag{2.6.6}$$

and

$$\lambda_n < \lambda_{n+1}. \tag{2.6.7}$$

$\mathtt{N}$ denotes thereby the number of contributing eigenvalues. In the case of a GOE matrix, this results in $r_{\mathrm{GOE}} = 4 - 2\sqrt{3} \approx 0.53$ [27, 28]. For comparison, the matrices corresponding to Fig. 1 possess $r \approx 0.5295$.
Methods that investigate the Gaussian nature of the elements are often used in this context. Thus, one can examine the distribution of the matrix elements or also only the variance of those. For the sake of completeness, some of these methods will be shortly mentioned here. Prior to explaining these, it should be pointed out that these methods do indeed examine the Gaussian properties of the matrix elements, but do not allow statements about whether and how the matrix elements are

correlated with each other. An indicator of this type is defined as

$$\Gamma(\omega) = \mathtt{N}_\omega \frac{\sum\limits_{nm} |A_{nm}|^2 \mathrm{rect}\left(\frac{(E_n - E_m) - \omega}{\Delta\omega}\right)}{\left(\sum\limits_{nm} |A_{nm}| \mathrm{rect}\left(\frac{(E_n - E_m) - \omega}{\Delta\omega}\right)\right)^2} \tag{2.6.8}$$

where $\Delta\omega$ is a small area of frequencies[23] and

$$\mathtt{N}_\omega = \sum_{nm} \mathrm{rect}\left(\frac{(E_n - E_m) - \omega}{\Delta\omega}\right). \tag{2.6.9}$$

If the matrix elements all correspond to a Gaussian distribution (with the same variance in the frequency range) $\Gamma_{\mathrm{GOE}} = \frac{\pi}{2}$ would hold, independent of ω [19]. Note again, that this indicator in contrast to $\bar{r}$ is blind to potential correlation between the elements.
Another way to investigate the Gaussian nature of the elements is to consider the rescaled transition strength

$$\tilde{y} = \frac{A_{nm}^2}{\left(\overline{A_{nm}^2}\right)} \tag{2.6.10}$$

where the $\overline{\bullet}$ denotes the mean over all elements. In the case of a GOE the distribution of these should hold

$$P(\tilde{y}) = \frac{\mathrm{e}^{-\frac{\tilde{y}}{2}}}{\sqrt{2\pi\tilde{y}}}, \tag{2.6.11}$$

which is called the Porter Thomas distribution [29].
To illustrate that this distribution shows that the matrix elements are Gaussian random numbers, but makes no statement about the independence among each other, the matrix from Fig. 2 b) shall be considered here. This matrix was generated from a realization of a GOE by sorting the elements within the diagonals according to their values. Thus, all elements individually are Gaussian random numbers, but it is clear that the elements are locally strongly correlated with each other. In Fig. 3 it can be seen that such matrices exhibit the Porter Thomas distribution, but the distribution of the eigenvalues deviates strongly from the WSC as seen in Fig. 4.
The correlations of the matrix elements are also reflected in the value $\overline{r} = 0.463$, which differs from the value of the unsorted GOE $\overline{r} = 0.529$. However, it should also be noted that the numerical data suggest that, especially in this situation, this indicator is not very sensitive. For example, Fig. 5 shows the distribution of the indicator for 10^7 different $2^4 \times 2^4$ GOEs for both cases, the sorted and unsorted ones. Even if the expectation values of both distributions are clearly distinguishable, it can be seen that both distributions are rather broad. Thus, single realizations can be indistinguishable in respect to $\overline{r}$. Even though the distributions are narrower for larger matrices, a distinction is not possible even then, because then the $\bar{r}$ for both cases tend to approach each other.
By the nature of random matrices, the possibility of generating an arbitrary (hermitian) matrix is always non-zero. However, the probability of obtaining deviations from the usual indicators for random matrices in individual realizations decreases as the size of the matrices increases. As an

[23] The limitation to a frequency range is necessary to assure that $f \approx$ const. holds and is thus redundant in true GOE matrices.

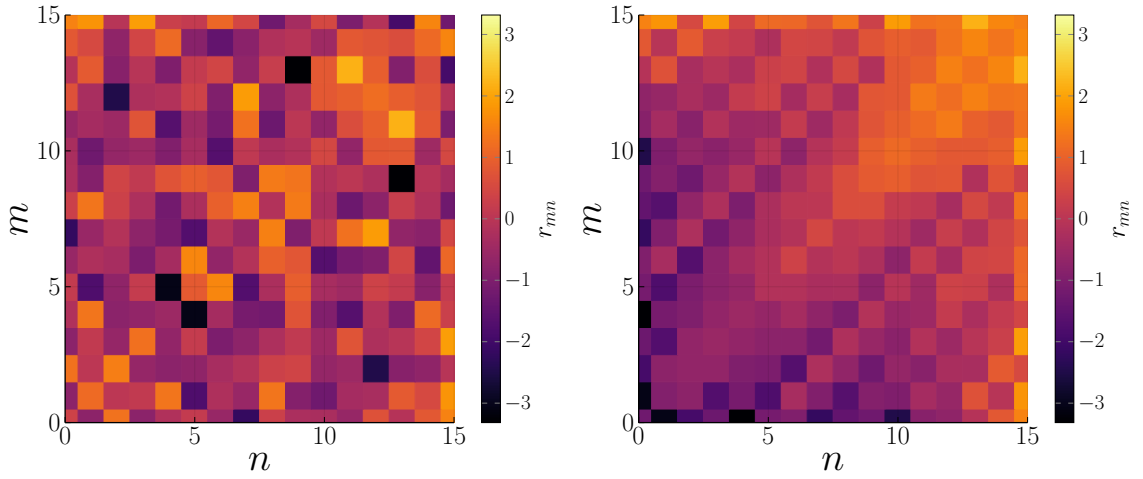

Fig. 2: a) Heatmap for a single realization of a $2^4 \times 2^4$ GOE matrix
b) Heatmap of a matrix with the same elements, but sorted along the (off-)diagonals.

example, consider the WSC of a single realization of a GOE of size $2^{10} \times 2^{1024}$, which is shown in Fig. 6. It is easy to see that the deviations for individual realizations are even rather small.
This property is particularly worth mentioning, since only one realization is ever considered when looking at an observable. Therefore, averaging is not possible in this case. Due to the property described above, a comparison with the expectations of GOE matrices for large systems is nevertheless useful.
One way to compare a matrix with a similar but correlation-free matrix is to use the sign-random method [24, 30, 31]. The method itself is not an indicator, instead it is a possibility to better estimate indicators. A sign-random version is generated from the observable $\hat{A}$, whose elements are randomly signed[25]:

$$\tilde{A}_{nm} = \begin{cases} A_{nm} & (50\%) \\ (-1) \cdot A_{nm} & (50\%) \end{cases} \tag{2.6.12}$$

Since MEC in this observation variable are broken, the indicators of this matrix can be compared with the original one. If a random matrix already existed before, the behavior of these indicators should not change by this method. Note that the Gaussian nature of the elements is preserved under sign randomization, so investigations involving only the Gaussian distribution remain unchanged (e.g. $\Gamma(\omega)$ or $P(\tilde{y})$).

[24] This would correspond to a spin system with 10 particles and is thus much smaller than the smallest systems studied within this thesis.
[25] To obtain the hermicity $\tilde{A}_{mn} = \tilde{A}^*_{nm}$ applies.

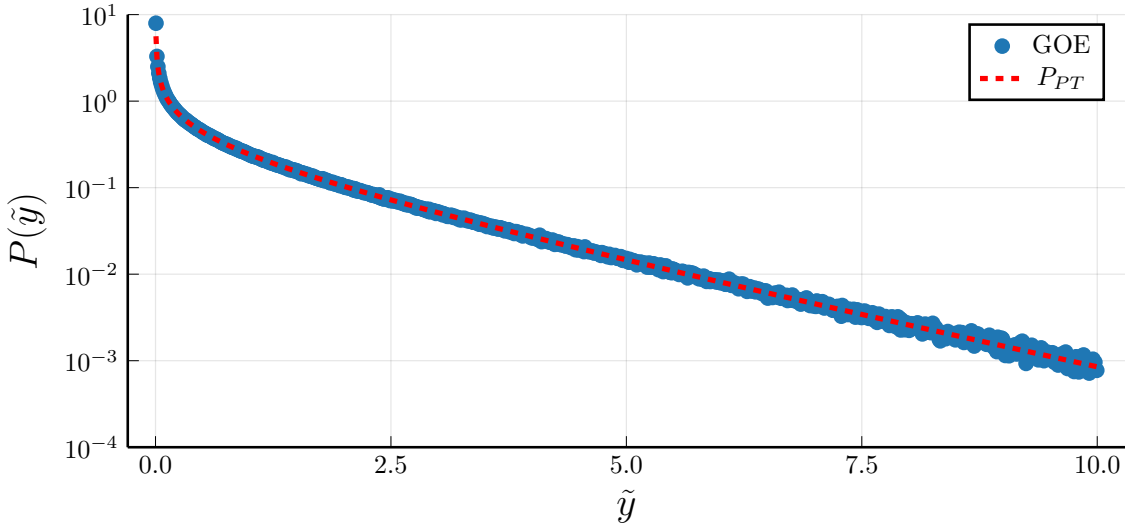

Fig. 3: Distribution of $\tilde{y}$ for modified $2^4 \times 2^4$ random matrices, as shown in Fig. 2 b), averaged over 5000 realizations compared to the Porter-Thomas distribution.

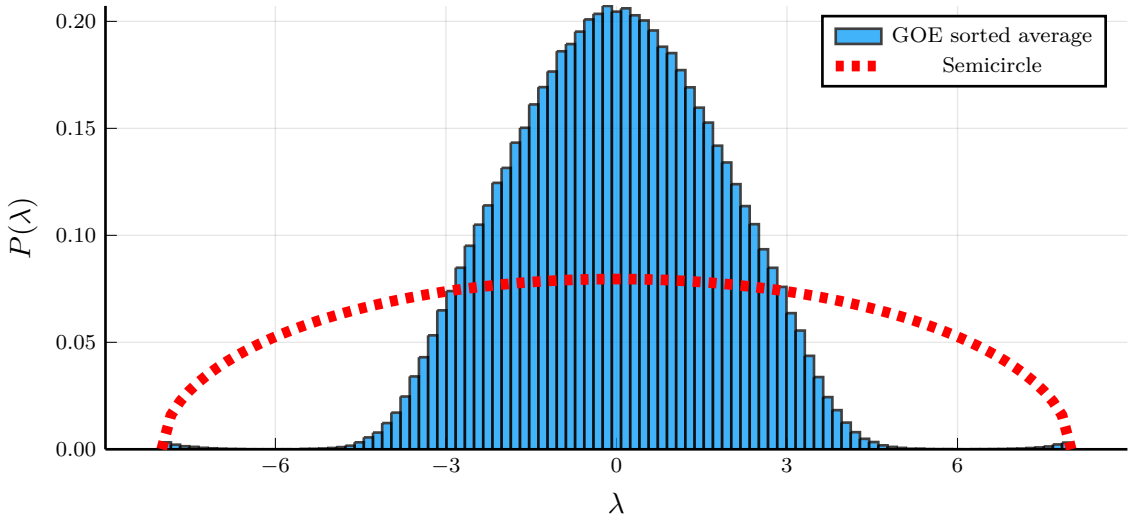

Fig. 4: Eigenvalue distribution for modified $2^4 \times 2^4$ random matrices, as shown in Fig. 2 b), averaged over 5000 realizations compared to the WSC. On average $\bar{r} = 0.463$ holds.

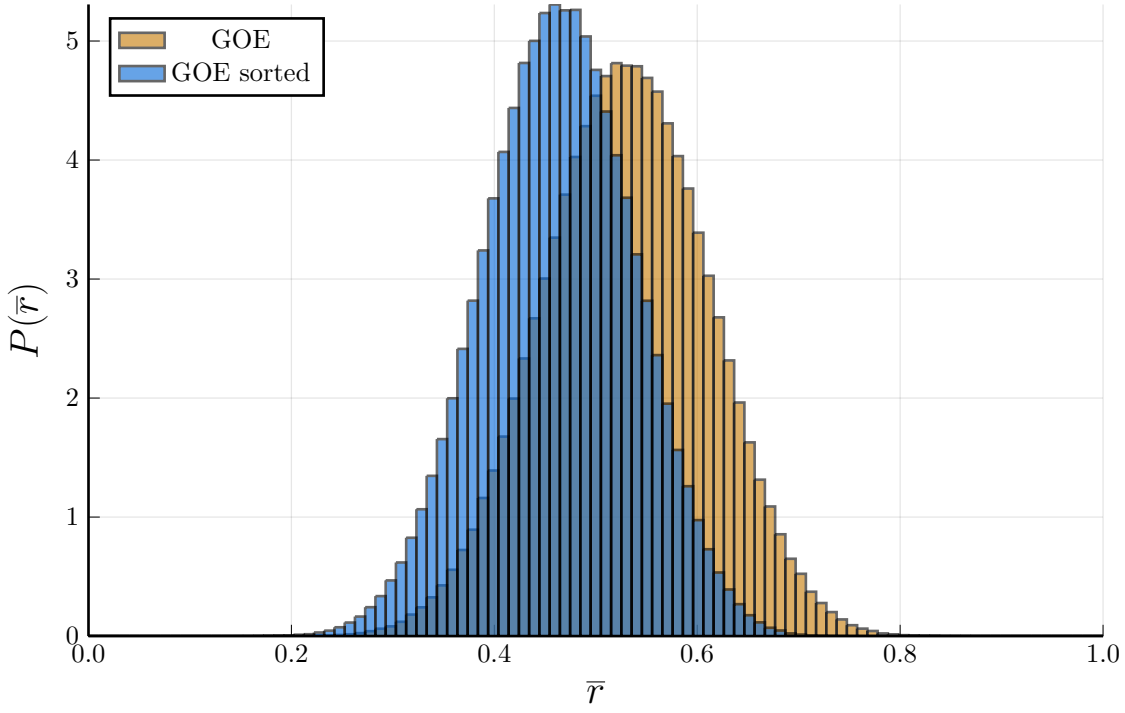

Fig. 5: Distribution of $\overline{r}$ for 10^7 different $2^4 \times 2^4$ sorted and unsorted GOE's.

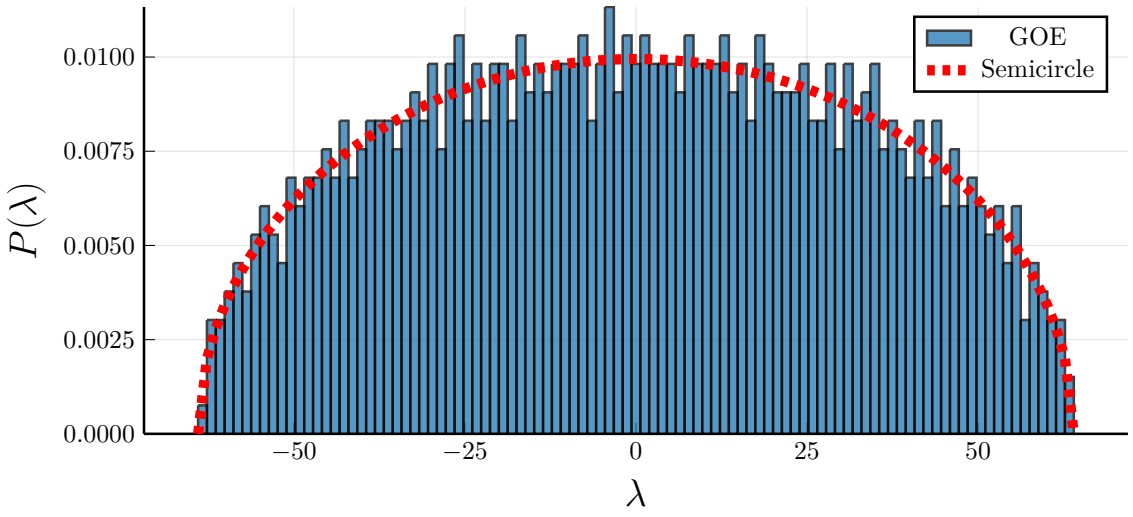

Fig. 6: Eigenvalue distribution of single realization of a GOE $2^{10} \times 2^{10}$ matrix, as well as Wigner's semicircle law with $R = 2^6$. $\bar{r} = 0.520$ holds.

2.7 Typicality Perturbation Theory

The theory explained in this subsection has some similarity to the DQT (Subsection 2.3) and the RMT (see Subsection 2.6), but unlike those, it is not a standard tool. The theory which is called Typicality Perturbation Theory (TPT) within this thesis is relatively new and would (if valid) be a powerful tool with great general predictive power. TPT was introduced in Ref. [32] and further refined in Refs. [33, 34]. Since validity is a subject of investigation within this thesis (see Section 4), that question shall be postponed. The focus of this subsection is to explain the basic idea of the theory, as well as its assumptions and statements. TPT treats perturbations of the following form

$$\hat{H} = \hat{H}_0 + \lambda \hat{V} \tag{2.7.1}$$

where $\hat{H}$ is the perturbed Hamiltonian of the system, λ denotes the perturbation strength, and $\hat{V}$ is the perturbation.
Let

$$A(t) = \mathrm{Tr}\left\{\hat{A}\mathrm{e}^{-\mathrm{i}\hat{H}_0 t}\hat{\rho}\mathrm{e}^{\mathrm{i}\hat{H}_0 t}\right\} \tag{2.7.2}$$

be the known unperturbed dynamics of the system, where $\hat{\rho}$ is the initial state. TPT makes statements about the perturbed dynamics

$$\tilde{A}(t) = \mathrm{Tr}\left\{\hat{A}\mathrm{e}^{-\mathrm{i}\hat{H} t}\hat{\rho}\mathrm{e}^{\mathrm{i}\hat{H} t}\right\}. \tag{2.7.3}$$

It can be shown that under some conditions,

$$\tilde{A}(t) \approx \overline{\tilde{A}} + |g(t)|^2 \cdot \left(A(t) - \overline{\tilde{A}}\right) \tag{2.7.4}$$

holds, where $\overline{\tilde{A}}$ is the long term value (see Subsection 2.4) of the perturbed dynamics and $g(t)$ is monotonically decreasing in time. TPT does not make any statements about the former, so the theory is unsuitable for investigating the long-time values.
The main idea behind TPT is to look at an ensemble of perturbations rather than individual specific perturbations. This ensemble should have some main properties of the perturbation under investigation, but otherwise be random.
To understand the necessary conditions for TPT, a few things should be explained first: First, it is important to consider the matrix elements of the perturbation in the basis of the unperturbed Hamiltonian

$$V^0_{\mu\nu} = {}_0\langle E_\mu|\hat{V}|E_\nu\rangle_0\,. \tag{2.7.5}$$

Secondly, the LDOS[26], which is proportional to the probability density to find an occupied energy-eigenstate in a given energy range for a given initial state, requires to be put into context. The LDOS is thereby the product of DOS and the population distribution $\langle E_n|\hat{\rho}|E_n\rangle$, where $\hat{\rho}$ is the initial state. The LDOS is used here as an indicator which part of the spectra is relevant for the dynamics of the system, e.g. if the LDOS equals zeros for some energy region, these parts are not relevant for the dynamics. The DOS can be used as an indicator for a constant mean level spacing ϵ, as a constant level spacing equals a constant DOS.
Even if the exact form of $g(t)$ depends on further conditions, four basic assumptions can be listed, which are necessary to develop the theory:

[26] For numerical calculation using DQT see Subsection 2.3.

i) The DOS in the non-perturbed system should be approximately constant in the region where the LDOS is not vanishingly small.

ii) The perturbation should not change any thermodynamic quantities of the system. This implies that the DOS should not be changed significantly either, because of its connection to entropy.

iii) The perturbation should be strong enough, such that the eigenstates of the unperturbed system $|E_\nu\rangle_0$ and those of the perturbed system $|E_m\rangle$ are well mixed.

iv) The perturbation $\hat{V}$ should be a (pseudo) random matrix in the non-perturbed eigenbasis with the following properties

$$\overline{V^0_{\mu\nu}} = 0 \tag{2.7.6}$$

$$\overline{|V^0_{\mu\nu}|^2} = \sigma^2(|E_\mu - E_\nu|) \tag{2.7.7}$$

where the bar denotes the mean over an ensemble of perturbations. The variance σ^2 is a smooth function of its arguments and will be called perturbation-profile.

At this point, some consequences of the assumptions shall be considered in more detail. Firstly, it can be seen from condition i) that the perturbation theory is not necessarily independent of the initial state $\hat{\rho}$. Even if a system does not exhibit constant DOS in all its parts, this would not be a problem as long as this region is not relevant to the dynamics.
For condition i), one could ask whether the DOS of the unperturbed or the perturbed Hamiltonian is meant. The irrelevance of this question is shown in condition ii), which states that both cases must not differ (strongly). Moreover, condition ii) excludes phase transitions.
These four conditions thus form the foundation of the theory, so to speak. In addition, further conditions apply, depending on which function is to be used for $g(t)$. For different cases there are different $g_i(t)$. Within this thesis the focus will be on 3 of these cases.
The first one is the case of weak perturbation (small λ), where

$$g_1(t) = \mathrm{e}^{-\Gamma\frac{|t|}{2}} \tag{2.7.8}$$

with

$$\Gamma = \frac{2\pi}{\epsilon}\lambda^2\sigma^2(0) \tag{2.7.9}$$

is appropriate for an approximation. Thereby, the weak perturbation should be strong enough to satisfy condition iii).
There is also an application of the theory for the case of strong perturbations (large λ). For this

$$g_2(t) = \frac{2J_1(\gamma t)}{\gamma t} \tag{2.7.10}$$

with

$$\gamma = \lambda\sqrt{\frac{8\Delta_v\sigma(0)^2}{\epsilon}} \tag{2.7.11}$$

and

$$\Delta_v = \frac{1}{\sigma^2(0)}\int_0^\infty \sigma^2(\omega)d\omega \tag{2.7.12}$$

is inserted. Here Δ_v is an indicator for the bandwidth of the perturbation $\hat{V}$ and $J_1(t)$ is the first kind Bessel function of order 1. It should be noted that even in this case the perturbation may not be arbitrarily strong, but is still limited by condition ii).
The crossover between these approximations should happen at a perturbation strength

$$\lambda_c := \sqrt{\frac{2\Delta_v \epsilon}{\pi^2 \sigma^2(0)}}. \tag{2.7.13}$$

In addition to these two cases, a third approximation was determined in Ref. [34], which is applied using

$$g_3(t) = \frac{\left(\gamma_+ - \frac{\Gamma}{2}\right) \mathrm{e}^{-\gamma_- |t|} + \left(\gamma_- - \frac{\Gamma}{2}\right) \mathrm{e}^{-\gamma_+ |t|} - \Gamma \mathrm{e}^{-\gamma_0 |t|}}{2(\gamma_0 - \Gamma)} \tag{2.7.14}$$

with

$$\gamma_{-,0,+} = \frac{2\Delta_v}{\pi} \left[1 \pm \sqrt{1 - \frac{\pi\Gamma}{2\Delta_v}}\right]. \tag{2.7.15}$$

Similar to the first approximation, this one applies in the range of weak perturbations, but is supposed to be valid over a larger range. However, it differs from the previous approximation in that further assumptions have been made for the derivation, i.e. it is only applicable under additional conditions. Strictly speaking, the new additional condition concerns the perturbation profile $\sigma^2(\omega)$, which is now assumed to be Lorentz-shaped

$$\sigma^2(\omega) = \frac{\sigma^2(0)}{1 + \left(\frac{\omega\pi}{2\Delta_v}\right)^2}. \tag{2.7.16}$$

It can be shown numerically in individual cases that g_3 also yields good results for other perturbation profiles, but those results are not a general proof, but only an indication of the stability of g_3 under violation of that condition.

2.8 Recursion Method

Even though the system behind an autocorrelation function can be arbitrarily complex, it can always be mapped to a transport problem in a one dimensional semi-infinite chain. The method of this mapping is called the Recursion Method [35].
Within this subsection it will be explained how this mapping works and how it relates to other representations. In addition, the problems with the implementation of that mapping will be briefly mentioned. For the interested reader Ref. [35] is recommended, which provides a more detailed look into this method.
A modified version of this method, which is often called Krylov subspace method, can also be used to approximately determine the dynamics of a pure state [36]. The normalized autocorrelation function, which is expressed in Eq. (2.2.2), takes the following form

$$\tilde{C}_{\hat{A}}(t) = \mathrm{Tr}\left\{\hat{A}\hat{A}(t)\right\} / \mathrm{Tr}\left\{\hat{A}^2\right\}. \tag{2.8.1}$$

Here $\hat{A}(t)$ satisfies the differential Eq. (2.1.18), therefore

$$\frac{d}{dt}\hat{A}(t) = \mathrm{i}\hat{\mathscr{L}}^{\mathrm{S}}\hat{A}(t) \tag{2.8.2}$$

holds, where $\hat{\mathscr{L}}^{\mathrm{S}}$ is a superoperator with

$$\hat{\mathscr{L}}^{\mathrm{S}} = \left[\hat{H}, \bullet\right] \tag{2.8.3}$$

which is called Liouvillian[27]. In addition, a new scalar product

$$(A|B) := \frac{1}{\mathcal{D}} \mathrm{Tr}\left\{\hat{A}^{\dagger}\hat{B}\right\} \tag{2.8.4}$$

and a corresponding norm

$$||\hat{A}|| := \sqrt{(A|A)} \tag{2.8.5}$$

are introduced. With these two definitions, the Lanczos algorithm can now be applied. As a starting point

$$|A_0) := |A) \qquad |A_1) := \frac{1}{b_1}\hat{\mathscr{L}}^{\mathrm{S}}|A_0) \tag{2.8.6}$$

$$b_0 := 0 \qquad b_1 := \sqrt{(A_0\hat{\mathscr{L}}^{\mathrm{S}}|\hat{\mathscr{L}}A_0)} \tag{2.8.7}$$

are used.
All further definitions are recursively given by

$$|B_n) := \hat{\mathscr{L}}^{\mathrm{S}}|A_{n-1}) - b_{n-1}|A_{n-2}) \tag{2.8.8}$$

$$b_n := ||B_n|| \tag{2.8.9}$$

$$|A_n) := \frac{1}{b_n}|B_n). \tag{2.8.10}$$

As a result, this procedure yields an orthogonal basis $\{|A_n)\}$, which is called the Krylov basis, and the so-called Lanczos coefficients b_n, which are positive real numbers. Within this basis the Liouvillian is tridiagonal:

$$\mathscr{L}^{\mathrm{S}}_{nm} = (A_n|\hat{\mathscr{L}}^{\mathrm{S}}|A_m) \tag{2.8.11}$$

$$:= \begin{pmatrix} 0 & b_1 & 0 & 0 & \cdots \\ b_1 & 0 & b_2 & 0 & \cdots \\ 0 & b_2 & 0 & b_3 & \cdots \\ 0 & 0 & b_3 & 0 & \ddots \\ \vdots & \vdots & \vdots & \ddots & \ddots \end{pmatrix} \tag{2.8.12}$$

Since the time evolution according to Eq. (2.8.2) is formally solved with

$$|A(t)) = \mathrm{e}^{\mathrm{i}\hat{\mathscr{L}}^{\mathrm{S}}t}|A_0), \tag{2.8.13}$$

it follows for the autocorrelation function

$$\tilde{C}_{\hat{A}}(t) = (A_0|\mathrm{e}^{\mathrm{i}\hat{\mathscr{L}}^{\mathrm{S}}t}|A_0). \tag{2.8.14}$$

[27]Since $\hat{\mathscr{L}}$ will latter represent a slightly modified variant of the Liouvillian, this form is marked here with an S.

Introducing a new basis $\{|\tilde{A}_n)\}$[28], which is derived from the Krylov basis by

$$|\tilde{A}_n) := \mathrm{i}^n |A_n) \tag{2.8.15}$$

and including the complex number i into the superoperator $\hat{\mathscr{L}}$,

$$\mathscr{L}_{mn} := \mathrm{i}(\tilde{A}_n|\hat{\mathscr{L}}^{\mathrm{S}}|\tilde{A}_m) \tag{2.8.16}$$

$$:= \begin{pmatrix} 0 & -b_1 & 0 & 0 & \cdots \\ b_1 & 0 & -b_2 & 0 & \cdots \\ 0 & b_2 & 0 & -b_3 & \cdots \\ 0 & 0 & b_3 & 0 & \ddots \\ \vdots & \vdots & \vdots & \ddots & \ddots \end{pmatrix} \tag{2.8.17}$$

is obtained. This antisymmetric matrix corresponds to a hopping on a semi-infinite[29] chain, the so-called Mori chain. Here x_n is the occupation on the n-th place. Since in the base transformation the first base state is unchanged, the autocorrelation function is given by

$$\tilde{C}_{\tilde{A}}(t) = (A_0|\mathrm{e}^{\hat{\mathscr{L}}t}|A_0). \tag{2.8.18}$$

In terms of hopping, the dynamics of the chain can also be described as a differential equation

$$\frac{\partial}{\partial t} x_n(t) = b_n x_{n-1}(t) - b_{n+1} x_{n+1}(t), \tag{2.8.19}$$

with $x_n(t=0) = \delta_{n0}$ as the initial condition. The advantage of the new basis is that the occupations of the sites are always real.
In this way, it is possible to reduce arbitrary autocorrelation functions of quantum systems to simple transport dynamics in one-dimensional systems with real values.
In addition, a representation for the Laplace transform of the autocorrelation can be obtained from this equation. By means of the Laplace transform

$$\mathcal{L}\{x(t)\}(s) = \int_0^\infty x(t) e^{st} dt = x(s) \tag{2.8.20}$$

follows from that equation

$$s x_n(s) - x_n(t=0) = b_n x_{n-1}(s) - b_{n+1} x_{n+1}(s). \tag{2.8.21}$$

Adding now the initial condition $x_n(t=0) = \delta_{n0}$, the two equations

$$x_0(s) = \frac{1}{s + b_1 \frac{x_1(s)}{x_0(s)}} \qquad \text{for } n = 0 \tag{2.8.22}$$

$$b_n \frac{x_{n-1}(s)}{x_n(s)} = s + b_{n+1} \frac{x_{n+1}(s)}{x_n(s)} \qquad \text{for } n \neq 0 \tag{2.8.23}$$

[28] Note that this basis is also orthonormal.
[29] The chain is semi-infinite only for infinite systems.

are obtained. If one now substitutes Eq. (2.8.23) into Eq. (2.8.22) and repeats this successively for the new equation, the result can be expressed by

$$x_0(s) = \cfrac{1}{s + \cfrac{b_1^2}{s + \cfrac{b_2^2}{s + \ddots}}}\,, \tag{2.8.24}$$

which is called Continued Fraction.
However, even though the full information is written in these coefficients, it is far from trivial to construct the autocorrelation function from this. For the exact behavior of this dynamic for a general case a ED is needed. Moreover, these dynamics are carried out in the so-called Liouville space, which is much larger than the Hilbert space otherwise used[30].
Even without the problem of the sheer size of the resulting matrices, the Lanczos algorithm itself is problematic, since it is numerically unstable: Even if mathematically it follows beyond doubt that the Krylov basis is orthonormal, in practice it turns out that due to the limited numerical accuracy, orthogonality is no longer fulfilled after a few steps. Even though there are numerical methods that improve the stability of the algorithm [38], they greatly increase the numerical cost, so they are not necessarily useful to apply.
An alternative approach will be introduced in Subsubsection 2.10.4, which does not change the numerical procedure itself, but exploits structures of the underlying model, so that the Lanczos method can be performed exactly.

2.8.1 Operator Grows Hypothesis

Although in general the Lanczos coefficients can only be determined numerically in finite numbers, the Operator Grows Hypothesis (OGH) presented in Ref. [39] states that for few-body observables in non-integrable systems, these coefficients b_n increase linearly[31] for large n. Such a behavior has already been proven for different cases [40], where the linear behavior could already be seen in the range in which the Lanczos coefficients are determinable.
Even if the determination of the coefficients is strongly limited by the numerical costs, by means of that procedure a meaningful continuation can be formed, which yields in many cases equivalent results to the autocorrelation functions determined by the usual methods (see Subsection 5.1). Moreover, this representation of a chain is suitable for further investigations, since many complicated dynamics in the original model can be reduced to a more intuitive picture of a one-dimensional chain.

2.9 Models

All systems studied within this thesis are spin-1/2 lattice systems. The Hamiltonians of these systems can be written in the most general form as follows

$$\hat{H} = \sum_{j,l} J_{jl} \left(\sum_u \Delta_u \hat{\sigma}_j^u \hat{\sigma}_l^u \right) + \sum_j \left(\sum_u h_{uj} \hat{\sigma}_j^u \right) \tag{2.9.1}$$

with

$$u \in \{x, y, z\}\,, \tag{2.9.2}$$

[30] In the worst case for the dimension of this space $\mathcal{K} = \mathcal{D}^2 - \mathcal{D} + 1$ holds, whereby $\mathcal{D}$ is the dimension of the Hilbert space [37].
[31] For 1-dimensional systems there exists a logarithmic correction $b_n \sim A\frac{n}{\ln(n)}$.

where $\hat{\sigma}_j^u$ is one of the Pauli matrices at site j. The first sum runs over all combinations of the different sites, J_{jl} indicating the coupling strength between the sites j and l, while Δ_u corresponds to the anisotropy in the different directions. The second sum is to be interpreted in the sense of an external magnetic field, where h_{uj} is the strength of the magnetic field at the site j in direction u. The Pauli matrices are defined as

$$\hat{\sigma}^x = \begin{pmatrix} 0 & 1 \\ 1 & 0 \end{pmatrix} \qquad \hat{\sigma}^y = \begin{pmatrix} 0 & -\mathrm{i} \\ \mathrm{i} & 0 \end{pmatrix} \qquad \hat{\sigma}^z = \begin{pmatrix} 1 & 0 \\ 0 & -1 \end{pmatrix} . \tag{2.9.3}$$

Since a Pauli matrix $\hat{\sigma}_j^u$ acts only on position j, the effect of the operator on the whole system can be expressed as

$$\hat{\sigma}_j^u = \bigotimes_{l=1}^{L} \left[\hat{1} \cdot (\delta_{lj} - 1) + \hat{\sigma}^u \delta_{lj}\right], \tag{2.9.4}$$

where $\bigotimes$ denotes a row of dyadic products and L is the number of sites within the system.
From Eq. (2.9.3) and (2.9.4) follows the commutation relation of those operators:

$$\left[\hat{\sigma}_j^u, \hat{\sigma}_l^v\right] = 2\mathrm{i}\varepsilon_{uvw}\hat{\sigma}_j^w \delta_{jl} \tag{2.9.5}$$

where ε is the antisymmetric Levi-Civita symbol.
For a more direct view, the spin operators $\hat{s}^u = 1/2 \cdot \hat{\sigma}^u$ are also frequently introduced, which accordingly have the commutation relation

$$\left[\hat{s}_j^u, \hat{s}_l^v\right] = \mathrm{i}\varepsilon_{uvw}\hat{s}_j^w \delta_{jl}. \tag{2.9.6}$$

For the special case that $h_{uj} = 0$ if $u \neq z$ holds, the model in this thesis is called the Heisenberg model. Moreover, for all Heisenberg models in this thesis, $\Delta_x = \Delta_y := \Delta_{xy}$ holds. These two properties allow a more efficient computation of dynamics of those systems. For this purpose, first the Hamiltonian is rewritten to

$$\hat{H} = \sum_{j,l} J_{jl}\left[\Delta_{xy}\left(\hat{\sigma}_j^x\hat{\sigma}_l^x + \hat{\sigma}_j^y\hat{\sigma}_l^y\right) + \Delta_z\hat{\sigma}_j^z\hat{\sigma}_l^z\right] + \sum_j h_j\hat{\sigma}_j^z \tag{2.9.7}$$

$$= \sum_{j,l} J_{jl}\left[2\Delta_{xy}\left(\hat{\sigma}_j^+\hat{\sigma}_l^- + \hat{\sigma}_j^-\hat{\sigma}_l^+\right) + \Delta_z\hat{\sigma}_j^z\hat{\sigma}_l^z\right] + \sum_j h_j\hat{\sigma}_j^z \tag{2.9.8}$$

with

$$\hat{\sigma}^+ = \begin{pmatrix} 0 & 1 \\ 0 & 0 \end{pmatrix} \qquad \hat{\sigma}^- = \begin{pmatrix} 0 & 0 \\ 1 & 0 \end{pmatrix} \tag{2.9.9}$$

which are called creation (annihilation) operators[32].
It is easy to see that the xy-term is equivalent to hopping: If there is an up spin at j and a down spin at l (or vice versa), then this term swaps both spins. It follows that this term preserves the total magnetization in the z-direction $\hat{S}^z = \frac{1}{2}\sum_j \hat{\sigma}_j^z$. Since the further terms consist only of $\hat{\sigma}^z$, and those operators always commute with all parts of the z-magnetization (see Eq. (2.9.5)), it turns out that $\hat{S}^z$ is commuted with the complete Hamiltonian and thus is obtained. This is particularly

[32]Note that even if the operators are called creation (annihilation) operators, the spin particles are neither created nor annihilated.

useful since constants of motions span subspaces in the Hilbert space $\mathcal{H}$, which can be considered separately from each other. Thus, in a divide and conquer manner, the numerics can be simplified. Thus, there are L different subspaces which can be investigated separately. The dimensions of these spaces are given by

$$\mathcal{D}_M = \binom{L}{M} = \frac{L!}{M!(L-M)!} \qquad \text{with } M = 0, 1, 2, ..., L. \tag{2.9.10}$$

So for a common system size of $L = 16$ the largest subspaces of magnetization only has one fifth of the total dimension.
Another reduction is the absence of external magnetic fields, so that the Hamiltonian takes the form

$$\hat{H} = \sum_j J \left[2\Delta_{xy} \left(\hat{\sigma}_j^+ \hat{\sigma}_{j+1}^- + \hat{\sigma}_j^- \hat{\sigma}_{j+1}^+ \right) + \Delta_z \hat{\sigma}_j^z \hat{\sigma}_{j+1}^z \right]. \tag{2.9.11}$$

This case is worth mentioning because it is integrable in terms of the so-called Bethe Ansatz[33][41, 42]. Moreover, such a system also corresponds to a system of spinless fermions by means of the Jordan-Wigner transformation [43] and a bosonic system via the HolsteinPrimakoff transformation [44].
Another named model used within this thesis is the mixed-field Ising model, which takes the following form

$$\hat{H} = \sum_{j,l} J_{jl} \hat{\sigma}_j^z \hat{\sigma}_l^z + \sum_j \left(\sum_u h_{uj} \hat{\sigma}_j^u \right). \tag{2.9.12}$$

In contrast to the Heisenberg model the total magnetization in z-direction is not conserved here, so that a separation into magnetization subspaces is not possible here[34].
In the special case of

$$\hat{H} = J \sum_j \hat{\sigma}_j^z \hat{\sigma}_{j+1}^z + h \sum_j \sigma_j^y, \tag{2.9.13}$$

this model (which then is also called XY chain) is integrable [42]. Remark that since a cyclic swapping of $\{x, y, z\}$ is just a change of the coordinates, which does not change the integrability property.
It should be mentioned that the usual computational basis is the Ising basis, which are the eigenstates of $\hat{\sigma}_l^z$ for all l. In this basis, it is easy to see that the Hamiltonian (as well as local observables) are sparse. This property can be used to speed up numerical calculations [45]. To see this, consider the Heisenberg chain in Eq. (2.9.11) in this basis: Since all states of the basis are eigenstates of $\hat{\sigma}_l^z$, this part of the Hamiltonian only contributes to the diagonal elements. The other part of the Hamiltonian corresponds to a flip of two neighboring spins. Even in the worst case, there are only L possible ways to do so. Thus, considering this worst case, every state of the basis connects to a maximum of L other basisstates. Since the number of basisstates is exponential, only $\frac{(L+1)}{4^L}\%$ of the elements are not zeros[35].
The models described here are used to describe ultracold trapped atoms [46, 47, 48] and quantum magnets [49]. In spite of those application possibilities, it is to be pointed out that those experimental relations are less relevant within this thesis and the models are to be regarded only as examples or objects of investigation.

[33] Which systems are considered integrable and which are not is still a topic of discussion in science today. However, the case of integrability in the sense of the Bethe approach is consensus.

[34] The exploitation of other symmetries is still possible, but is not used within this work, since the symmetries are broken by additional magnetic fields.

[35] Similar arguments in the Ising chain lead to a similar result.

2.10 Numerical methods

In this subsection the numerical methods used within this thesis will be explained. The focus lies strongly on the applicability of these methods and less on the theoretical background. The goal is to enable the reader to reproduce the basic results of the thesis.

2.10.1 Exact Diagonalization

The most direct way to compute the dynamics of a system numerically is by exact diagonalization. As already shown in the previous sections, the Schrödinger equation is formally solved by

$$|\phi(t)\rangle = \sum_n \mathrm{e}^{-\mathrm{i}E_n t} \underbrace{\langle \phi(0)|E_n\rangle}_{c_n} |E_n\rangle \tag{2.10.1}$$

where $\hat{H}\,|E_n\rangle = E_n\,|E_n\rangle$, thus E_n are eigenvalues and the corresponding eigenstates of the Hamiltonian $\hat{H}$.
Therefore, the state can be directly determined at any time if c_n and E_n are known. These values can be determined by standard methods of diagonalization. These methods are already highly efficient in many linear algebra packages (e.g. LAPACK [50]) and can be further optimized by exploiting the hermicity of the Hamiltonian.
Even though ED is in principle applicable to any finite system and highly optimized methods are available, its use is still severely limited. On the one hand, this is due to the poorly scaling runtime of $\mathcal{O}(\mathcal{D}^3)$, on the other hand, the required storage space grows with $\mathcal{D}^2$. For example, for 18 spin $1/2$ particles one requires ~ 1 TB of memory.
Since much larger systems are to be considered within this thesis in order to minimize possible finite size effects, other methods are mostly used for dynamics, which scale better.

2.10.2 Runge-Kutta-4 Method

Since ED is not possible for large systems, within this thesis different methods are used which can describe the dynamical behavior of pure states in a very good approximation without the need to determine the eigenvalues (and eigenvectors) of the Hamiltonian.
The first method presented here is the Runge-Kutta-4 method. This is an iterative method which allows to solve a differential equation of the form

$$\frac{dy}{dt}(t) = f(y(t), t) \tag{2.10.2}$$

successively.
By using this method $y(t_0 + \delta t)$ can be determined approximately:

$$y(t_0 + \delta t) = y(t_0) + \frac{\delta t}{6}\left(k_1 + 2k_2 + 2k_3 + k_4\right) + \mathcal{O}(\delta t^4) \tag{2.10.3}$$

$$k_1 = f(t_0, y(t_0)) \tag{2.10.4}$$

$$k_2 = f(t_0 + \frac{\delta t}{2}, y(t_0) + \frac{\delta t}{2} \cdot k_1) \tag{2.10.5}$$

$$k_3 = f(t_0 + \frac{\delta t}{2}, y(t_0) + \frac{\delta t}{2} \cdot k_2) \tag{2.10.6}$$

$$k_4 = f(t_0 + \delta t, y(t_0) + \delta t \cdot k_3) \tag{2.10.7}$$

Thus, $y(t_0 + \delta t)$ can be determined with arbitrary accuracy as long as δt is chosen small enough[36]. Plugging in the Schrödinger Eq. (2.1.14) results in:

$$|\psi(t_0 + \delta t)\rangle = |\psi(t_0)\rangle + \frac{\delta t}{6}\left(|k_1\rangle + 2\,|k_2\rangle + 2\,|k_3\rangle + |k_4\rangle\right) + \mathcal{O}(\delta t^4) \tag{2.10.8}$$

$$|k_1\rangle = -\mathrm{i}\hat{H}\,|\psi(t_0)\rangle \tag{2.10.9}$$

$$|k_2\rangle = -\mathrm{i}\hat{H}\left(|\psi(t_0)\rangle + \frac{\delta t}{2}\,|k_1\rangle\right) \tag{2.10.10}$$

$$|k_3\rangle = -\mathrm{i}\hat{H}\left(|\psi(t_0)\rangle + \frac{\delta t}{2}\,|k_2\rangle\right) \tag{2.10.11}$$

$$|k_4\rangle = -\mathrm{i}\hat{H}\left(|\psi(t_0)\rangle + \delta t\,|k_3\rangle\right) \tag{2.10.12}$$

By this method a temporal dynamic can be developed by multiple application of the Hamiltonian to a vector; a diagonalization is no longer necessary for this. The most expensive operation within the method is a matrix-vector multiplication, which has a running time of $\mathcal{O}(\mathcal{D}^2)$ (compare ED running time $\mathcal{O}(\mathcal{D}^3)$). In turn, matrix-vector multiplication must be performed very often in consecutive order. Since within this thesis the Hilbertspaces are large and the dynamics have been developed only for relatively short times, this method offers an advantage over ED.
By exploiting sparseness of the used Hamiltonian (see 2.9) and high parallelization, the matrix-vector multiplication can be greatly improved, especially when using the graphics processing unit (GPU).

2.10.3 Chebyshev Method

Another approach to iterative evolution of dynamics is the Chebyshev method, which is based on the Chebyshev polynomials [51, 52].
Just as in the previous subsubsections, the focus here will be on the application rather than on the derivation. For the time evolution of

$$|\psi(t)\rangle = \mathrm{e}^{-\mathrm{i}\hat{H}t}\,|\psi\rangle \tag{2.10.13}$$

by means of this method, the largest (smallest) energy eigenvalue $E_{\max}$ ($E_{\min}$) must first be determined.
Now introduce a new scaled Hamiltonian

$$\hat{H}_{\text{scal.}} = \frac{\hat{H} - b\hat{1}}{a}. \tag{2.10.14}$$

with

$$b = \frac{(E_{\max} + E_{\min})}{2} \qquad\qquad a = \frac{(E_{\max} - E_{\min})}{2}. \tag{2.10.15}$$

This new Hamiltonian has the eigenvalues

$$|\tilde{\lambda}_n| \leq 1. \tag{2.10.16}$$

This rescaling is necessary because the Chebyshev method is only applicable if the eigenvalues are between -1 and 1. In practice, the maximum energy eigenvalues can be approximated by standard

[36] For too small δt also the dynamic changes become too small, so that these are lost in the numerical rounding. However, this is not a problem in practice, since there is a large range in which δt is small enough to satisfy the approximation very precisely, but large enough so that the dynamic changes do not become too small.

estimation. This is easily applicable if the Hamiltonian is built up from several local operators whose maximum eigenvalues are known. This is for example the case in models of spin lattices/chains. If the Hamiltonian has the following form

$$\hat{H} = \sum_j \hat{A}_j \cdot \hat{B}_j, \tag{2.10.17}$$

it follows via the triangle inequality and the sub-multiplicative

$$||\hat{H}|| \leq \sum_j ||\hat{A}_j|| \cdot ||\hat{B}_j||, \tag{2.10.18}$$

where $||\bullet||$ denotes the absolute value of the absolute largest eigenvalue of the operator. It is easy to see that $E_{\max} \leq ||\hat{H}||$ and $E_{\min} \geq -||\hat{H}||$, so that an estimation of the maximum eigenvalues is obtained[37]. In addition to this rough estimate, it is possible to determine the maximum (and minimum) eigenvalue more precisely using Von Mises iteration [53] or the Lanczos iteration [54]. The time evolution of the state $|\psi(t)\rangle$ can be expressed by the rescaled Hamiltonian as follows

$$|\psi(t)\rangle = \mathrm{e}^{-\mathrm{i}\left(a\hat{H}_{\text{scal.}} + b\hat{1}\right)t} |\psi\rangle \tag{2.10.19}$$

$$= \mathrm{e}^{-\mathrm{i}b\hat{1}t} \mathrm{e}^{-\mathrm{i}\hat{H}_{\text{scal.}}at} |\psi\rangle . \tag{2.10.20}$$

Since the first part of the equation only provides a constant phase factor, which is not relevant for most dynamics[38], this part shall be disregarded. Using the Chebyshev polynomials one obtains

$$\mathrm{e}^{-\mathrm{i}\hat{H}_{\text{scal.}}at} |\psi\rangle = \mathcal{J}_0(at) |\psi\rangle + 2\sum_{n=1}^{\infty} (-\mathrm{i})^n \mathcal{J}_n(at) \mathcal{T}_n\left(\hat{H}_{\text{scal.}}\right) |\psi\rangle . \tag{2.10.21}$$

Here $\mathcal{J}_n$ are the Bessel functions of nth order and $\mathcal{T}_n$ are the Chebyshev polynomials, which can be constructed recursively:

$$\mathcal{T}_0\left(\hat{H}_{\text{scal.}}\right) = \hat{1} \tag{2.10.22}$$

$$\mathcal{T}_1\left(\hat{H}_{\text{scal.}}\right) = \hat{H}_{\text{scal.}} \tag{2.10.23}$$

$$\mathcal{T}_n\left(\hat{H}_{\text{scal.}}\right) = 2\hat{H}_{\text{scal.}} \cdot \mathcal{T}_{n-1}\left(\hat{H}_{\text{scal.}}\right) - \mathcal{T}_{n-2}\left(\hat{H}_{\text{scal.}}\right) \tag{2.10.24}$$

Since the main interest is only in $\mathcal{T}_n\left(\hat{H}_{\text{scal.}}\right) |\psi\rangle$ the focus is set on the recursive construction of those states

$$|\psi_0\rangle = |\psi\rangle \tag{2.10.25}$$

$$|\psi_1\rangle = \hat{H}_{\text{scal.}} |\psi\rangle \tag{2.10.26}$$

$$|\psi_n\rangle = 2\hat{H}_{\text{scal.}} |\psi_{n-1}\rangle - |\psi_{n-2}\rangle . \tag{2.10.27}$$

The Bessel functions $\mathcal{J}_n(at)$ are available in many packages as highly optimized functions, so that the computation of those values needs virtually no time. Thus, the recursive determination of $|\psi_n\rangle$ is

[37] Note that too large an estimate is not a problem in principle. It only slows down the procedure, while too small an estimate leads to incorrect results.

[38] For the calculation of the LDOS this phase factor is indeed important.

mainly causing the running time of the method. Of course, the infinite sum can never be computed in finite time. This is not necessary, because $\mathcal{J}_n(a\delta t) \sim (\frac{a\delta t}{n})^n$ holds for $n \gg at$ and thus higher orders are negligible. It can be clearly seen that an overestimation of a can be compensated by using higher orders or smaller time steps.
Similar to the Runge-Kutta-4 method, the runtime is mainly caused by matrix-vector multiplications. Thus, this method also has a running time of $\mathcal{O}(\mathcal{D}^2)$.

2.10.4 Determination of Lanczos coefficients by means of Pauli strings

As mentioned in Subsection 2.8, the determination of Lanczos coefficients by means of the Lanczos algorithm is highly unstable, so that even mathematically trivial properties such as orthogonality of the basis are no longer satisfied after only a few iterations. In practice, the stability of the method can be optimized, but this would increase the runtime [38]. This approach would thus result in a trade-off between precision and computational speed.
Here an alternative method is briefly explained, which is based on an exact description of the expressions, which was introduced in Ref. [39]. However, this method is severely limited in its application, as it is only useful for spin-1/2 systems.
For this, first a new basis $\{\tau_n\}$ is introduced, where each basis state has the form

$$\tau_n := \bigotimes_l \hat{\sigma}_l^u \tag{2.10.28}$$

with $u \in \{x, y, z, 0\}$[39]. From the commutator relation in Eq. (2.9.5), it follows that

$$\hat{\sigma}^u \hat{\sigma}^v = \delta_{uv}\hat{1} + \mathrm{i}\epsilon_{uvw}\hat{\sigma}^w \tag{2.10.29}$$

holds for Pauli matrices on the same site. By this expression, it is clear that this new basis is orthonormal in the sense of the scalar product from Eq. (2.8.4).
Another representation of this basis is given by

$$\tau_n = \mathrm{i}^{\delta_n}(-1)^{\epsilon_n} \bigotimes_l (\hat{\sigma}_l^z)^{v_l^n} (\hat{\sigma}_l^x)^{w_l^n} \tag{2.10.30}$$

where n denotes the basis state and l the site of the Pauli operator. $\delta_n, \epsilon_n, w_l^n, v_l^n \in \{0, 1\}$ are binary numbers. It should be noted that not all states that can be represented in this way are necessary to span the complete space. In this way, it is possible to describe each of these base states uniquely by two binary numbers δ_n, ϵ_n and two binary vectors $\vec{v}_n, \vec{w}_n$. In addition, this representation of the base states offers the advantage that the product of two such states can be simply represented as

$$\tau_n \cdot \tau_m = \tau_k \tag{2.10.31}$$

with

$$\delta_k = \delta_n + \delta_m \tag{2.10.32}$$
$$\epsilon_k = \epsilon_n + \epsilon_m + \delta_n\delta_m + \vec{w}_n \cdot \vec{v}_m \tag{2.10.33}$$
$$\vec{v}_k = \vec{v}_n + \vec{v}_m \tag{2.10.34}$$
$$\vec{w}_k = \vec{w}_n + \vec{w}_m, \tag{2.10.35}$$

[39] Thereby the identity on one site is also denoted by $\sigma_l^0 = \hat{1}_l$.

where all additions are performed over $\mathbb{Z}_2$. From this, we can see that the commutator can be nonzero if and only if $\vec{w}_n \cdot \vec{v}_m \neq \vec{w}_m \cdot \vec{v}_n$. The trivial case that observables acting on different sites commute is thus fulfilled. Moreover, it is shown that the commutator of two basis states consists of at most two basis states.
Mostly one examines local observables, which can be represented particularly simply by means of this representation. In this case only few basis states are needed, which in addition also have only few nonzero elements in the vectors $\vec{v}_n$ and $\vec{w}_n$.
Moreover, mostly Hamiltonians are considered, which consist of few-body operators, whereby those also have few entries not equal to 0. Unlike the single local operator, a Hamiltonian is usually a superposition of many shifted such operators. Thus, it can be seen that both the Hamiltonian and relevant observables can be easily transferred into this representation. By further application of Eq. (2.8.8), the Lanczos algorithm can be implemented with high precision. The choice of the representation in Eq. (2.10.30) has the advantage that the representation of the operators is much more precise compared to storing whole matrices and also requires less memory. Also the coefficients can be determined with high accuracy due to the orthogonality of the base states. Another advantage of this representation is that it deals directly with the infinite system. Nevertheless, even with this method, only a few dozen coefficients can be determined, since the required memory grows exponentially even for the very efficient representation by means of binary parameters.

3 Eigenstate Thermalization Hypothesis and its deviations from Random-Matrix Theory beyond the thermalization time

As explained in Subsection 2.5, one of the basic assumptions of ETH is that the elements of local observables in the energy eigenbasis are independent random numbers, or at least this is the case within energy windows. In the following section this is to be examined with the help of a new method at the example of 6 different systems. Here, a system is always considered to be a combination of an observable and Hamiltonian. The sizes of the investigated systems do not allow an exact diagonalization so that common indicators for the randomness are no longer applicable.
The section will be divided into three parts: First, in Subsection 3.1, a new method for the application of an energy filter will be explained. Without this filter the investigation within energy windows would not be possible. Even though it is a numerical method, it has been omitted from Subsection 2.10 because it is a result of this thesis and therefore should be mentioned separately from the already established methods.
In Subsection 3.2, a new indicator Λ is introduced to study the independent randomness of elements within a matrix.
Numerical results of that indicator for different systems are presented in Subsection 3.3.
Subsequently, in Subsection 3.4 a comparison with common indicators will be made. Furthermore, it will be examined whether ETH is fulfilled independently of the randomness of the elements.
The results of this section have been published in [P1].

3.1 Energy filter

Since the investigations are to be carried out in energy windows of systems, which lies outside the range of the ED, first a method must be introduced, which allows to regard an energy window isolated[40]. Such an introduction is the goal of this subsection.

[40] It is to be mentioned here that the dimension of the energy window can lie quite within the range of the ED, however for the determination of the window nevertheless a diagonalization of the full system would be necessary.

First, let $\hat{\mathcal{P}}_{\Delta E}^{E_c}$ be an energy filter which reduces a state to a ΔE wide energy window around E_c:

$$\hat{\mathcal{P}}_{\Delta E}^{E_c} = \sum_n \operatorname{rect}\left(\frac{E_c - E_n}{\Delta E}\right) |E_n\rangle \langle E_n| \, E_n \tag{3.1.1}$$

$$= \sum_n \int_{-\infty}^{\infty} \operatorname{rect}\left(\frac{E_c - \tau}{\Delta E}\right) \cdot \delta(E_n - \tau) d\tau \, |E_n\rangle \langle E_n| \, E_n \tag{3.1.2}$$

$$= \sum_n \frac{\Delta E}{2\pi} \int_{-\infty}^{\infty} \mathcal{F}\left\{\operatorname{sinc}\left(t\frac{\Delta E}{2\pi}\right)\right\} (E_c - \tau) \cdot \mathcal{F}\left\{\mathrm{e}^{\mathrm{i}E_n t}\right\} (\tau) \, d\tau \, |E_n\rangle \langle E_n| \, E_n \tag{3.1.3}$$

$$= \sum_n \frac{\Delta E}{\sqrt{2\pi}} \mathcal{F}\left\{\operatorname{sinc}\left(t\frac{\Delta E}{2\pi}\right) \mathrm{e}^{\mathrm{i}E_n t}\right\} (E_c) \, |E_n\rangle \langle E_n| \, E_n \tag{3.1.4}$$

$$= \sum_n \frac{\Delta E}{2\pi} \int_{-\infty}^{\infty} \operatorname{sinc}\left(t\frac{\Delta E}{2\pi}\right) \mathrm{e}^{\mathrm{i}E_n t} \mathrm{e}^{-\mathrm{i}E_c t} dt \, |E_n\rangle \langle E_n| \, E_n \tag{3.1.5}$$

$$= \frac{\Delta E}{2\pi} \int_{-\infty}^{\infty} \operatorname{sinc}\left(t\frac{\Delta E}{2\pi}\right) \mathrm{e}^{\mathrm{i}\hat{H} t} \mathrm{e}^{-\mathrm{i}E_c t} dt \tag{3.1.6}$$

$$= \frac{\Delta E}{2\pi} \int_{-\infty}^{\infty} \operatorname{sinc}\left(t\frac{\Delta E}{2\pi}\right) \mathrm{e}^{-\mathrm{i}\hat{H} t} \mathrm{e}^{\mathrm{i}E_c t} dt \tag{3.1.7}$$

with

$$\operatorname{sinc}(t) = \frac{\sin(\pi t)}{\pi t}. \tag{3.1.8}$$

Within this derivation the convolution theorem

$$\sqrt{2\pi}\mathcal{F}\{f \cdot g\}(\omega) = \int_{-\infty}^{\infty} \mathcal{F}\{f\}(\omega - \nu) \, \mathcal{F}\{g\}(\nu) \, d\nu \tag{3.1.9}$$

was used. It is easy to see that the expression (3.1.7) serves as an energy filter, as described above. Applying the right-hand side of Eq. (3.1.7) to an arbitrary state $|\psi\rangle$, one obtains

$$\frac{\Delta E}{2\pi} \int_{-\infty}^{\infty} \operatorname{sinc}\left(t\frac{\Delta E}{2\pi}\right) \mathrm{e}^{\mathrm{i}E_c t} \, |\psi(t)\rangle \, dt = \hat{\mathcal{P}}_{\Delta E}^{E_c} \, |\psi\rangle \, . \tag{3.1.10}$$

This way of representing the filter can already be implemented numerically. For this, the dynamics of the state in small steps δt is needed, so that for the integration approximately results in

$$\hat{\mathcal{P}}_{\Delta E}^{E_c} \, |\psi\rangle \approx \frac{\Delta E}{2\pi} \delta t \sum_{n=-\infty}^{\infty} \operatorname{sinc}\left(n\delta t\frac{\Delta E}{2\pi}\right) \mathrm{e}^{\mathrm{i}E_c n\delta t} \, |\psi(n\delta t)\rangle \, . \tag{3.1.11}$$

Of course, an infinite sum is outside the realm of the numerically possible. However, already numerically realizable values of n are sufficient. By adding further sums and smaller time steps the

sharpness of the filter can be increased arbitrarily. Time evolution can be performed using the usual methods (see Subsection 2.10).
The choice of the Chebyshev method (see Subsubsection 2.10.3) allows further optimization of the numeric. For this one inserts Eq. (2.10.21) into (3.1.10)

$$\frac{\Delta E}{2\pi}\int_{-\infty}^{\infty}\operatorname{sinc}\left(t\frac{\Delta E}{2\pi}\right)\mathrm{e}^{\mathrm{i}E_c t}\left|\psi(t)\right\rangle dt \tag{3.1.12}$$

$$=\frac{\Delta E}{2\pi}\int_{-\infty}^{\infty}\operatorname{sinc}\left(t\frac{\Delta E}{2\pi}\right)\mathrm{e}^{\mathrm{i}E_c t}\mathrm{e}^{-\mathrm{i}bt}\left[\mathcal{J}_0(at)\left|\psi\right\rangle+2\sum_{n=1}^{\infty}(-\mathrm{i})^n\mathcal{J}_n(at)\left|\psi_n\right\rangle\right]dt. \tag{3.1.13}$$

The n-th order Bessel function of the first kind $\mathcal{J}_n(t)$ can be Fourier transformed using the integral notation

$$\mathcal{J}_n(t)=\frac{1}{2\pi}\int_{-\pi}^{\pi}\mathrm{e}^{\mathrm{i}(n\tau-t\sin(\tau))}d\tau \tag{3.1.14}$$

such that

$$\mathcal{F}\left\{\mathcal{J}\right\}(\omega)=\frac{1}{\sqrt{2\pi}}\int_{-\infty}^{\infty}\left(\frac{1}{2\pi}\int_{-\pi}^{\pi}\mathrm{e}^{\mathrm{i}(n\tau-t\sin(\tau))}d\tau\right)\mathrm{e}^{-\mathrm{i}\omega t}dt \tag{3.1.15}$$

$$=(2\pi)^{-\frac{3}{2}}\int_{-\pi}^{\pi}\left(\int_{-\infty}^{\infty}\mathrm{e}^{-\mathrm{i}(\omega+\sin(\tau))t}dt\right)\mathrm{e}^{\mathrm{i}n\tau}d\tau \tag{3.1.16}$$

$$=\frac{1}{2\pi}\int_{-\pi}^{\pi}\delta\left(\omega+\sin(\tau)\right)\mathrm{e}^{\mathrm{i}n\tau}d\tau \tag{3.1.17}$$

$$=\frac{1}{2\pi}\left(\frac{\mathrm{e}^{\mathrm{i}n\tau_1}}{|\cos(\tau_1)|}+\frac{\mathrm{e}^{\mathrm{i}n\tau_2}}{|\cos(\tau_2)|}\right), \tag{3.1.18}$$

with

$$\tau_1=-\operatorname{asin}(\omega)\qquad\qquad\tau_2=\pi-\tau_1\,. \tag{3.1.19}$$

So that in all one receives

$$\mathcal{F}\left\{\mathcal{J}\right\}(\omega)=\frac{\mathrm{e}^{\mathrm{i}n\tau_1}+(-1)^n\mathrm{e}^{-\mathrm{i}n\tau_1}}{2\pi|\cos(\tau_1)|} \tag{3.1.20}$$

$$=\frac{\mathrm{e}^{-\mathrm{i}n\operatorname{asin}(\omega)}+(-1)^n\mathrm{e}^{\mathrm{i}n\operatorname{asin}(\omega)}}{2\pi\sqrt{1-\omega^2}}. \tag{3.1.21}$$

With this knowledge, consider now one part of Eq. (3.1.12) again, which will be called

$$C_n = (-\mathrm{i})^n \frac{\Delta E}{2\pi} \int_{-\infty}^{\infty} \operatorname{sinc}\left(t\frac{\Delta E}{2\pi}\right) \mathrm{e}^{\mathrm{i}E_c t}\mathrm{e}^{-\mathrm{i}bt} \mathcal{J}_n(at)dt \tag{3.1.22}$$

$$= \frac{(-\mathrm{i})^n \Delta E}{\sqrt{2\pi}} \mathcal{F}\left\{\operatorname{sinc}\left(t\frac{\Delta E}{2\pi}\right)\mathcal{J}_n(at)\right\}(b-E_c) \tag{3.1.23}$$

$$= \frac{(-\mathrm{i})^n}{a} \int_{-\infty}^{\infty} \operatorname{rect}\left(\frac{b-E_c-\omega}{\Delta E}\right) \mathcal{F}\{\mathcal{J}\}\left(\frac{\omega}{a}\right) d\omega \tag{3.1.24}$$

$$= (-\mathrm{i})^n \int_{\kappa_-}^{\kappa_+} \mathcal{F}\{\mathcal{J}\}(\tilde{\omega})\, d\tilde{\omega} \tag{3.1.25}$$

$$= (-\mathrm{i})^n \int_{\kappa_-}^{\kappa_+} \frac{\mathrm{e}^{-in\operatorname{asin}(\tilde{\omega})} + (-1)^n \mathrm{e}^{in\operatorname{asin}(\tilde{\omega})}}{2\pi\sqrt{1-\tilde{\omega}^2}} d\tilde{\omega} \tag{3.1.26}$$

$$= \begin{cases} \frac{\operatorname{asin}(\kappa_+)-\operatorname{asin}(\kappa_-)}{\pi} & \text{if } n=0 \\ \frac{(-\mathrm{i})^{n-1}}{2\pi n}\left[\left(\mathrm{e}^{-in\operatorname{asin}(\kappa_+)} - \mathrm{e}^{-in\operatorname{asin}(\kappa_-)}\right) + (-1)^n\left(\mathrm{e}^{in\operatorname{asin}(\kappa_-)} - \mathrm{e}^{in\operatorname{asin}(\kappa_+)}\right)\right] & \text{else} \end{cases} \tag{3.1.27}$$

$$= \begin{cases} \frac{\operatorname{asin}(\kappa_+)-\operatorname{asin}(\kappa_-)}{\pi} & n=0 \\ \frac{(-1)^{n-1}}{\pi n}\left[\cos\left(n\operatorname{asin}\left(\kappa_+\right) - \cos\left(n\operatorname{asin}\left(\kappa_-\right)\right)\right]\right. & n \text{ odd} \\ \frac{(-1)^{n/2}}{\pi n}\left[\sin\left(n\operatorname{asin}\left(\kappa_-\right) - \sin\left(n\operatorname{asin}\left(\kappa_+\right)\right)\right]\right. & n \text{ even} \end{cases} \tag{3.1.28}$$

with

$$\kappa_\pm = \frac{b - E_c \pm \frac{\Delta E}{2}}{a}. \tag{3.1.29}$$

This concludes in an easy expression for

$$\hat{\mathcal{P}}_{\Delta E}^{E_c} |\psi\rangle = C_0 |\psi\rangle + 2 \cdot \sum_{n=1}^{\infty} C_n |\psi_n\rangle \tag{3.1.30}$$

where again the sum is only carried along up to a certain order, so that the accuracy meets the requirements. In practice, the required length of the sum depends on the width of the filter ΔE; wider energy windows require fewer summands. As a result, smaller windows are numerically more costly.
Since this method is based on time evolution using Chebyshev polynomials, many tips from Subsection 2.10 are transferable. Thus, a and b can be estimated again from the composition of the Hamiltonian, or determined through iterative methods. Moreover, an too large estimate of a ensures that more sums are needed for the same accuracy. A too small estimation of a on the other hand provides a general failure of the energy filter. Therefore, as for the case of time evolution, an overestimation of a is preferable to an underestimation.

It should be pointed out that the Eq. (3.1.30) can be understood as a superposition of polynomials, which converge to the rectangle function. The chosen polynomials are the Chebychev polynomials, since they are well understood and a common tool in the topic of quantum dynamics. However, this choice is not unique and one could also try to construct the rectangle function with different kinds of polynomials. This could lead to different convergence behavior, for better or worse.
Finally, it should be pointed out what this method cannot do. It does not allow observation of the elements from the given observables in the energy window, nor does it provide a reduction of the (numerical) dimension of the system; even if the effective dimension can be strongly reduced, the same number of parameters is still needed to describe a state in the computational basis. Thus, this filtering method does not allow speeding up programs by reducing the effective dimension.

3.2 The Λ-indicator

Now that a method for isolating individual energy windows is available, this subsection is devoted to introducing a new indicator for analyzing MEC.
As a new indicator of independent randomness of matrix elements, let

$$\Lambda = \frac{\mathcal{M}_2^2}{\mathcal{M}_4} \tag{3.2.1}$$

be introduced with

$$\mathcal{M}_n := \frac{\mathrm{Tr}\left\{(\hat{\mathcal{P}}\hat{A})^n\right\}}{d} \tag{3.2.2}$$

and

$$d := \mathrm{Tr}\left\{\hat{\mathcal{P}}\right\}. \tag{3.2.3}$$

For the sake of clarity, the exact description of the energy filter (width and center) is omitted. Furthermore, $\mathrm{Tr}\left\{\hat{\mathcal{P}}\hat{A}\right\} = 0$ is assumed, this can always be achieved by a constant shift of the spectrum. In case the elements of $\hat{A}$ within the energy window are independent random numbers,

$$\Lambda_{\mathrm{GOE}} = \frac{1}{2} \tag{3.2.4}$$

should hold. In the case that those numbers are distributed in a Gaussian way, the consideration of the WSC is sufficient for this insight: $\mathcal{M}_n$ are the higher moments of the distribution of the eigenvalues, which in that case obey the WSC. For those moments then holds

$$\mathcal{M}_n = \int_{-R}^{R} x^n \frac{2\sqrt{R^2-x^2}}{\pi R^2} dx \tag{3.2.5}$$

$$= \begin{cases} 0 & \text{for odd } n \\ \frac{R^n}{2^{n-1}}\left[\frac{n!}{(\frac{n}{2}!)^2} - \frac{(n+2)!}{4((\frac{n}{2}+1)!)^2}\right] & \text{for even } n \end{cases}. \tag{3.2.6}$$

The first 4 moments (higher moments are not relevant for the indicator) are shown in Tab. 1. The advantage of this reasoning is that it works without any further assumptions. However, it is limited

n	0	1	2	3	4
$\mathcal{M}_n$	1	0	$\frac{R^2}{4}$	0	$\frac{R^4}{8}$

Table 1: First few moments of the WSC

to the case of independent Gaussian random numbers. A more general justification for independent random numbers will be given as well. For this purpose, the fourth moment $\mathcal{M}_4$ is considered first:

$$\mathcal{M}_4 = \frac{1}{d} \sum_{mnkl} A^{\mathcal{P}}_{mn} A^{\mathcal{P}}_{nk} A^{\mathcal{P}}_{kl} A^{\mathcal{P}}_{lm} \,. \tag{3.2.7}$$

Here $A^{\mathcal{P}}_{mn}$ are the elements of $\hat{\mathcal{P}}\hat{A}\hat{\mathcal{P}}$ in the eigenbasis of the Hamiltonian. If those elements are now independent random numbers with zero mean, only the quadratic terms provide a contribution for the fourth moment, ergo

$$\begin{aligned}
\mathcal{M}_4 &= \frac{1}{d} \sum_{mnl} |A^{\mathcal{P}}_{mn}|^2 |A^{\mathcal{P}}_{lm}|^2 + \frac{1}{d} \sum_{mnk} |A^{\mathcal{P}}_{mn}|^2 |A^{\mathcal{P}}_{kn}|^2 - \frac{1}{d} \sum_{mn} |A^{\mathcal{P}}_{mn}|^4 && (3.2.8)\\
&= \frac{2}{d} \sum_{mnl} |A^{\mathcal{P}}_{mn}|^2 |A^{\mathcal{P}}_{lm}|^2 - \frac{1}{d} \sum_{mn} |A^{\mathcal{P}}_{mn}|^4 && (3.2.9)\\
&= \frac{2}{d} \sum_{m} \left(\sum_{n} |A^{\mathcal{P}}_{mn}|^2 \right) \left(\sum_{l} |A^{\mathcal{P}}_{lm}|^2 \right) - \frac{1}{d} \sum_{mn} |A^{\mathcal{P}}_{mn}|^4 && (3.2.10)\\
&= \frac{2}{d} \sum_{m} \left(\sum_{n} |A^{\mathcal{P}}_{mn}|^2 \right)^2 - \frac{1}{d} \sum_{mn} |A^{\mathcal{P}}_{mn}|^4 && (3.2.11)\\
&= \frac{2}{d} \sum_{m} \mathcal{F}_m^2 - \frac{1}{d} \sum_{mn} |A^{\mathcal{P}}_{mn}|^4 && (3.2.12)
\end{aligned}$$

with

$$\begin{aligned}
\mathcal{F}_m &:= \sum_{n} |A^{\mathcal{P}}_{mn}|^2 && (3.2.13)\\
&= \langle E_m | \hat{\mathcal{P}}\hat{A}\hat{\mathcal{P}}\hat{A}\hat{\mathcal{P}} | E_m \rangle \,. && (3.2.14)
\end{aligned}$$

This can be expressed via the mean

$$\overline{\mathcal{F}} = \frac{1}{d} \sum_{m} \mathcal{F}_m \tag{3.2.15}$$

and the variance

$$\begin{aligned}
\hat{\sigma}^2_{\mathcal{F}} &= \frac{1}{d} \sum_{m} \left(\mathcal{F}_m - \overline{\mathcal{F}} \right)^2 && (3.2.16)\\
&= \left(\frac{1}{d} \sum_{m} \mathcal{F}_m^2 \right) - \overline{\mathcal{F}}^2 && (3.2.17)
\end{aligned}$$

of $\mathcal{F}_m$ as

$$\mathcal{M}_4 = 2\overline{\mathcal{F}}^2 + 2\hat{\sigma}_{\mathcal{F}}^2 - \frac{1}{d}\sum_{mn}|A_{mn}^{\mathcal{P}}|^4 \tag{3.2.18}$$

$$= 2\left(\frac{1}{d}\sum_{m}\mathcal{F}_m\right)^2 + 2\hat{\sigma}_{\mathcal{F}}^2 - \frac{1}{d}\sum_{mn}|A_{mn}^{\mathcal{P}}|^4 \tag{3.2.19}$$

$$= 2\left(\frac{1}{d}\sum_{m}\langle E_m|\hat{\mathcal{P}}\hat{A}\hat{\mathcal{P}}\hat{A}\hat{\mathcal{P}}|E_m\rangle\right)^2 + 2\hat{\sigma}_{\mathcal{F}}^2 - \frac{1}{d}\sum_{mn}|A_{mn}^{\mathcal{P}}|^4 \tag{3.2.20}$$

$$= 2\left(\frac{1}{d}\mathrm{Tr}\left\{\hat{\mathcal{P}}\hat{A}\hat{\mathcal{P}}\hat{A}\hat{\mathcal{P}}\right\}\right)^2 + 2\hat{\sigma}_{\mathcal{F}}^2 - \frac{1}{d}\sum_{mn}|A_{mn}^{\mathcal{P}}|^4 \tag{3.2.21}$$

$$= 2\mathcal{M}_2^2 + \underbrace{2\hat{\sigma}_{\mathcal{F}}^2 - \frac{1}{d}\sum_{mn}|A_{mn}^{\mathcal{P}}|^4}_{\Delta_\Lambda}. \tag{3.2.22}$$

Inserting this into the definition of Λ in Eq. (3.2.1) then yields the expression

$$\Lambda = \frac{\mathcal{M}_2^2}{2\mathcal{M}_2^2 + \Delta_\Lambda}. \tag{3.2.23}$$

Note that this relation does not require a Gaussian distribution of the elements. It was only used that only the elements are drawn independently and have a mean of 0. A comparison with the moments of the WSC (see Tab. 1) exhibits that for the case of a GOE $\Delta_\Lambda = 0$ holds.
In the remainder of this work, no exact compliance with the WSC is required, but only that Δ_Λ is assumed to be small. Thus, in linear approximation

$$\Lambda \approx \frac{1}{2} - \frac{\Delta_\Lambda}{4\mathcal{M}_2} \tag{3.2.24}$$

holds. That this linear approximation is reasonable can be shown by data from the ED range, which can be seen in Fig. 9.
Additionally, those contributions are small enough to be further neglected. Therefore, it follows that

$$\Lambda \approx \frac{1}{2} = \Lambda_{\mathrm{GOE}}, \tag{3.2.25}$$

even without the assumption that the spectrum satisfies the WSC.
Note that in the limit of large numbers Δ_Λ approaches 0, if the drawn numbers are gaussian. Thus, non-zeros Δ_Λ can be caused by two reasons. On the one hand, by using non-gaussian random numbers. This can even in the limit of large numbers cause deviation from 0.
On the other hand, even gaussian independent drawn numbers can exhibit $\Delta_\Lambda \neq 0$ as a finite size effect. Remark that the limit of large numbers was already used before considering $\Delta_\Lambda = 0$. Thus, even if Δ_Λ is (close to) 0, Λ itself could still suffer from finite size effects.
Using the DQT (see Subsection 2.3) and the energy filter $\mathcal{P}$ introduced in Subsection 3.1, it is possible to determine that indicator efficiently for different systems:

$$\mathcal{M}_n = \frac{\mathrm{Tr}\left\{(A^{\mathcal{P}})^n\right\}}{\mathrm{Tr}\left\{\mathcal{P}\right\}} \tag{3.2.26}$$

$$\approx \frac{\langle\psi|(A^{\mathcal{P}})^n|\psi\rangle}{\langle\psi|\mathcal{P}|\psi\rangle} \tag{3.2.27}$$

3.3 Numerical results

In this subsection numerical results of the Λ-indicator for different cases shall be investigated. In particular, the focus will be on the progression of Λ as a function of the width of energy windows, keeping the mean energy constant.
The main system of those investigations is a mixed-field Ising model (see Subsection 2.9), whose Hamiltonian is given by

$$\hat{H}_{\mathrm{Is}} = h_2\hat{\sigma}_2^z + h_5\hat{\sigma}_5^z + \sum_{l=1}^{L}\hat{h}_l \tag{3.3.1}$$

where

$$\hat{h}_l = \hat{\sigma}_l^z\hat{\sigma}_{l+1}^z + \frac{1}{2}\left(\hat{\sigma}_l^x + \hat{\sigma}_{l+1}^x\right) + \frac{1}{4}\left(\hat{\sigma}_l^z + \hat{\sigma}_{l+1}^z\right) \tag{3.3.2}$$

and

$$h_2 = 0.1665 \qquad\qquad h_5 = -0.2415 \tag{3.3.3}$$

hold. The magnetic fields in z-direction ensure that that system has no symmetry subspaces anymore, so that the investigations are carried out in the full Hilbert space ($\mathcal{D} = 2^L$).
In this system 3 different observables are to be considered, which are related to transport within the model in different ways. By means of

$$\hat{\mathcal{E}}_q = \frac{1}{\sqrt{L}}\sum_{l=1}^{L}\cos\left(\frac{2\pi}{L}ql\right)\hat{h}_l \tag{3.3.4}$$

two observables with $q = 1$ and $q = \frac{1}{L}$, respectively, are introduced. Since the total energy in the system is conserved, a local change can only occur by transport along the chain. Thus, the above observable for $q = 1$ ($q = 1/L$) corresponds to the slowest (fastest) mode of the energy[41].
Additionally, also

$$\hat{\mathcal{B}} = \frac{1}{\sqrt{L}}\sum_{l=1}^{L}\hat{\sigma}_l^x \tag{3.3.5}$$

should be considered. That observable hereby exhibits no transport behavior and decays rapidly (see Fig. 7).
Since focusing on an energy window blocks out high frequencies, this can be compared to a dephasing of those after a certain time. It should be noted that the case considered here is different from straight frequency cutting. The latter would lead to a banded matrix, while here block matrices are considered. Therefore, the investigations performed here are blind to correlations which are in the same banded matrix but not in the same energy window.
Motivated by the connection between energy window and temporal dephasing, it is now determined on which timescales the considered autocorrelation functions take place. These dynamics are shown in Fig. 7 for different system sizes. Methods of the iterative time evolution (see Subsection 2.10) as well as the DQT (see Subsection 2.3) were used for the determination. The relaxation time $\tau_{rel.}$ introduced in Eq. (2.5.7) is used to describe the timescale. It is shown that $\tau_{rel.}$ for $\hat{B}$ and the fastest

[41] The magnetic fields used to break the symmetry should be neglected for this purpose.

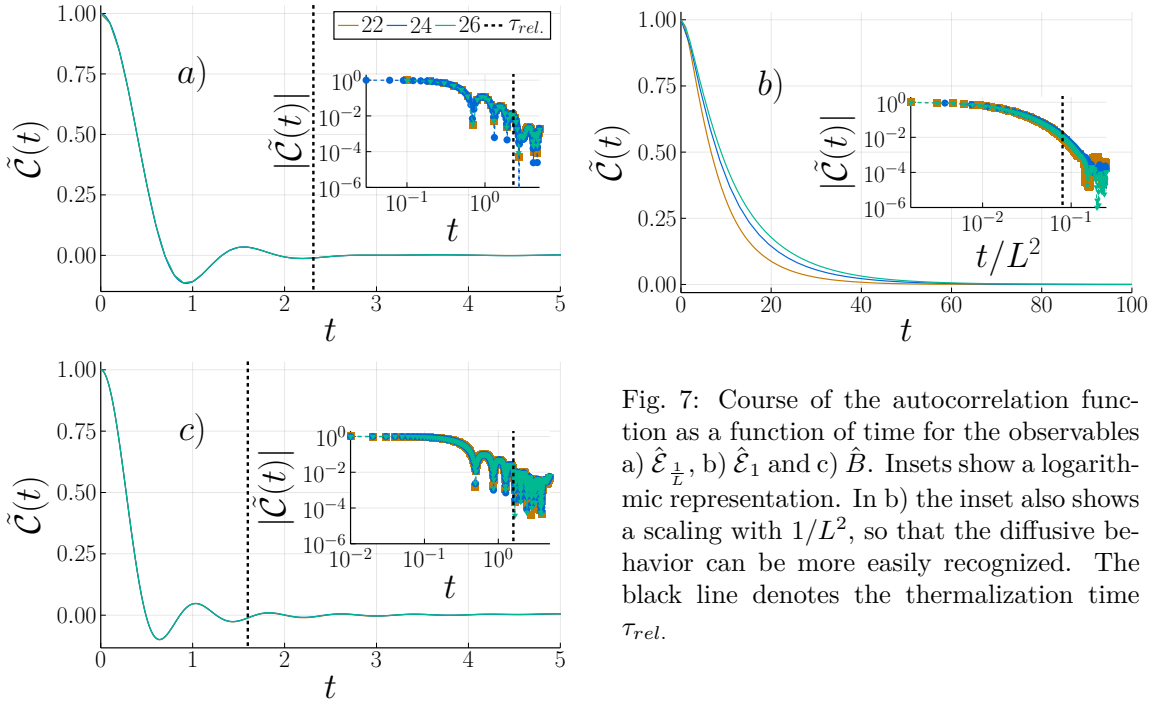

Fig. 7: Course of the autocorrelation function as a function of time for the observables a) $\hat{\mathcal{E}}_{\frac{1}{L}}$, b) $\hat{\mathcal{E}}_1$ and c) $\hat{B}$. Insets show a logarithmic representation. In b) the inset also shows a scaling with $1/L^2$, so that the diffusive behavior can be more easily recognized. The black line denotes the thermalization time $\tau_{rel.}$

mode are independent of the system size. For the slowest mode however, $\tau_{rel.} \propto L^2$ holds due to the diffusive nature of the system.
Furthermore, Fig. 8 shows coarse grained images for the observables within different energy windows. The coarse graining is understood to be the average over the absolute values of all elements within an energy block. By means of

$$\mathtt{A}_{jk} = \frac{1}{\mathtt{N}_{jk}} \sum_{nm} |A_{nm}| \mathrm{rect}\left(\frac{E_j - E_n}{\delta E}\right) \mathrm{rect}\left(\frac{E_k - E_m}{\delta E}\right) \tag{3.3.6}$$

with

$$\mathtt{N}_{jk} = \sum_{nm} \mathrm{rect}\left(\frac{E_j - E_n}{\delta E}\right) \mathrm{rect}\left(\frac{E_k - E_m}{\delta E}\right) \tag{3.3.7}$$

such a coarse grained matrix can be created. Here δE is to be chosen in such a way that there are enough elements within a section so that a statistical averaging is reasonable, but not so large that the structure can no longer be recognized. In the sense of ETH, this is to be understood as a visualization of $|f(\omega, \bar{E})|$. The energy windows were chosen in such a way that one describes a time before the thermalization and one afterward. In Fig. 8 it can be seen that a structure for a previous time can still be recognized, but after the thermalization it is no longer visible[42].

[42]Except for the diagonal of $\hat{B}$, which is also in agreement with ETH.

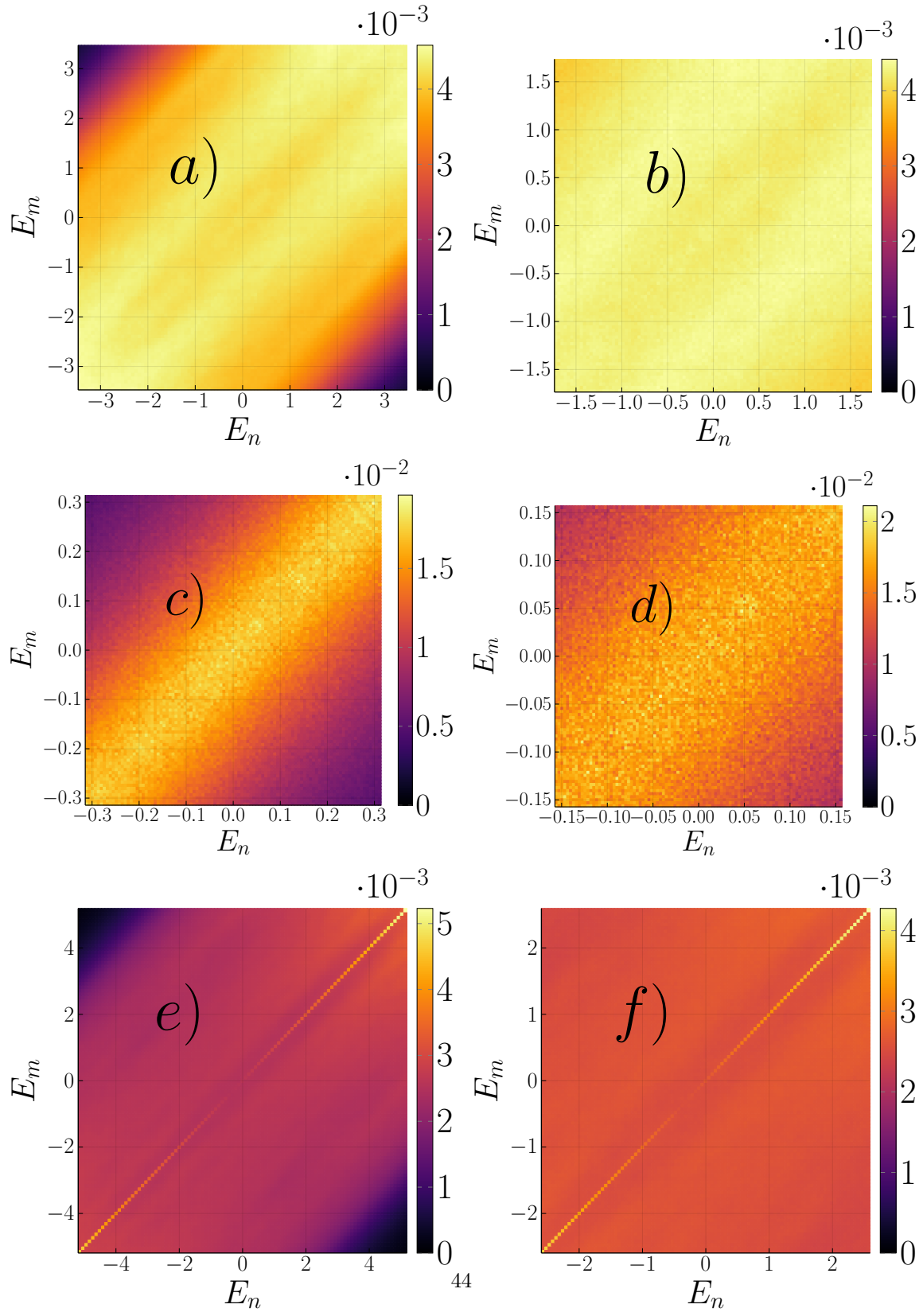

Fig. 8: Coarse-grained matrix of observables for different energy windows centered around $E_c = 0$: a) $\hat{\mathcal{E}}_{\frac{1}{L}}$; $\Delta E = \frac{2\pi}{\tau}$ b) $\hat{\mathcal{E}}_{\frac{1}{L}}$; $\Delta E = \frac{\pi}{\tau}$ c) $\hat{\mathcal{E}}_1$; $\Delta E = \frac{2\pi}{\tau}$ d) $\hat{\mathcal{E}}_1$; $\Delta E = \frac{\pi}{\tau}$ e) $\hat{B}$; $\Delta E = \frac{2\pi}{\tau}$ f) $\hat{B}$; $\Delta E = \frac{\pi}{\tau}$.

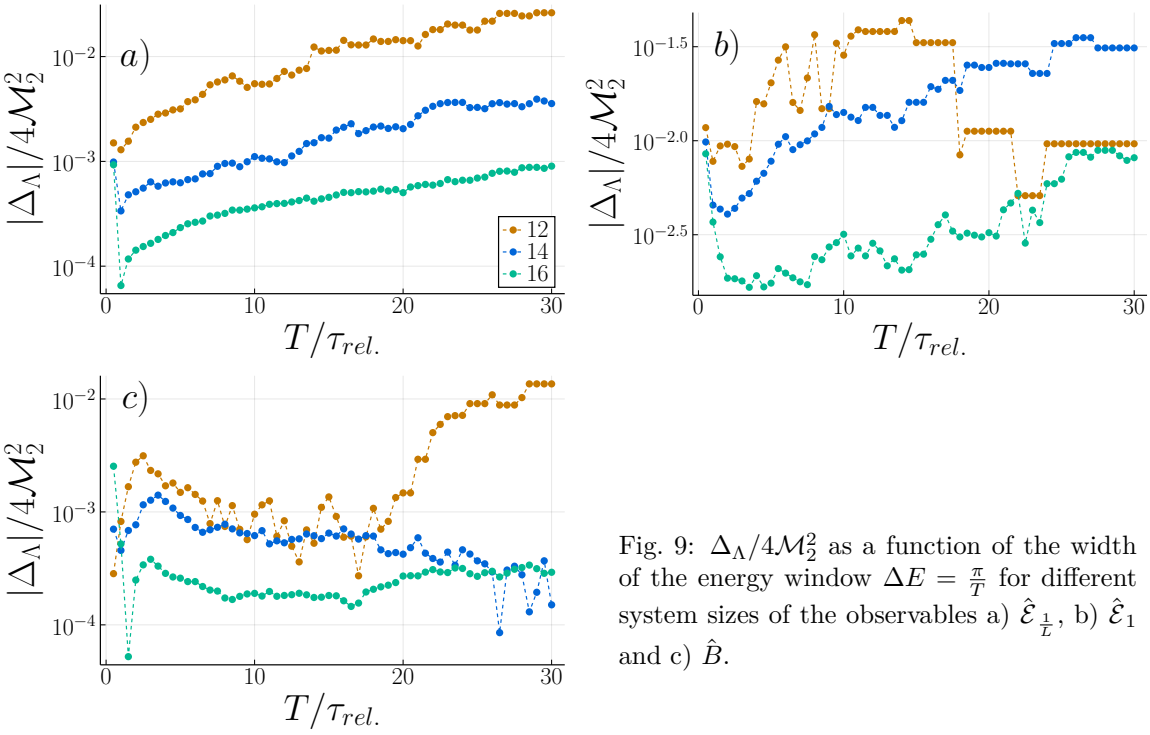

Fig. 9: $\Delta_\Lambda/4\mathcal{M}_2^2$ as a function of the width of the energy window $\Delta E = \frac{\pi}{T}$ for different system sizes of the observables a) $\hat{\mathcal{E}}_{\frac{1}{L}}$, b) $\hat{\mathcal{E}}_1$ and c) $\hat{B}$.

Before the results of the Λ-indicator are shown, first the approximation from the previous subsection (see Eq. (3.2.22)) for those observables shall be analyzed. Since an investigation of that approximation is only possible using ED, smaller systems must be considered here. The results for this can be seen in Fig. 9, where $E_c = 0$ was chosen[43]. One recognizes first that all results are very small in comparison to $\Lambda_{\text{GOE}} = 0.5$, and thus at least for those cases the approximation is reasonable. It can be seen that the negligible expression becomes smaller as the system size L increases. Assuming that this trend also continues in the sizes outside the range of the ED, it can be expected that the above approximation is reasonable. Another trend in the data can be seen in the case of observables with transport properties. It is seen that the negligible expression becomes larger for smaller energy windows. The increasing deviation for very large windows ($T < \tau_{rel.}$) is not problematic, since the main focus is on the regime of larger times and the deviation is still rather small. In contrast, the tendency for smaller windows is rather disadvantageous for the investigation, however, it also emerges that for larger systems the first trend dominates, so that for the systems discussed in the following, also smaller energy windows should not be problematic. Furthermore, especially in the case of the slowest mode, it can be seen that the data form plateaus. This can be explained by the small number of matrix elements within the energy window. Since the relaxation time of the slowest mode is much larger than that of the other observables, the corresponding energy window is much smaller. Accordingly, the number of matrix elements is not sufficient for statistical analysis. Since this behavior occurs already at $L = 14$ in the case of the slowest mode, an investigation of smaller systems is omitted.
Now that the approximation is justified, Λ is shown in Fig. 10 for the different observables as a function of the width of the energy windows. It can be seen that Λ for small energy windows ap-

[43] This corresponds to infinite temperature.

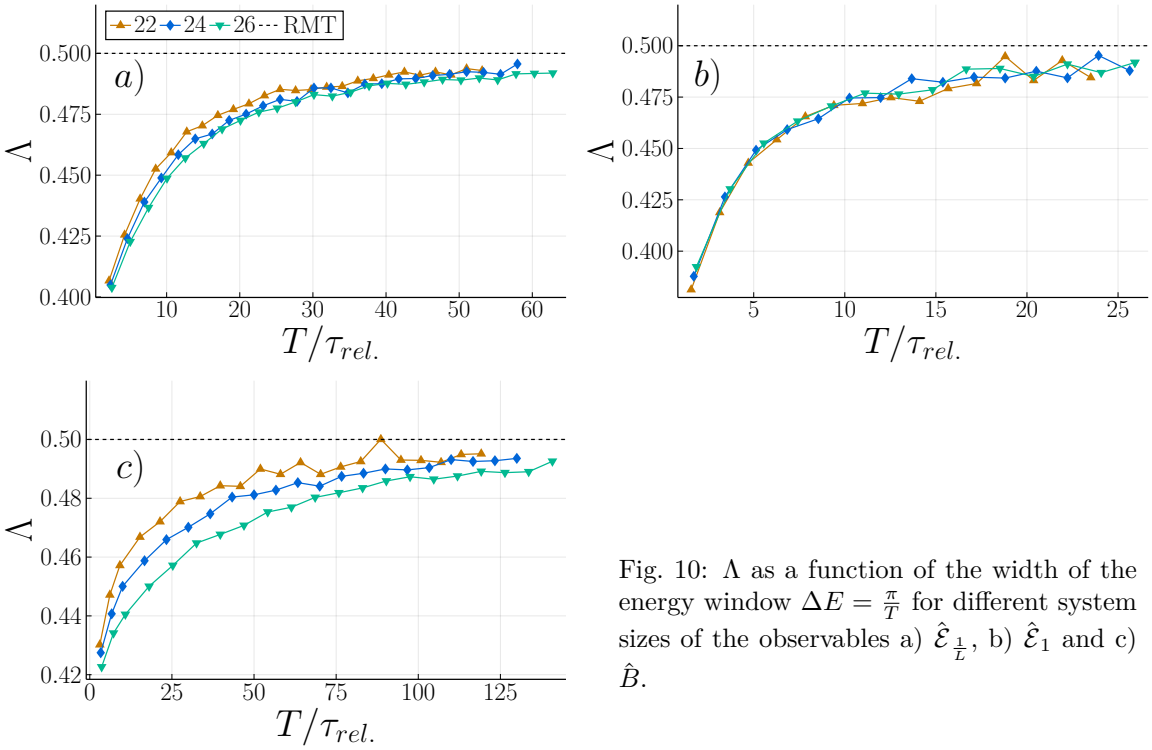

Fig. 10: Λ as a function of the width of the energy window $\Delta E = \frac{\pi}{T}$ for different system sizes of the observables a) $\hat{\mathcal{E}}_{\frac{1}{L}}$, b) $\hat{\mathcal{E}}_1$ and c) $\hat{B}$.

proaches the expected value for GOE $\Lambda_{GOE} = 0.5$, but does not reach this value (permanently). In particular, Λ still exhibits a large distance to Λ_{GOE} for energy windows corresponding to the relaxation time. This has two implications, since in those energy windows $f(\omega, \bar{E}) \approx$ const. holds (see Fig. 8), those deviations here cannot be explained by a rough structure, but only by MEC. Furthermore, these findings are in contradiction with the assumption that for energy windows smaller than the Thouless energy ΔE_{Th} the matrix consists of independent, identically distributed random elements (see Subsection 2.5). At that point, it is worth briefly pointing out possible problems of the implementation of the Λ-indicator in the range of small energy windows. First, the runtime of the simulations, the smaller the desired energy window, the more summands are needed for the implementation of the energy filter (see Subsection 3.1). Furthermore, the effective dimension d_{eff} of the considered observables becomes smaller due to the restriction of the energy. As mentioned in Subsection 2.3, the variance of the expectation values determined by DQT is proportional to that dimension. This means that the precession of the results decreases with smaller energy windows[44]. These two points are not directly problems of the Λ-indicator itself, but only concern the method chosen here to determine that quantity. Another possible problem concerns again the effective dimension. If the effective dimension becomes too small, it could happen that there are not enough elements left in the matrix to make a statistical statement. However, this is a problem that affects every investigation that makes statistical statements about the elements within an energy window. In addition to the investigations of the above-mentioned model, the Λ-indicator was also investigated in systems which have other conservation values in addition to the energy, so that other observables with transport properties can also be investigated. For this purpose, a Heisenberg model is used,

[44]To counteract this, averaging over more random states would be an option.

whose Hamiltonian can be described by means of

$$\hat{H}_{\mathrm{XXZ}} = \sum_{l=1}^{N} \frac{1}{4}\hat{\sigma}_l^x\hat{\sigma}_{l+1}^x + \frac{1}{4}\hat{\sigma}_l^y\hat{\sigma}_{l+1}^y + \Delta_1\hat{\sigma}_l^z\hat{\sigma}_{l+1}^z \tag{3.3.8}$$

$$+ \sum_{l=1}^{N} \Delta_2\hat{\sigma}_l^z\hat{\sigma}_{l+2}^z + h_1\hat{\sigma}_1^z + h_{\lfloor L/3\rfloor+1}\hat{\sigma}_{\lfloor L/3\rfloor+1}^x \tag{3.3.9}$$

where parameters $\Delta_1 = \frac{3}{8}$, $\Delta_2 = \frac{1}{8}$, $h_1 = 0.05$ and $h_{\lfloor L/3\rfloor+1} = 0.0375$ are chosen and periodic boundary conditions apply. In this system, the total magnetization in z direction is thereby preserved. Here the consideration is done in the magnetization space with $\sum \sigma_l^z = 0$. A reduction to the smallest subspace is necessary, because otherwise the structure of further subspaces can influence the Λ-indicator. All further symmetries (translation and mirror symmetry) were again broken by relatively small magnetic fields.
As observables again the limiting modes of transport within the system are chosen, now however around transport of the magnetization in z-direction, so that

$$\hat{S}_q = \sum_{l=1}^{L} \cos\left(\frac{2\pi}{L}ql\right)\hat{\sigma}_l^z, \tag{3.3.10}$$

with $q = 1$ ($q = L/2$) denotes the slowest (fastest) mode. The Hamiltonian of another system considered here can be described by

$$\hat{H}_3 = \sum_{l=1}^{L-1} \frac{1}{4}\hat{\sigma}_l^x\hat{\sigma}_{l+1}^x + \frac{1}{4}\hat{\sigma}_l^y\hat{\sigma}_{l+1}^y + \Delta_1\hat{\sigma}_l^z\hat{\sigma}_{l+1}^z \tag{3.3.11}$$

$$+ \sum_{l=1}^{L-2} \Delta_2\hat{\sigma}_l^z\hat{\sigma}_{l+2}^z + h_1\hat{\sigma}_1^z. \tag{3.3.12}$$

The parameters $\Delta_1 = \frac{3}{8}$, $\Delta_2 = \frac{3}{10}$ and $h_1 = 0.05$ were chosen. In contrast to the previous system, open boundary conditions are present here. The chosen observable of interest is $\hat{\sigma}_{\frac{L}{2}}^z$. Also the investigation will be done within the magnetization subspace with $\sum \sigma_l^z = 0$. This system has already been investigated in detail in Ref. [24], whereas the new methods here now allow investigations for larger systems[45].
A plot of the dynamics can be seen in Fig. 11. It shows that for $\hat{H}_{XXZ}$ there is a diffusive transport, so that the relaxation time of the slowest mode is $\tau_{rel.} \propto L^2$. The relaxation time of the fastest mode, on the other hand, is again independent of the system size. Moreover, it turns out that the local operator under $\hat{H}_3$ exhibits a relaxation time which does not support a simple scaling. Therefore, in this context, no consistent scaling based on that timescale is to be used.
Fig. 12 shows the results for Λ as a function of the width of the considered energy window. The mean energy of these windows are chosen as $E_c = -0.3\frac{L}{16}$ in the case of $\hat{H}_{XXZ}$ and $E_c = -0.1 \cdot L$ for $\hat{H}_3$. The value of the latter one was taken from Ref. [24]. It is recognizable that the observables of the slowest (fastest) mode show a similar behavior as the previously considered observables. Thus, it is shown that even for small energy windows the value $\Lambda_{\mathrm{GOE}} = 0.5$ is not reached and the distance is still large, in particular, if one considers energy windows corresponding to the relaxation time.

[45] It should be noted that within that work no consideration was made in the energy window but within a limited frequency range.

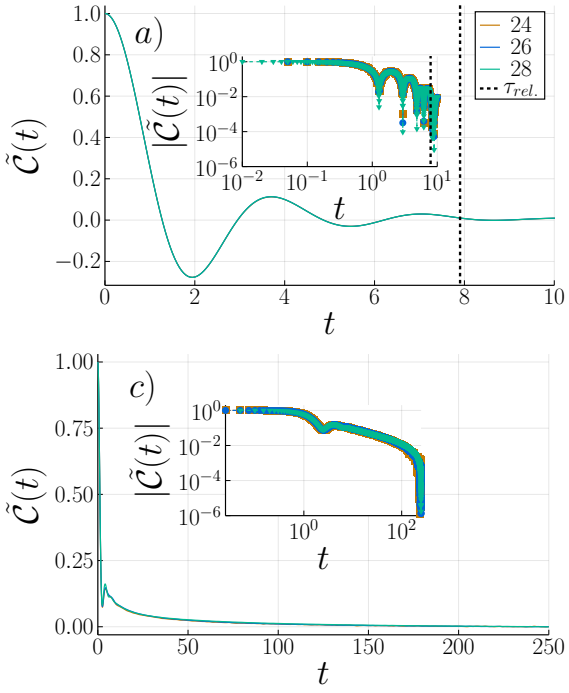

Fig. 11: The autocorrelation function $\tilde{\mathcal{C}}(t)$ against the time t for different system sizes and the observables a) $\hat{S}_{\frac{1}{L}}$, b) $\hat{S}_1$ and c) $\hat{\sigma}_{L/2}$. The insets show a logarithmic scale, whereby the slowest mode is also scaled by L^2 to show the diffuse behavior.

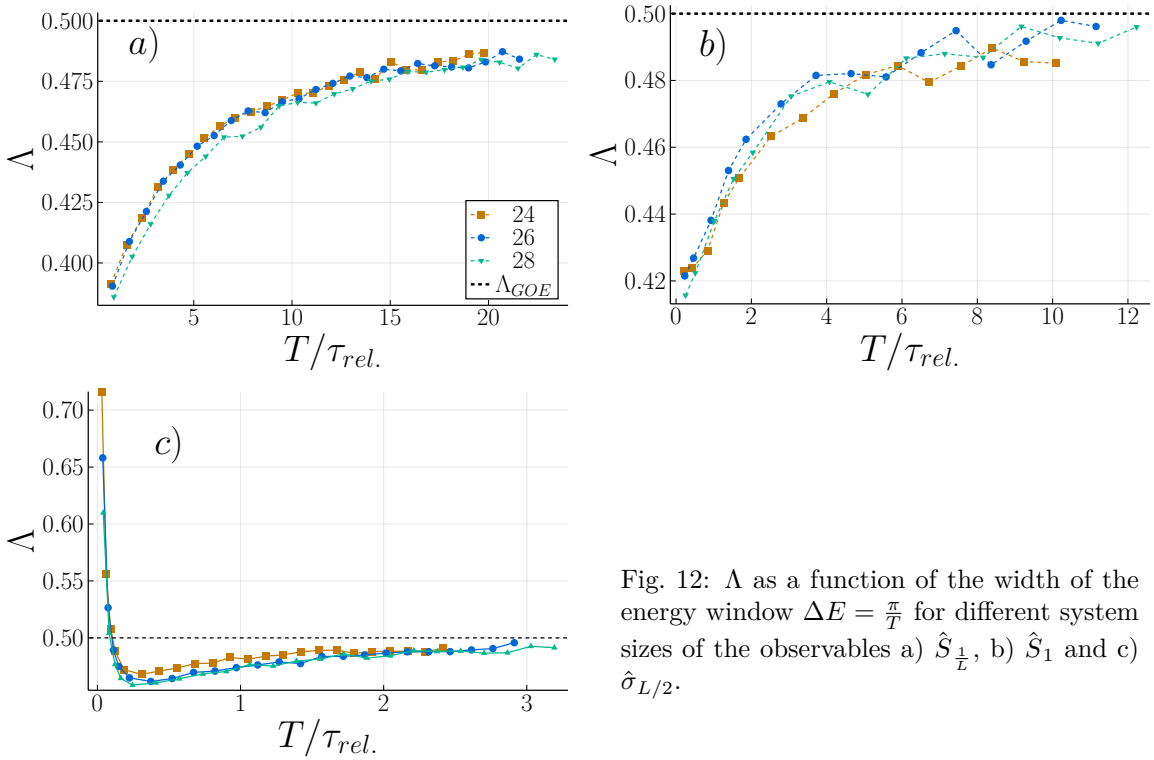

Fig. 12: Λ as a function of the width of the energy window $\Delta E = \frac{\pi}{T}$ for different system sizes of the observables a) $\hat{S}_{\frac{1}{L}}$, b) $\hat{S}_1$ and c) $\hat{\sigma}_{L/2}$.

A clearly different behavior can be observed for the local operator: Here Λ first approaches Λ_{GOE} from above[46], then drops below that value, and then approaches the value again, this time from below. The first phase of this behavior is thus consistent with the results of Ref. [24], where various indicators showed a sharp transition between random matrix and correlated matrix elements. However, the Λ-indicator shows that even after a first strong approach to Λ_{GOE} there is a further deviation as well as a renewed slow approach. Thus, also those investigations show that an energy window, which corresponds to the Thouless time, nevertheless still contains MEC. These findings confirm the analytical considerations from Ref. [55]. There it was shown that a lower bound for the RMT time τ_{RMT} exists which scales with L^3. Since the Thouless time τ_{Th} only grows with L^2, there must still be MEC for sufficiently large systems within the corresponding energy window.

3.4 Comparison with other indicators

Within this subsection, other common indicators of ETH will be considered using the example of Ising systems. Since the usual investigation methods work on the carrier of ED, smaller system sizes are considered here $N = 14, 16$. In addition to the randomness of the matrix elements, the smoothness of the functions from Eq. (2.5.1) is a significant condition of ETH. As a first indication of this property can be seen in Fig. 8. Thus, at least a coarse structure of the observables does not reveal any discontinuities. However, the coarse resolution could prevent the visibility of deviations from single elements[47]. To exclude this case, in Fig. 13 the diagonal elements are shown in dependence of the energy. It can be seen that the diagonal elements represent a dense point cloud, which becomes narrower with increasing system size. Thus, for the thermodynamic limit case $L \to \infty$, a smooth function of the diagonal elements is expected.
Since the matrices considered here are real (and symmetric), the ratio of the variance of the diagonal elements should be twice that of the offdiagonal elements [57] (see Eq. 2.6.2). For an investigation of that property

$$\Sigma(\nu, \mu) = \frac{\sigma_{\mathrm{d}}^2(\nu, \mu)}{\sigma_{od}^2(\nu, \mu)} \tag{3.4.1}$$

is considered. Here $\sigma_{\mathrm{d}}^2(\nu, \mu)$ denotes the variance of the diagonal elements within an energy window of the n-th energy eigenstates with $n \in [\mu \pm \nu/2]$, $\sigma_{\mathrm{od}}^2(\nu, \mu)$ corresponds to the variance of the offdiagonal elements in that window. The results of Ising systems accordingly can be seen in Fig. 14. Two different sizes with $\nu = 100, 1000$ were chosen. It can be seen that for the transport bound observables the expected ratio is obtained for both quantities. In the case of $\hat{B}$, however, one recognizes that the ratio deviates strongly from the expectation in the case of larger windows. This can be explained by means of diagonal element variation (see Fig. 13): in the case of larger windows, the change in those elements is dominated by the change in energy compared to static noise. This conjecture is confirmed by the fact that the deviation of Σ becomes smaller for larger systems: Since the energy states are denser for larger systems, the same number of states covers a smaller energy range. Thus, the change of $f(\omega, \bar{E})$ in this range also decreases.

[46] For the case without energy filter, $\Lambda(T = 0) = 1$.
[47] In case these deviations decay exponentially with system size, this is also called weak ETH [56].

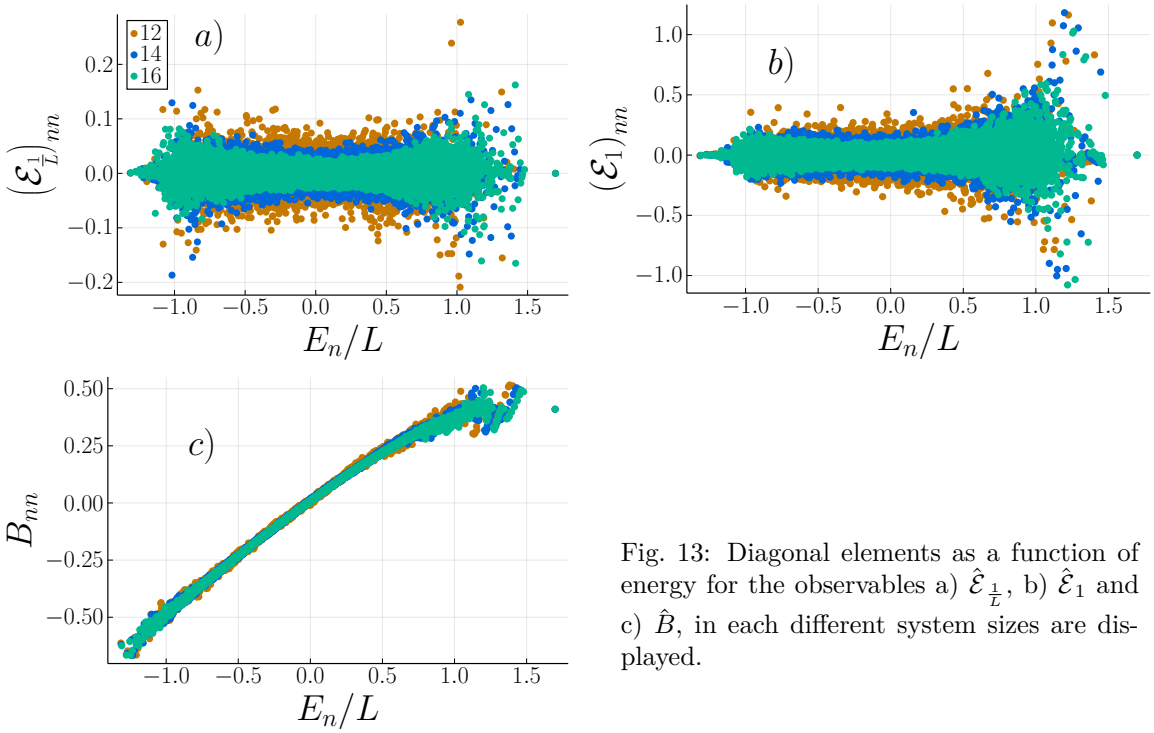

Fig. 13: Diagonal elements as a function of energy for the observables a) $\hat{\mathcal{E}}_{\frac{1}{L}}$, b) $\hat{\mathcal{E}}_1$ and c) $\hat{B}$, in each different system sizes are displayed.

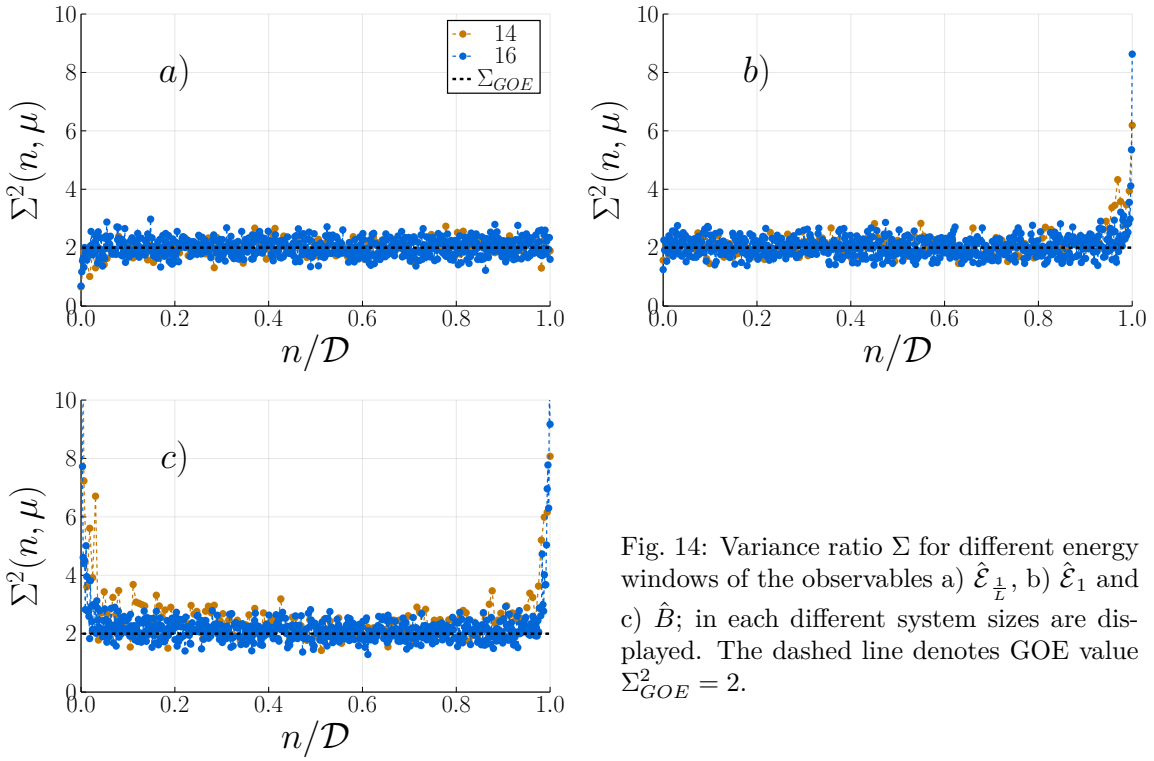

Fig. 14: Variance ratio Σ for different energy windows of the observables a) $\hat{\mathcal{E}}_{\frac{1}{L}}$, b) $\hat{\mathcal{E}}_1$ and c) $\hat{B}$; in each different system sizes are displayed. The dashed line denotes GOE value $\Sigma^2_{GOE} = 2$.

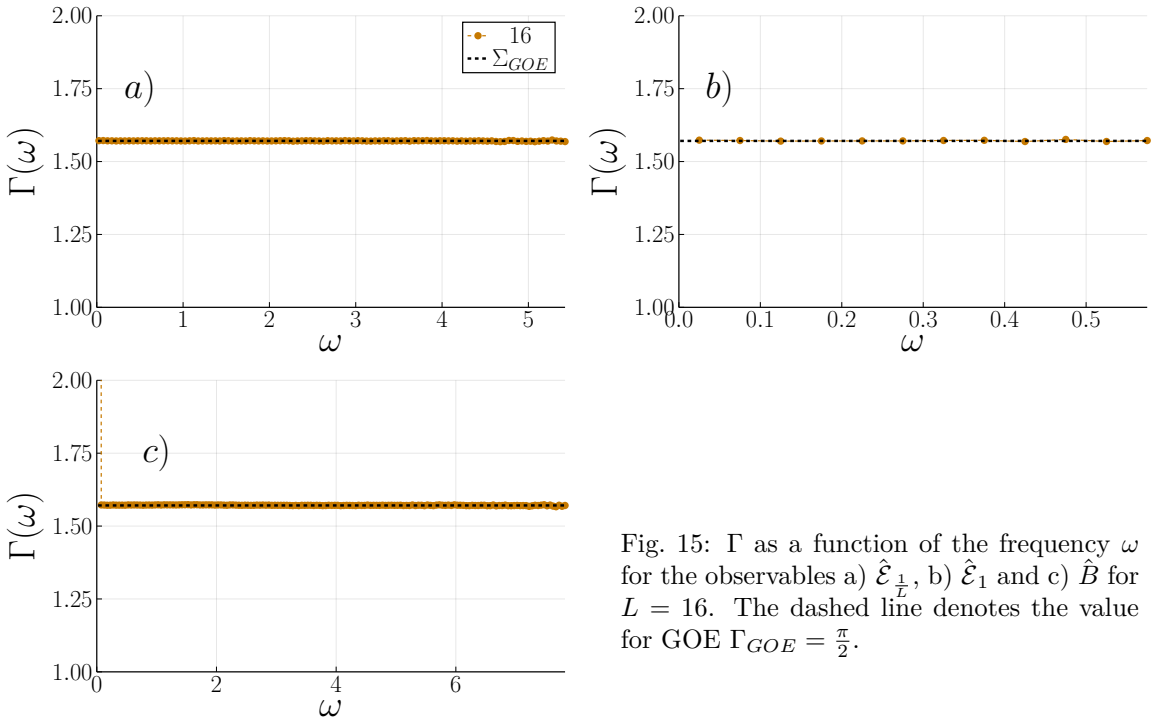

Fig. 15: Γ as a function of the frequency ω for the observables a) $\hat{\mathcal{E}}_{\frac{1}{L}}$, b) $\hat{\mathcal{E}}_1$ and c) $\hat{B}$ for $L = 16$. The dashed line denotes the value for GOE $\Gamma_{GOE} = \frac{\pi}{2}$.

The Gaussian nature of the elements will be studied by means of two indicators already introduced in Subsection 2.6. First, consider the quantity $\Gamma(\omega)$ (see Eq. (2.6.8)). Let $\Delta\omega = 0.05$ be chosen as frequency width. The investigation was performed in the energy window corresponding to half the relaxation time. The results are shown in Fig. 15. It can be seen that even in this window, before relaxation, the indicator corresponds to the expectations of the RMT. The only exception here is $\hat{B}$ at $\omega = 0$. This can be explained since the diagonal elements, which have to be considered for $\omega = 0$, are not fully random numbers, but shifted by $\mathcal{A}(\bar{E})$ (see Eq. (2.5.1)). In addition, it should be noted that the number of measurement points for the slowest mode is much smaller than for the other cases. This is due to the fact that $\tau_{rel.}$ is much larger there and thus the corresponding window is much narrower.

Furthermore, in Fig. 16 the distribution of the rescaled transition strength is shown, which is also an indicator sensitive to the Gaussian nature of the random numbers, but blind to MEC. The investigation was carried out in energy windows corresponding to the relaxation time. A large agreement can be shown for systems of different magnitudes.

It should be pointed out again that even if all previous results are in agreement with the GOE expectations (with potential deviations at the diagonal), the results are not conclusive for possible correlations. For this purpose, the indicator $\bar{r}$ (see Eq. (2.6.5)) will now be considered, since this indicator does not only rely on the gaussian nature of the elements but also on the independence of these (see Subsection 2.6). The values displayed in Fig. 17 show that that indicator already agrees well with the expectations for GOE under one relaxation for all observables. The larger deviations in the results for the slowest mode of energy transport are due to the very narrow energy windows, which result in large statistical deviations. In comparison with the results of the Λ-indicator, the large sensitivity of that new indicator becomes apparent; while $\bar{r}$ already corresponds to the value

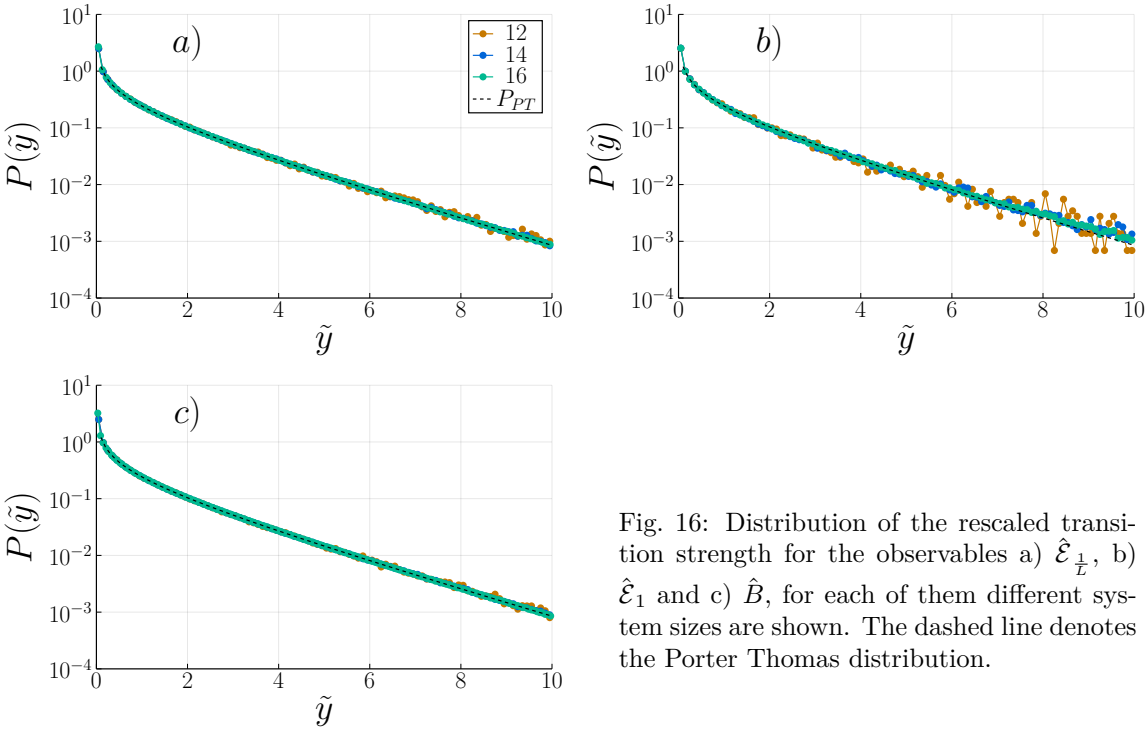

Fig. 16: Distribution of the rescaled transition strength for the observables a) $\hat{\mathcal{E}}_{\frac{1}{L}}$, b) $\hat{\mathcal{E}}_1$ and c) $\hat{B}$, for each of them different system sizes are shown. The dashed line denotes the Porter Thomas distribution.

of GOE (in the range of statistical fluctuations) at $\frac{\tau_{rel.}}{2}$, Λ shows a significant deviation from Λ_{GOE}. Even though the cases are not fully comparable, remember that in Subsection 2.6 $\bar{r}$ also exhibits some uncertainties.

Another common method for investigating randomness is to compare the spectra of the original observables and a sign-randomized version[48] of those (see Eq. (2.6.12) and therefore). In Fig. 18 $\hat{B}$ can be seen. Here, 3 different energy windows were investigated, corresponding to time points before, during, and after the relaxation time. It can be seen here that even at the time of relaxation the spectra still show strong differences, whereas after $t = 25\tau_{rel.}$ the spectra coincide. This behavior can also be seen for $\hat{\mathcal{E}}_{L/2}$ in Fig. 19. This reinforces the results of the Λ indicator, which also still shows deviations from Λ_{GOE} for the relaxation time point. In Fig. 20, the spectra of $\hat{\mathcal{E}}_1$ are compared. A comparison long after the relaxation time is omitted, since the number of matrix elements is already too small for the consideration of the distribution to be useful.

Furthermore, in connection with Out-Of-Time-Correlations (OTOC) [58, 59, 60] another consequence of the randomness of the matrix elements will be shown. In this context, OTOC[49] is defined as the dynamics of

$$F_T(t) = \mathrm{Tr}\left\{\hat{A}(t)\hat{A}\hat{A}(t)\hat{A}\right\} \tag{3.4.2}$$

$$= \sum_{mnkl} A_{mn}A_{nk}A_{kl}A_{lm}e^{-\mathrm{i}(E_n-E_m+E_l-E_k)t}. \tag{3.4.3}$$

[48] A trace-free variant is always considered, since otherwise the sign-randomization causes trivial changes.

[49] Note that OTOC is not always clearly defined within the literature. Thus, $\mathrm{Tr}\left\{[A(t),A]^2\right\}$ is sometimes also called OTOC.

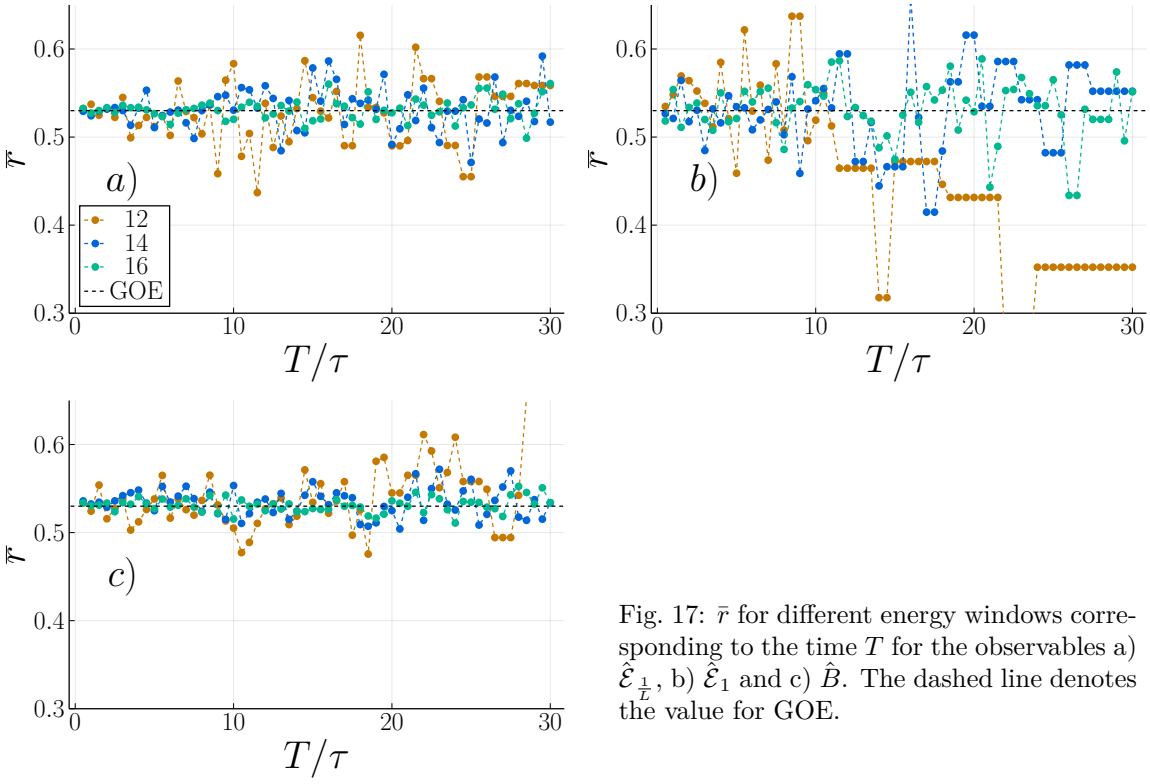

Fig. 17: $\bar{r}$ for different energy windows corresponding to the time T for the observables a) $\hat{\mathcal{E}}_{\frac{1}{L}}$, b) $\hat{\mathcal{E}}_1$ and c) $\hat{B}$. The dashed line denotes the value for GOE.

In the following, $\hat{A}$ shall always correspond to the observables in the energy window associated to T. As before in the derivation of the Λ-indicator, let now consider the case where the elements are independent random numbers. Therefore, only the quadratic terms contribute to the sum, hence the following applies:

$$F_T(t) \approx \sum_m \left(\sum_n |A_{nm}| e^{-\mathrm{i}(E_n - E_m)t} \sum_l |A_{ln}| e^{-\mathrm{i}(E_l - E_m)t} \right) \tag{3.4.4}$$

$$+ \sum_n \left(\sum_m |A_{nm}| e^{-\mathrm{i}(E_n - E_m)t} \sum_k |A_{nk}| e^{-\mathrm{i}(E_n - E_k)t} \right) \tag{3.4.5}$$

$$= \sum_m \left(\sum_n |A_{nm}|^2 e^{-\mathrm{i}(E_n - E_m)t} \right)^2 + c.c. \tag{3.4.6}$$

$$= 2 \sum_m \mathcal{R} \left[\langle m|\hat{A}(t)\hat{A}|m\rangle^2 \right] := Q_T(t). \tag{3.4.7}$$

This expression is only accessible via ED, so the inspection of that equivalence is also limited to small systems. In Fig. 21, OTOC and $Q_T(t)$ are shown for different energy windows. It can be seen that that equivalence is given for very small energy windows, while in larger windows there still exist MEC which breaks the equivalence. In Ref. [61], that difference between OTOC and Q_T is more significant as part of an extended ETH (generalized ETH) [62], in which multi-point correlations are taken into account.

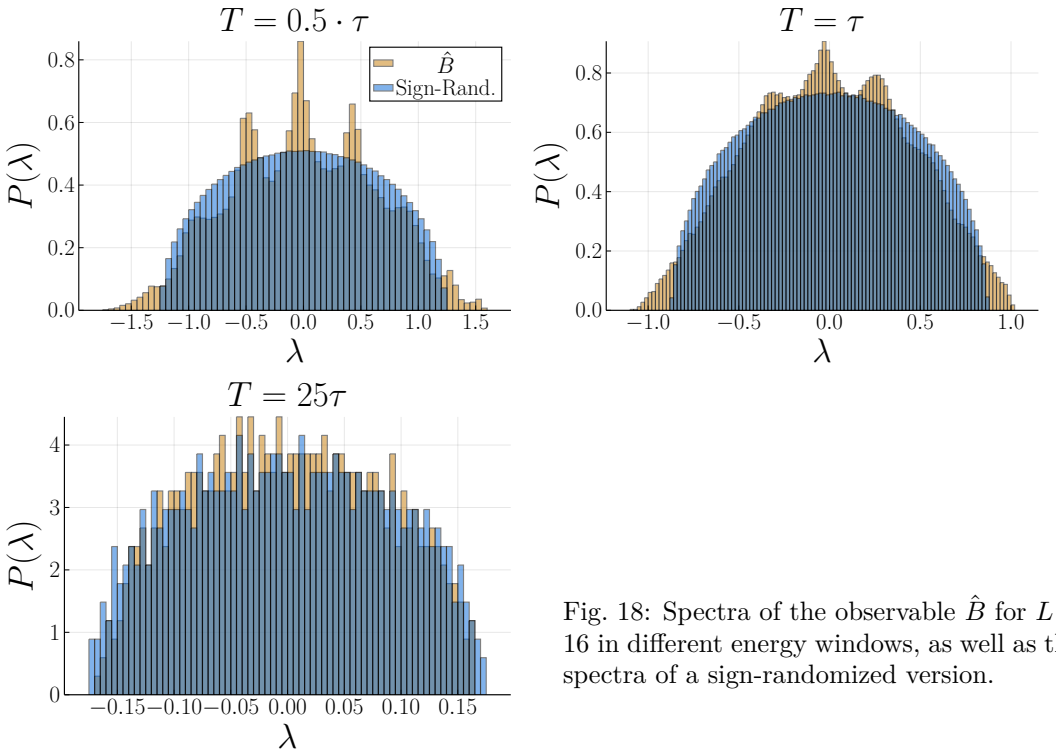

Fig. 18: Spectra of the observable $\hat{B}$ for $L = 16$ in different energy windows, as well as the spectra of a sign-randomized version.

3.5 Conclusion

In the case of the Ising system used here, it was shown that the ETH properties are fulfilled except for MEC. It was shown that the new Λ-indicator has advantages over the usual methods in two respects: First, it is now possible to investigate much larger systems that are beyond the reach of the ED. Furthermore, the new indicator is apparently more sensitive compared to the common methods, so that the use of Λ could also be useful in areas of the ED.
In all systems considered, MEC could be determined long after the relaxation time, so that the assumption often made that these regions can be described as GOE is contradicted here. The consequence of MEC on real physical systems is at large extent not yet to be grasped and requires further investigations. However, by means of the OTOC it is already to be recognized that correlations can have an effect on the dynamics of systems.
Furthermore, the method introduced in Subsection 3.1 for the energetic filtering of states can also be applied outside the investigation of MEC, for example for the determination of long-term values of microcanonical states.

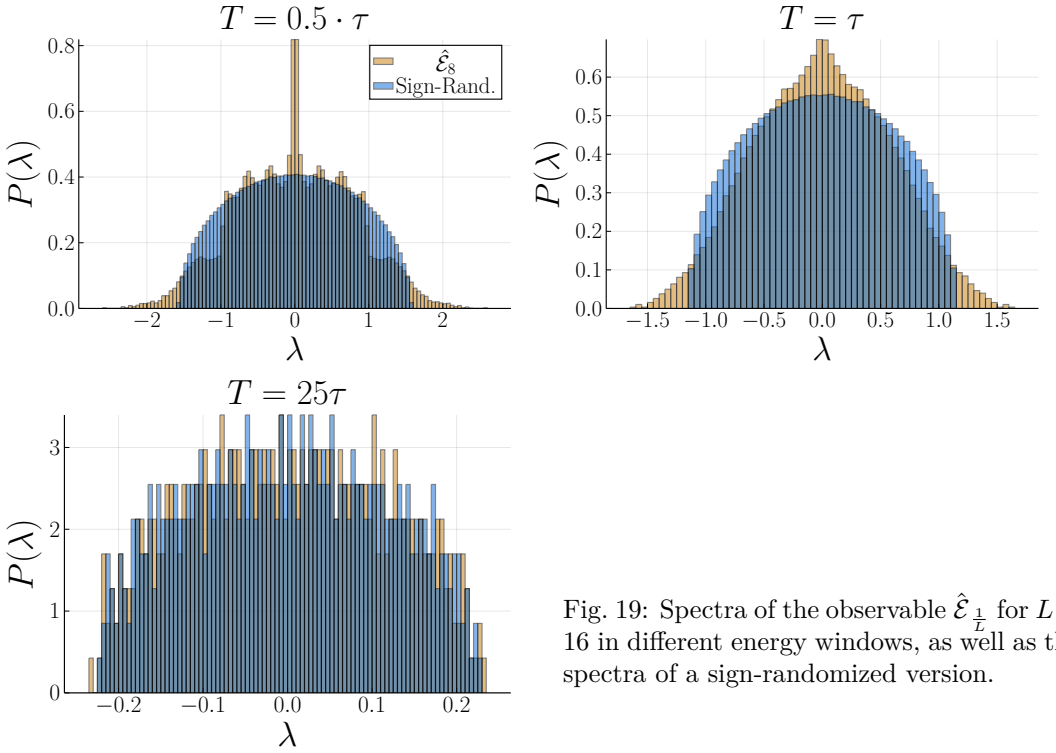

Fig. 19: Spectra of the observable $\hat{\mathcal{E}}_{\frac{1}{L}}$ for $L = 16$ in different energy windows, as well as the spectra of a sign-randomized version.

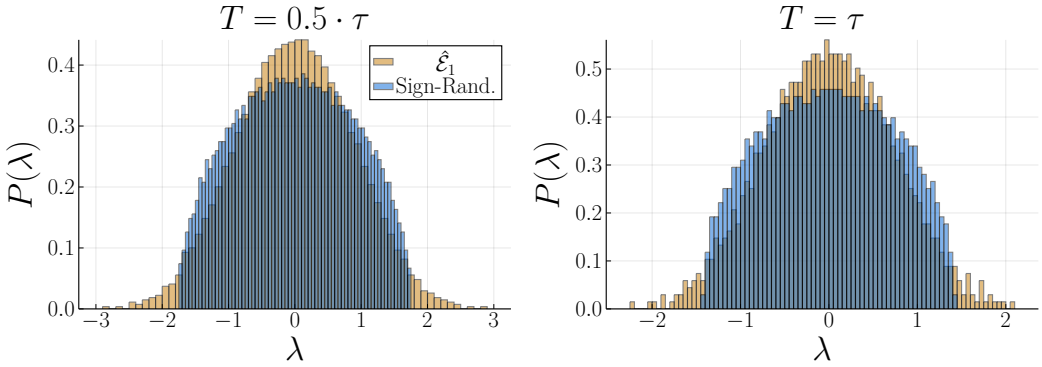

Fig. 20: Spectra of the observable $\hat{\mathcal{E}}_L$ for $L = 16$ in different energy windows, as well as the spectra of a sign-randomized version.

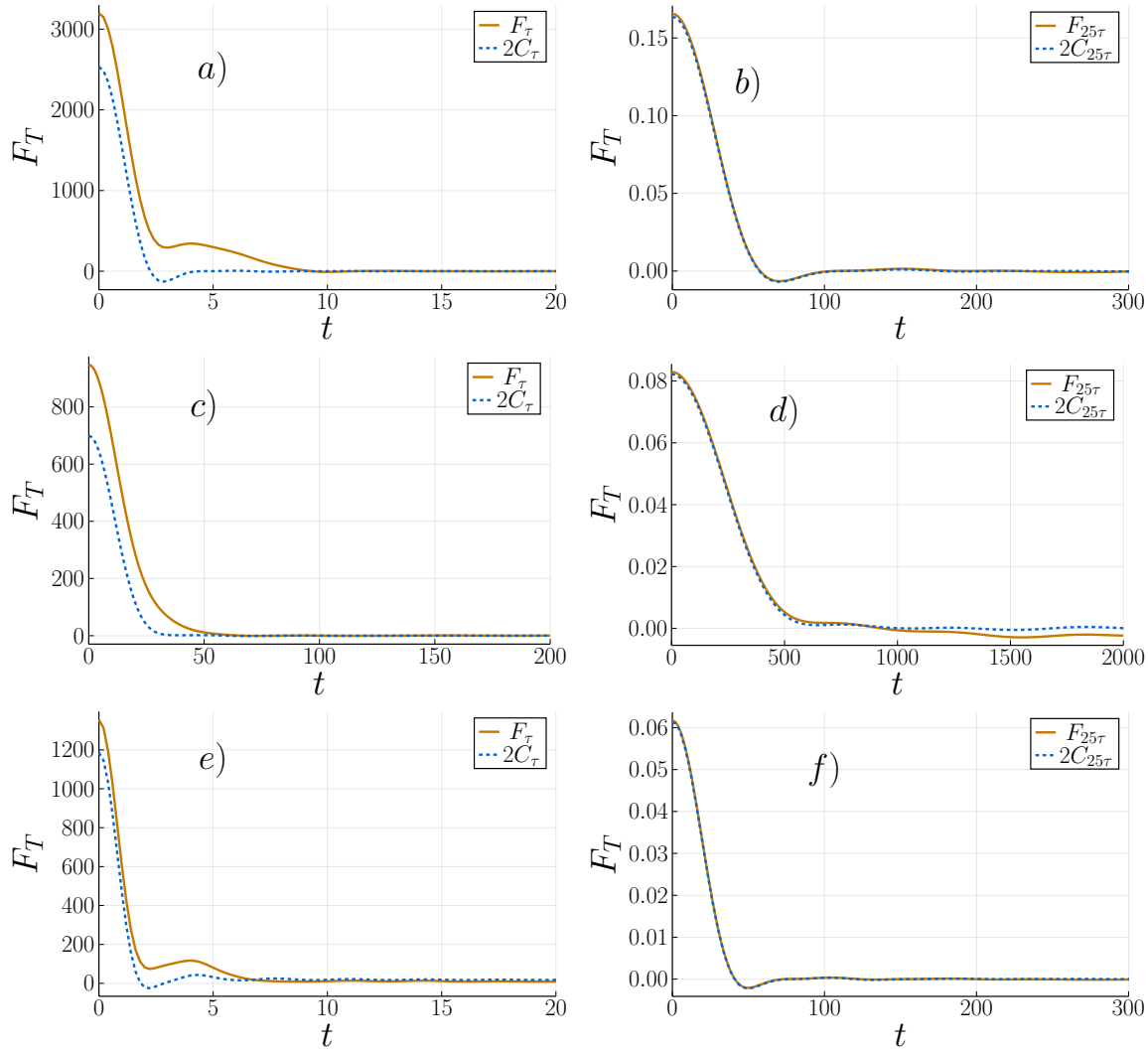

Fig. 21: OTOC for different energy windows corresponding to the time T for the observables a) & d) $\hat{\mathcal{E}}_{\frac{1}{L}}$, b) & e) $\hat{\mathcal{E}}_1$ and c) & f) $\hat{B}$ with $L = 16$. The dashed line denotes the expectation for no MEC.

4 Typical perturbation theory: conditions, accuracy and comparison with a mesoscopic case

The TPT (see Subsection 2.7) could be a powerful tool within the framework of quantum mechanics, since it has high universality and is able to make predictions about perturbed dynamics. In Refs. [32, 33, 34] it has already been shown on various systems that the theory matches the numerical results.
However, a thorough investigation of the necessary conditions (see Subsection 2.7) was omitted in the papers. This was justified by the robustness of the theory. Within this section, these conditions shall be investigated for different cases and whether a relation between the holding of the conditions and the effectiveness of the theory can be seen. The systems studied here are all spin 1/2 systems (see Subsection 2.9), which are also used as examples of where TPT yields good results in Ref [34].
The section is divided into 5 parts. In Subsections 4.1-4.3, three different systems are introduced and in each case their (perturbed) dynamics are compared with the results of TPT. In addition, the assumptions within these systems are also examined. Thereby, the investigations of the different systems partly differ in order to take into account results from previous works. Since the investigations also take place within different energy shells, Subsection 4.4 compares those energy ranges with those expected in mesoscopic cases. Subsection 4.5 condenses all results to a conclusion.
The results of this section have been published in Ref. [P2][50].

4.1 Spin ladder with cross-perturbation

The first system corresponds to a spin ladder whose Hamiltonian $\hat{H}$ and perturbation $\hat{V}$ has the following form:

$$\hat{H}_0 = \hat{h} + \sum_{j=1}^{2}\sum_{l=1}^{L} \overrightarrow{\hat{s}}_{l,j}\,\overrightarrow{\hat{s}}_{l+1,j} + \sum_{l=1}^{L} \overrightarrow{\hat{s}}_{l,1}\,\overrightarrow{\hat{s}}_{l,2} \tag{4.1.1}$$

$$\hat{h} = -0.16 \cdot \hat{s}^z_{1,1} + 0.2 \cdot \hat{s}^z_{4,2} + 0.1 \cdot \hat{s}^z_{5,2} \tag{4.1.2}$$

$$\hat{V} = \sum_{l=1}^{L} \hat{s}^z_{l,1}\hat{s}^z_{l+1,2} + \hat{s}^z_{l,2}\hat{s}^z_{l+1,1} \tag{4.1.3}$$

where the boundary conditions are periodic ($\overrightarrow{\hat{s}}_{L+1,j} \widehat{=} \overrightarrow{\hat{s}}_{1,j}$). Here $\overrightarrow{\hat{s}}_{l,j}$ denotes the vectorial spin operator at the l-th rung and j the respective ladder leg. This system is illustrated in sketch form in Fig. 22.

[50] To maintain a constant notation within this thesis ΔE denotes the full width of the energy window, while in the published work it denotes the half of this width.

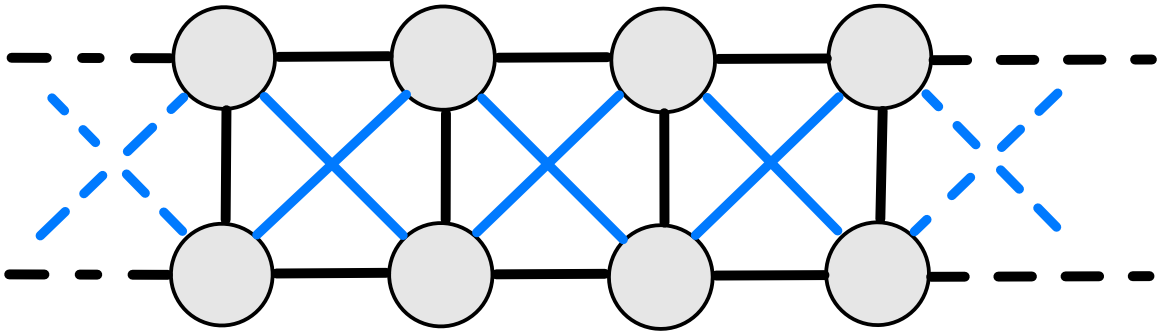

Fig. 22: Sketch of the model from Subsection 4.1:
The gray circles symbolize the spin sites, the black lines represent the Heisenberg interaction of the unperturbed Hamiltonian and the blue lines represent the perturbation. The dashed lines indicate the periodic boundaries of this system.

The focus of the investigation is in the magnetization subspace where the total magnetization in z-direction is 0. By using $\hat{h}$, all other symmetries in this system are broken, so the investigation can be carried out into a single symmetry subspace. While this is not mandatory for TPT, symmetry subspaces can complicate the application, since TPT would have to be applied individually to each of these subspaces[51]. The TPT is to be examined here on the basis of the observable

$$\hat{s}_q = \sum_{l=1}^{L} \cos\left(\frac{2\pi}{L} \cdot l\right) \left(\hat{s}^z_{l,1} + \hat{s}^z_{l,2}\right). \tag{4.1.4}$$

$\hat{s}_q$ is to be understood as the slowest mode of z-magnetization alongside the ladder legs. A similar case was already examined in Ref. [63]. This was done under the consideration of the TPT as well as the perturbation theory of the memory kernel [64]. Thereby the TPT showed up as less useful for the description of the perturbed dynamics, however, an investigation of the conditions was renounced to a large extent. A possible explanation for the failure of the TPT in this case is that the DOS is not constant. Therefore, in this subsection it will be investigated whether the TPT gives good results when the system is considered only in an energy window where the DOS is constant. For this purpose, the energy filter $\hat{\mathcal{P}}^{E_c}_{\Delta E}$ introduced in Subsection 3.1 is used, so that systems outside the ED range can also be studied in an energy-filtered manner. The dynamics on which the TPT is to be checked is represented by

$$\langle \hat{s}_q(t) \rangle = \mathrm{Tr}\left\{\hat{\rho}\hat{s}_q(t)\right\} \tag{4.1.5}$$

with

$$\hat{\rho} \propto \hat{\mathcal{P}}^{E_c}_{\Delta E} \left(\hat{s}_q - \kappa\hat{1}\right) \hat{\mathcal{P}}^{E_c}_{\Delta E}. \tag{4.1.6}$$

Here κ is the smallest eigenvalue of $\hat{s}_q$. To the energy filter it is to be mentioned that it refers to the unperturbed Hamiltonian. This has two differences in contrast to the case that the filter works in the perturbed Hamiltonian. First, in the former case, the initial state is independent of the perturbation strength. Since the TPT is designed for equal initial states, this case is therefore preferable. Secondly, the DOS in the perturbed case is no longer sharply cut off, but shows soft

[51] The special case that all subspaces have the same parameters for g is not ruled out, but it is not generally valid.

edges, which depend on the perturbation strength. This can be seen in Fig. 23. In the limiting cases $\lambda \to 0$ or $\Delta E \to \infty$ this dynamics corresponds to a (shifted) autocorrelation function

$$C_{\hat{s}_q}(t) = \frac{\mathrm{Tr}\left\{\hat{s}_q(t)\hat{\mathcal{P}}^{E_c}_{\Delta E}\hat{s}_q(t)\hat{\mathcal{P}}^{E_c}_{\Delta E}\right\}}{\mathrm{Tr}\left\{\hat{\mathcal{P}}^{E_c}_{\Delta E}\right\}} \tag{4.1.7}$$

$$\propto \langle \hat{s}_q(t)\rangle + C. \tag{4.1.8}$$

4.1.1 Conditions

First, conditions i) and ii) are examined. For this purpose, the DOS/LDOS is investigated. The system considered here is 26 spins large and thus exhibits a $\mathcal{D} = 10400600$ large Hilbert space. Since such a size makes ED impossible, the DOS (LDOS) is determined using the procedures explained in Subsection 2.3. This is done for energy filters of different widths and different perturbation strengths, where the central energy is always $E_c = 0$. The results can be seen in Fig. 23. It can be seen that for the case without energy filter ($\Delta E = \infty$) the assumption that the DOS is constant is not fulfilled. Furthermore, the smaller the width, the better this condition is met. Thus, there are different cases in which the condition i) is satisfied differently well.
In the same figure, it should also be noted that condition ii) is always satisfied, since the DOS does not show a large change for the perturbation strengths used. Condition iv) is investigated using the sign-randomization method (see Subsection 2.6). Since the trace of the perturbation is not 0 and thus under sign-randomization the spectrum would trivially change, here the investigation is done using a trace-free version of the perturbation

$$\hat{V}_{tf} = \mathcal{P}^{E_c}_{\Delta E}\hat{V}\mathcal{P}^{E_c}_{\Delta E} - \frac{\mathrm{Tr}\left\{\mathcal{P}^{E_c}_{\Delta E}\hat{V}\mathcal{P}^{E_c}_{\Delta E}\right\}}{\mathrm{Tr}\left\{\mathcal{P}^{E_c}_{\Delta E}\right\}} \cdot \mathcal{P}^{E_c}_{\Delta E}. \tag{4.1.9}$$

The spectra of both matrix versions of the perturbation are compared. The results are shown in Fig. 24. It can be seen that even in the smallest energy window there is a clear difference between the two spectra, which strongly indicates correlations between the matrix elements. This investigation was done in a smaller system ($L = 9$,$\mathcal{D} = 48620$) to use ED. An investigation of condition iii) is omitted within this thesis, since it is assumed that the chosen perturbation strengths λ are sufficiently large to provide for mixing.

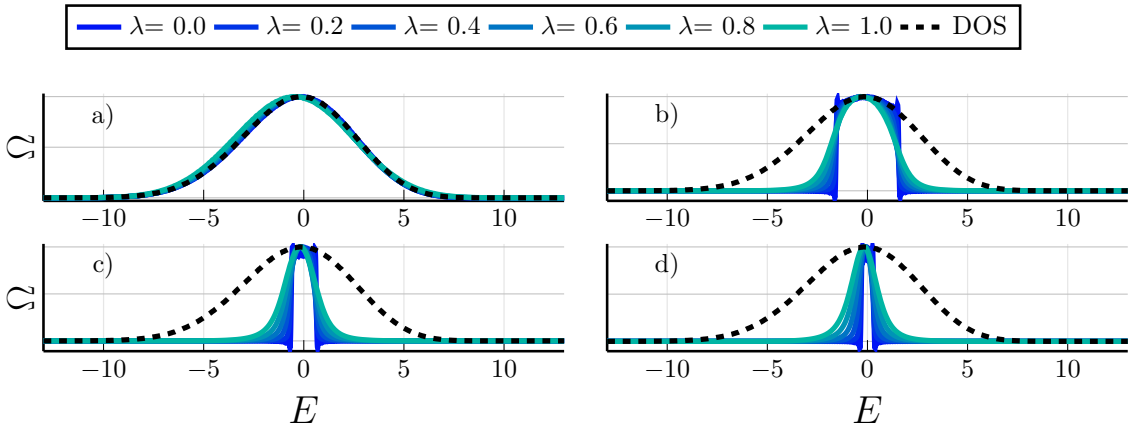

Fig. 23: LDOS for various perturbation strengths λ and energy windows in the system of Subsection 4.1. a) Full spectrum, b) $\Delta E = \pi$, c) $\Delta E = \frac{2\pi}{5}$ and d) $\Delta E = \frac{\pi}{5}$. Scaled for better comparability.

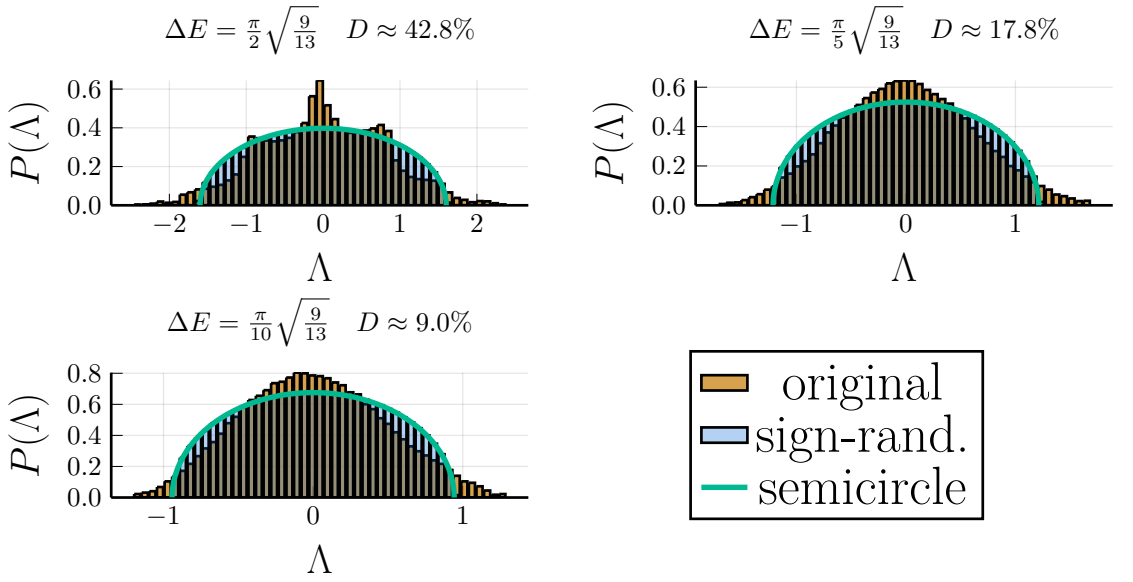

Fig. 24: Spectra of the (trace free) perturbation $\hat{V}_{\Delta E}$ and the sign-randomized version $\tilde{V}$ for different energy windows ΔE, for $L = 9$. In addition, the results are compared with the Wigner-semicircle law, which gives the distribution for a random matrix. D indicates what percentage of the total system is in the chosen energy window.

4.1.2 Comparison

To compare the TPT results with the direct numerical results for the perturbed dynamics, the quantity

$$\Delta_{g_l}(\lambda) = \frac{1}{\tau \left\langle \hat{s}_q(0) \right\rangle^2_{\text{num.}}} \int_0^\tau \left| \left\langle \hat{s}_q(t) \right\rangle_{g_l} - \left\langle \hat{s}_q(t) \right\rangle_{\text{num.}} \right|^2 \mathrm{d}t \tag{4.1.10}$$

is introduced. $\left\langle \hat{s}_q(t) \right\rangle_{\text{num.}}$ is the numerically determined [52] perturbed dynamics, while $\left\langle \hat{s}_q(t) \right\rangle_{g_l}$ is the prediction of TPT. τ is the relaxation time of the numerically determined dynamics. The relaxation time is the time after which

$$\tilde{C}(t) = \frac{C(t) - C(t \to \infty)}{C(0) - C(t \to \infty)} < 0.01 \tag{4.1.11}$$

is (and remains) valid. The long-term value $C(t \to \infty)$ is determined numerically by averaging over the values for late times.
The difference between perturbed and unperturbed dynamics is defined in a similar way:

$$\Delta_0(\lambda) = \frac{1}{\tau \left\langle \hat{s}_q(0) \right\rangle^2_{\text{num.}}} \int_0^\tau \left| \left\langle \hat{s}_q(t) \right\rangle_0 - \left\langle \hat{s}_q(t) \right\rangle_{\text{num.}} \right|^2 \mathrm{d}t \tag{4.1.12}$$

where $\left\langle \hat{s}_q(t) \right\rangle_0$ denotes the unperturbed dynamics. To illustrate these quantities, Fig. 25 shows perturbed and unperturbed dynamics and their difference, which is with $\Delta_0 = 43.4 \cdot 10^{-4}$ the largest in this system. In addition, Fig. 26 shows the perturbed dynamics compared to the unperturbed dynamics for different perturbation levels and energy shells. Since the parameters $(\Delta_v, \sigma^2(0))$ needed for the TPT cannot be determined without using ED, but the system considered is too large for this, those parameters are used here as fitting parameters. It should be noted that proper results using fitting is a necessary but not sufficient condition for the validity of the TPT, since the real parameters could still yield poor results.
Since the parameters are independent of the interference strength λ, the fitting is performed so that the

$$\Delta_{tot} = \sum_{i=0}^{N} \frac{\Delta_{g_l}(\lambda_i)}{\lambda_i} \tag{4.1.13}$$

is minimized. The deviations are weighted reciprocally to the perturbation strength λ, since the TPT is supposed to be valid for weak perturbations[53]. Although alternative weights such as λ_i^{-2} would be also possible and useful, the results are qualitatively the same as for the weighting chosen here. Since in any case the TPT exhibits a limiting case $\sigma^2(0) \to 0$ where the prediction of the theory transitions to the unperturbed case, the worst case is that for every perturbation strength $\Delta_{g_l}(\lambda) = \Delta_0(\lambda)$ holds[54].

[52] via Chebyshev method, see Subsubsection 2.10.3
[53] Even g_2 which is supposed to be valid for large λ is not valid for arbitrarily large λ, see Subsection 2.7.
[54] Individual dynamics may exhibit larger deviations than Δ_0.

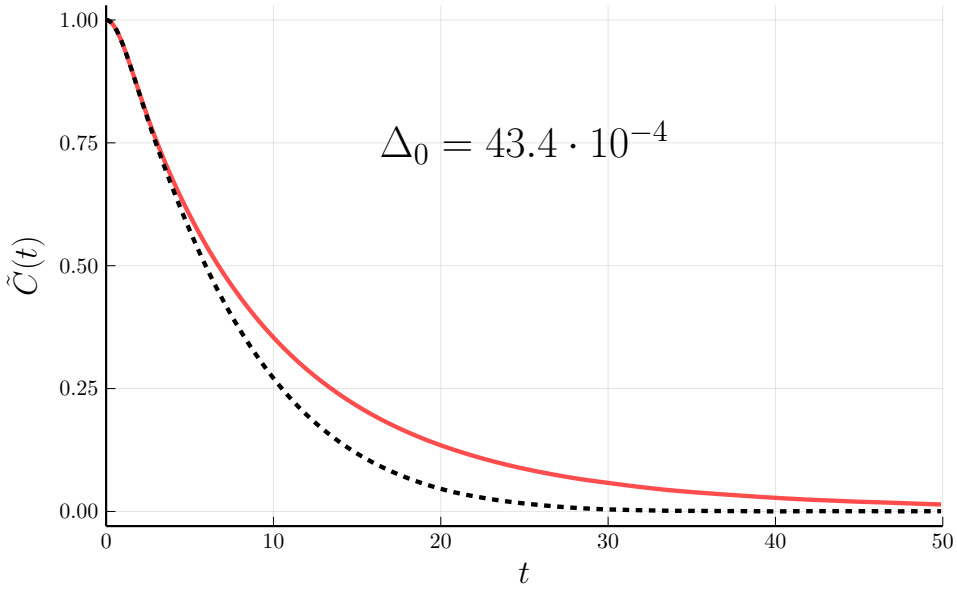

Fig. 25: Example of the difference between perturbed (solid) and unperturbed (dashed) dynamics. ($\Delta E = \infty, \lambda = 1.0$)

In addition to the $g_{1,2,3}(t)$ derived in Refs. [32, 33, 34], two arbitrary functions without theoretical background are also considered:

$$g_{\text{Gau}} = \exp(-\alpha \cdot (\lambda t)^2) \tag{4.1.14}$$

$$g_{\text{Lor}} = \frac{1}{1 + \alpha \cdot (\lambda t)^2} \tag{4.1.15}$$

where α corresponds here to a free parameter. These functions satisfy $g(0) = 1$ and $g(\infty) = 0$, so that trivial properties of perturbed dynamics are fulfilled. The results of this fitting are shown in Fig. 27. It can be seen that the previously discussed worst case occurs for the three largest energy shells and thus the TPT is unsuitable for these cases to make statements about the perturbed dynamics. Only in the smallest energy window the predictions of the TPT are better than the worst case, but this can be understood outside the theory: Since $\hat{\mathcal{P}}$ filters energy in the sense of the unperturbed Hamiltonian $\hat{H}_0$, any perturbation causes a softening of that window. That softening results in higher frequencies being available. Since the initial state is far from equilibrium, it is not surprising that those frequencies accelerate the dynamics at the beginning. This is supported by the fact that the acceleration of the dynamics appears only at small times. Since the TPT always accelerates the dynamics (for $\sigma^2(0) \neq 0$), the softening of the window favors the TPT. However, without theoretical justification, the two g achieve success to the same extent as g_1. Better results yielded $g_{1,3}$, but g_3 with two parameters can also cover a wider range of functions than the other functions.

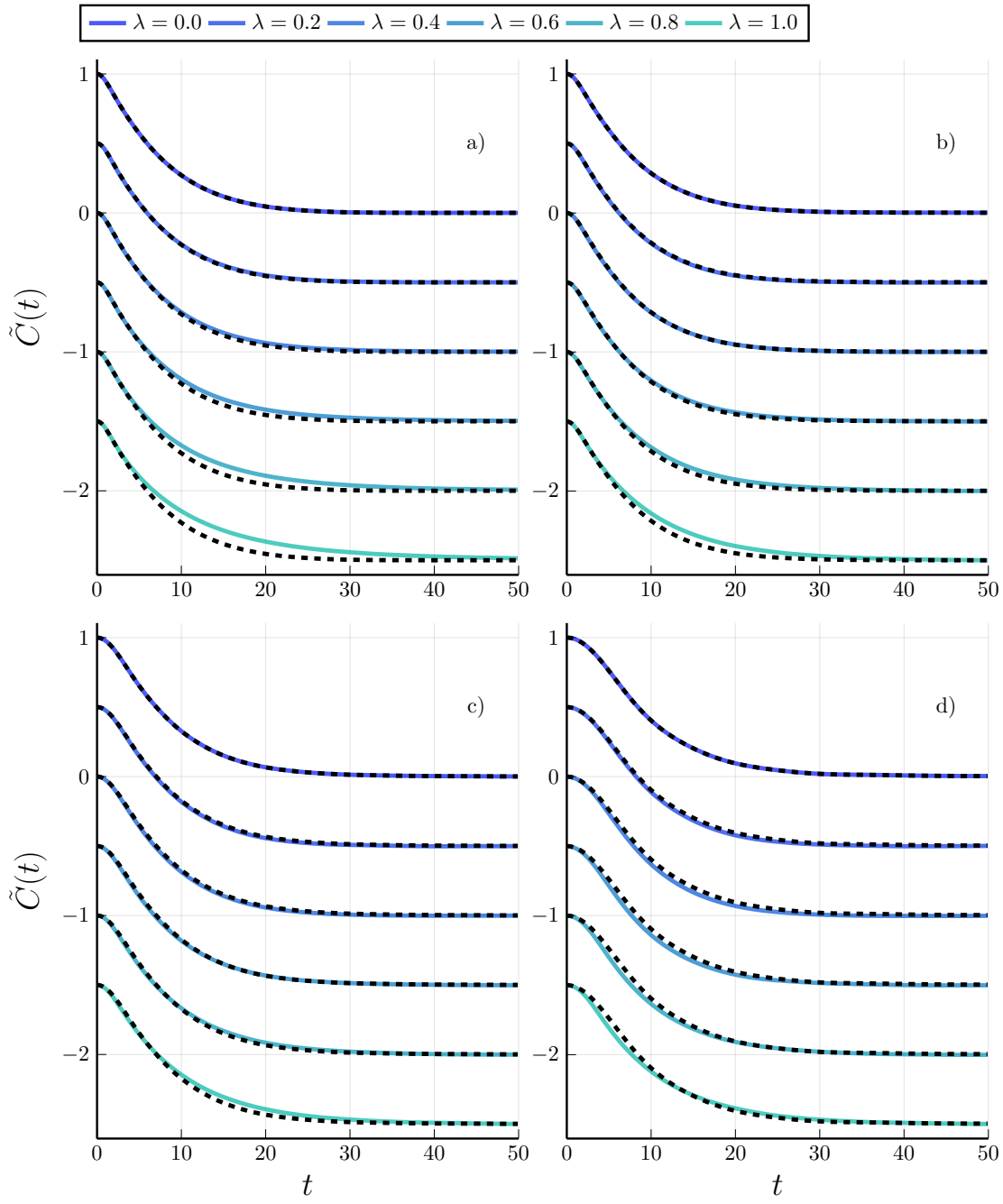

Fig. 26: Dynamics for various perturbation strengths λ and energy windows in the system of Subsection 4.1. The dashed lines denote the unperturbed dynamics within the corresponding energy window. The curves are normalized and shifted by 0.5.
a) Full spectrum, b) $\Delta E = \pi$, c) $\Delta E = \frac{2\pi}{5}$ and d) $\Delta E = \frac{\pi}{5}$.

4.1.3 Conclusion

Condition iv) does not seem to be fulfilled even for the smallest energy window, since there are deviations between the sign-randomized version of the matrix and the original one. Conditions i) and ii), on the other hand, are well satisfied for the smaller energy windows. Only in the smallest energy window the TPT shows relevant results at all, but these can be explained outside the theory. In addition, these results can as well be achieved with relatively arbitrary functions.

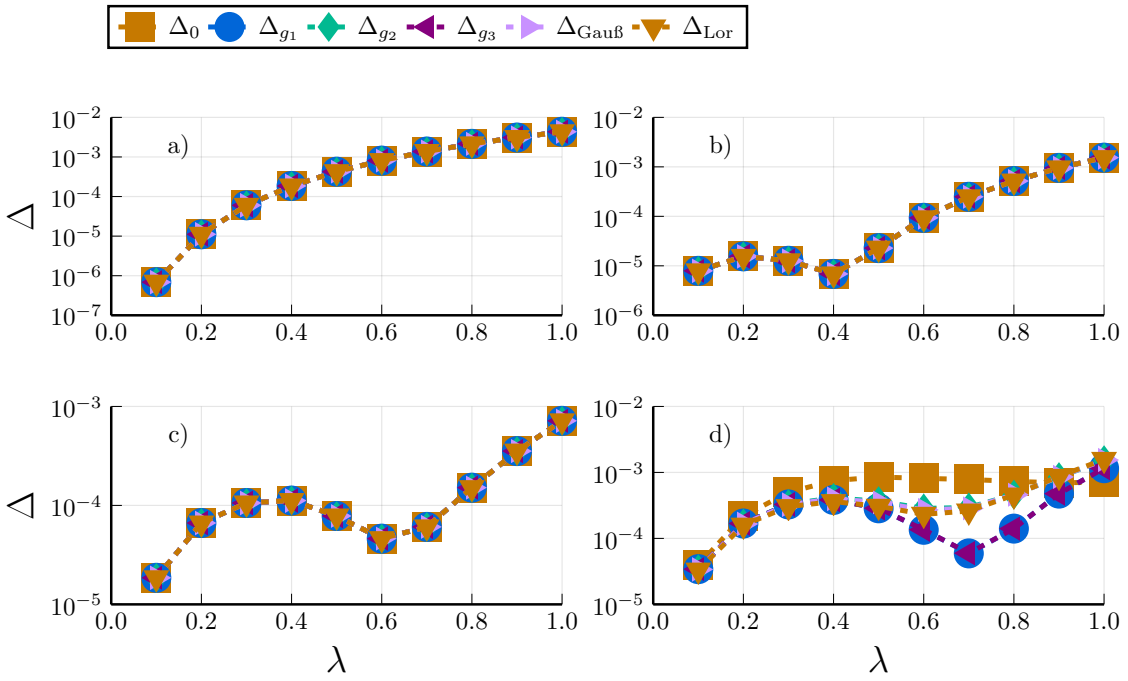

Fig. 27: Deviation between the prediction of the perturbation theory and perturbed dynamics as well as the deviation between the perturbed and unperturbed dynamics for various perturbation strengths λ and energy windows in the system of Subsection 4.1.
a) Full spectrum, b) $\Delta E = \pi$, c) $\Delta E = \frac{2\pi}{5}$ and d) $\Delta E = \frac{\pi}{5}$.

4.2 Spin chains to spin ladder

As shown in Fig. 28 the next model corresponds to two spin chains, which then transition to a spin ladder by the perturbation. The Hamiltonian $\hat{H}_0$ and the perturbation $\hat{V}$ have the form

$$\hat{H}_0 = \hat{h} + \sum_{j=1}^{2} \sum_{l=1}^{L} \vec{\hat{s}}_{l,j} \vec{\hat{s}}_{l+1,j} \tag{4.2.1}$$

$$\hat{V} = \sum_{l=1}^{L} \vec{\hat{s}}_{l,1} \vec{\hat{s}}_{l,2} \tag{4.2.2}$$

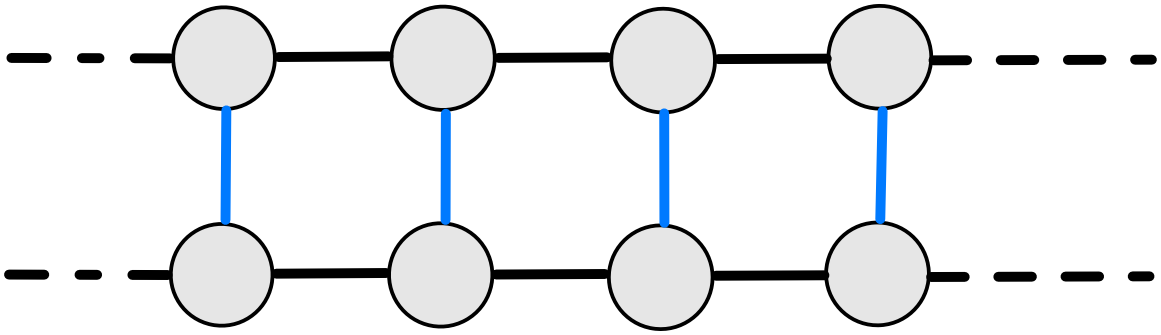

Fig. 28: Sketch of the model from Subsection 4.2:
The gray circles symbolize the spin sites, the black lines represent the Heisenberg interaction of the unperturbed Hamiltonian, the blue lines represent the perturbation. The dashed lines indicate the periodic boundaries of this system.

where $\hat{h}$ can be seen in Eq. (4.1.2) and is also used to break the symmetries in this case. The investigation was carried out in the subspace with vanishing total z-magnetization, which can not be subdivided in further subspaces. It is worth mentioning that this system is integrable without $\hat{h}$ and $\lambda = 0$. Therefore, this system is close to integrable without perturbation and turns into a non-integrable system under perturbation. In Ref. [65], a system differing only by $\hat{h}$ was studied and in Ref. [32] these results were compared with the TPT.
The autocorrelation function of the spin current along the legs is taken as the dynamics

$$C_{\hat{J}}(t) = \frac{\mathrm{Tr}\left\{\hat{J}(t)\hat{J}\right\}}{\mathcal{D}} \tag{4.2.3}$$

with

$$\hat{J} = \sum_{j=1}^{2}\sum_{l=1}^{L} \hat{s}^x_{l,j}\hat{s}^y_{l+1,j} - \hat{s}^y_{l,j}\hat{s}^x_{l+1,j}. \tag{4.2.4}$$

The autocorrelation function corresponds to the dynamics of a density operator

$$C_{\hat{J}} \propto \mathrm{Tr}\left\{\hat{\rho}\hat{J}(t)\right\} =: \langle \hat{J}(t)\rangle \tag{4.2.5}$$

$$\hat{\rho} \propto \hat{1} + \zeta\hat{J} \tag{4.2.6}$$

with a sufficiently small ζ. Since it has already been shown in Ref. [32] that this dynamic yields good results even without an energy filter, such a filter is not applied here. Those results were obtained without determining the parameters, which were treated as fitting parameters there.

4.2.1 Conditions

From the consideration of Eq. (4.2.6), it can be seen directly that condition i) is not fulfilled, since the dynamics takes place over the whole spectrum. Fig. 29 shows the DOS of the system with $L = 13$ for different perturbation strengths, which does not change much until $\lambda = 1.0$. Thus, condition ii) is fulfilled for all smaller perturbation strengths.

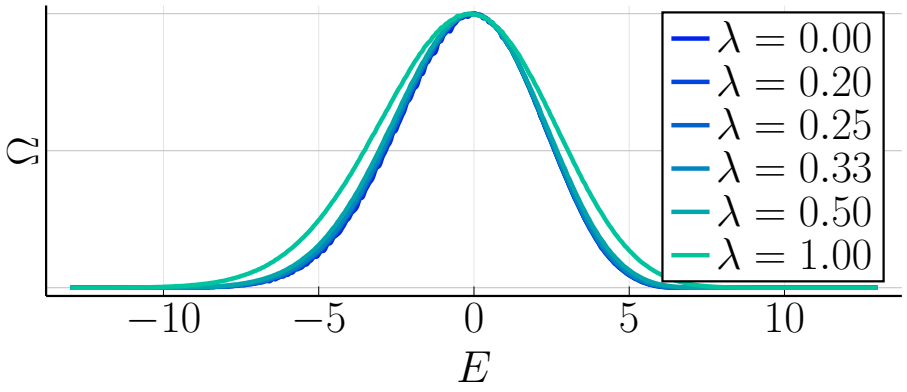

Fig. 29: DOS at different perturbation strengths λ from the spin ladder described in Subsubsection 4.2. Scaled for better comparability.

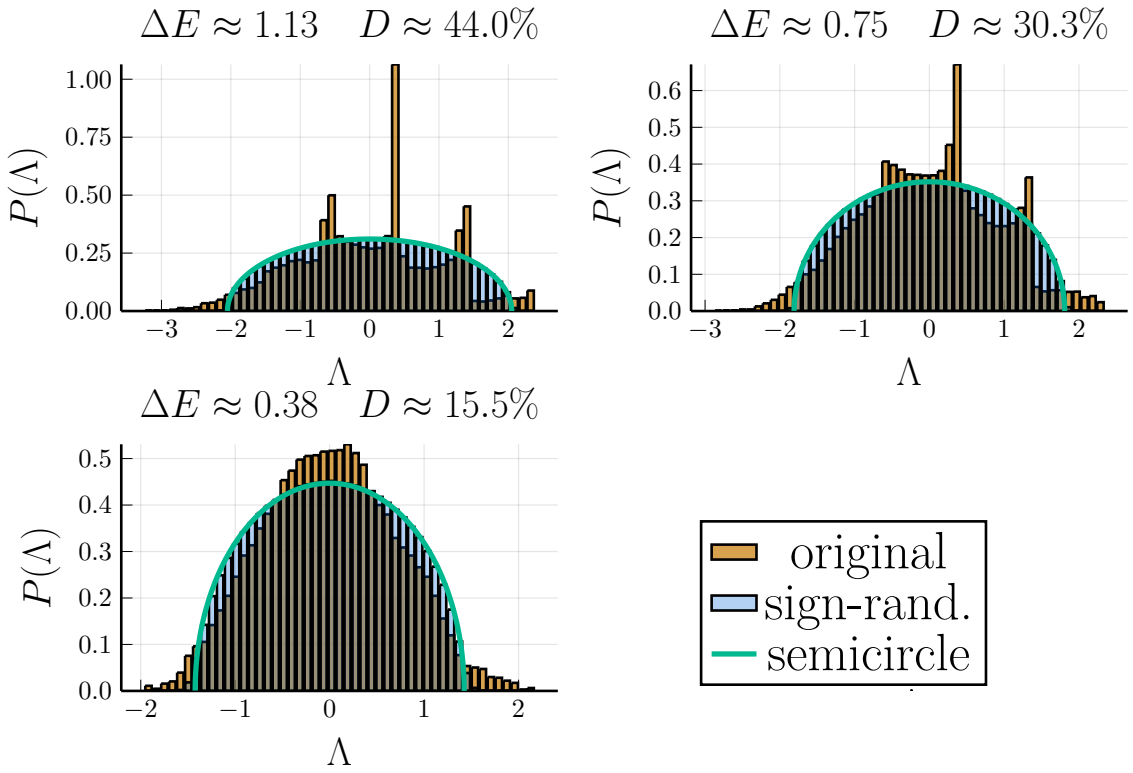

Fig. 30: Spectra of the (trace free) perturbation $\hat{V}_{\Delta E}$ and the sign-randomized version $\tilde{V}$ for different energy windows ΔE, for $L = 9$. In addition, the results are compared with the Wigner-semicircle law, which gives the distribution for a random matrix. D indicates what percentage of the total system is in the chosen energy window.

Even though the dynamics were determined without an energy filter, smaller energy windows are considered to investigate correlations between the elements of the perturbation. This is done with the same approach as before by comparing the spectra of the original perturbation and a sign-randomized version of it. Systems with $L = 9$ are used, since ED is needed for the spectral investigation. The results are shown in Fig. 30, where it can be seen that correlations between the elements exist even for small energy windows. These are given by

$$\Delta E = \{0.6, 0.4, 0.2\} \cdot 2\sigma_{\hat{H}} \tag{4.2.7}$$

$$= \{0.6, 0.4, 0.2\} \cdot 2\sqrt{\frac{\mathrm{Tr}\left\{\hat{H}_0^2\right\}}{\mathcal{D}}} \tag{4.2.8}$$

$$\approx \{0.6, 0.4, 0.2\} \cdot 4.48, \tag{4.2.9}$$

so that those are small compared to the standard deviation of the unperturbed Hamiltonian.

4.2.2 Comparison

Since the dynamics studied were for system sizes outside the range of the ED, the parameters required for the TPT are not determined here. Instead, those parameters are considered as fitting parameters. It should be noted again that good results from those fitting parameters are necessary but not sufficient for the validity of the TPT. The (un)perturbed dynamics are shown in Fig. 31.

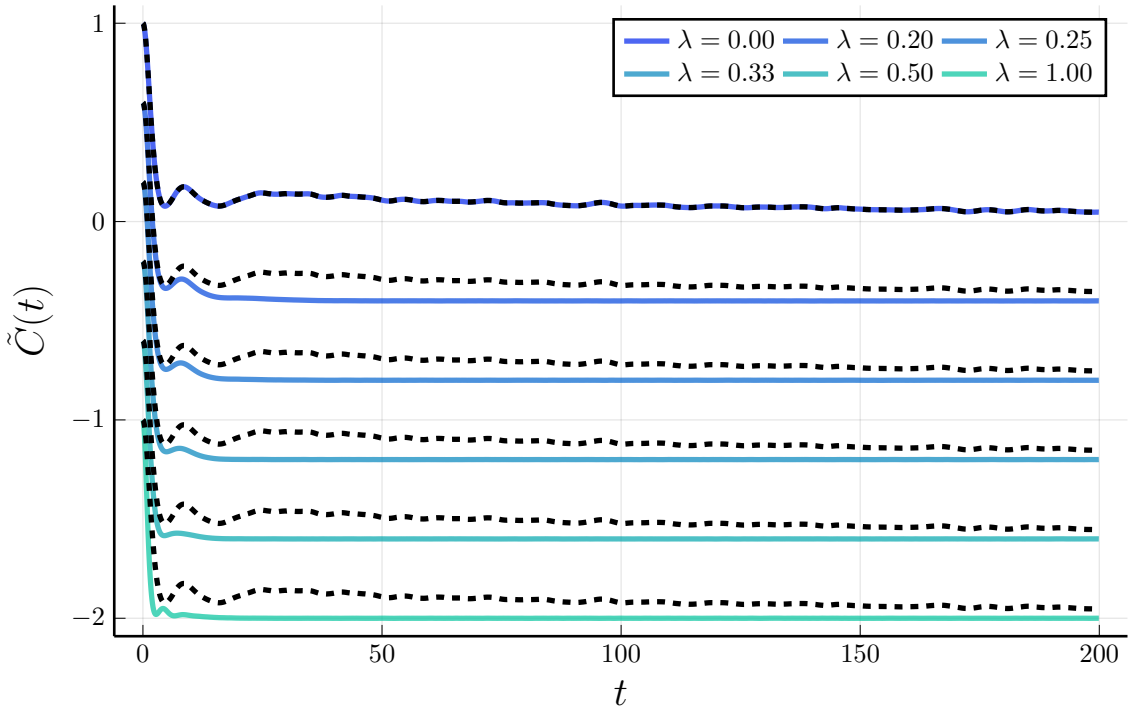

Fig. 31: Dynamics for various perturbation strengths λ in the system of Subsection 4.2. The dashed lines denote the unperturbed dynamics. The curves are normalized and shifted by 0.4.

By comparison with the unperturbed dynamics, it can be seen that large deviations occur even with weak perturbations. Those large deviations can be understood by means of prethermalization [66]. This occurs when systems are close to integrability. This is the case for the unperturbed system. Prethermalization describes that the dynamics consists of two parts, first the dynamics decays relatively fast to a point close to the long term value. Then the second part of the dynamics occurs, which describes a slow approach to that long term value. If the system is perturbed, then the property of prethermalization is lost as the system has been moved further away from integrability. Due to the absence of the second part of the dynamics, the perturbed dynamics is strongly accelerated, which can be well described by the TPT.

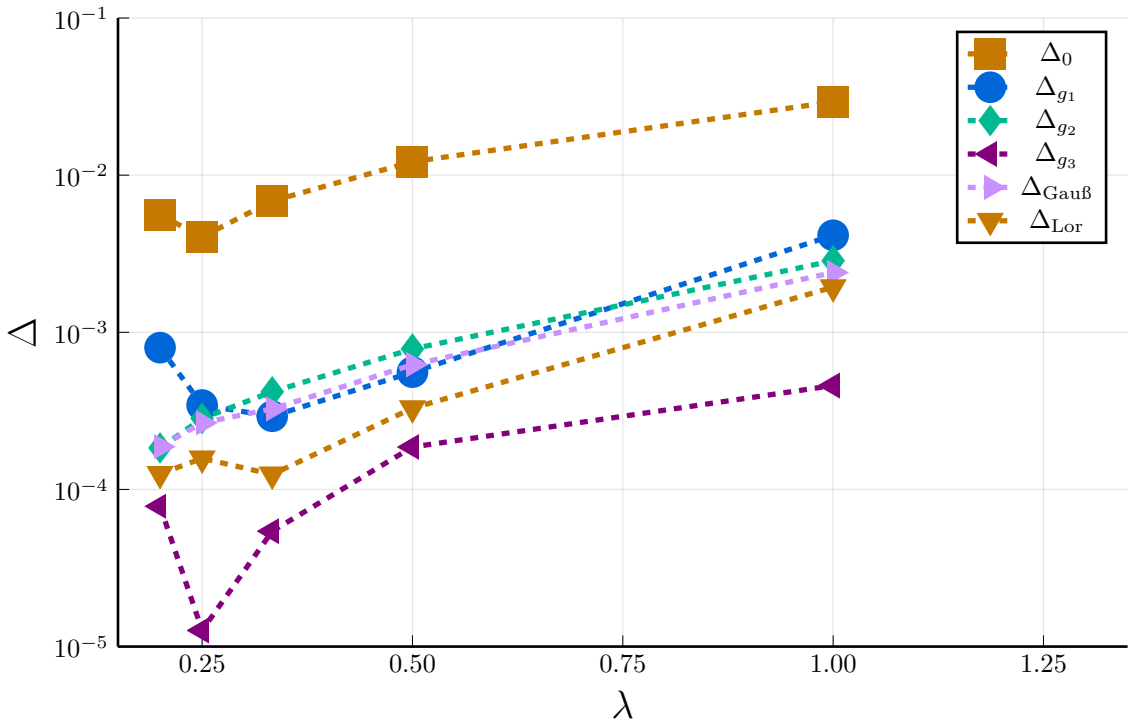

Fig. 32: Deviation between the prediction of the perturbation theory and perturbed dynamics, as well as the deviation between the perturbed and unperturbed dynamics in the system of Subsection 4.2.

In Ref. [32] the system is described without $\hat{h}$ (see Eq. (4.1.2)), so the integrable case is described there. In this case the prethermalization does not occur, but the long term value changes when the perturbation breaks the integrability. This is a free fitting parameter in the TPT, which cannot be determined by the theory. Thus, both cases (near and true integrable) are particularly well suited for the TPT to yield good results, whereas in the latter case this is only possible by a free parameter. The indicators of the deviations can be seen in Fig. 32. It is visible that the TPT is at least an improvement on the unperturbed case. However, functions without a theoretical basis yield equally good or even better results than the functions belonging to TPT. This underlines that the accelerating effect of the perturbation is advantageous for TPT as long as the associated function

decays quickly and the long term value can be chosen freely. g_3 yields the best results, but it also has the largest range of possible functions with two free parameters (plus long term value). Moreover, it is to be recognized that, contrary to the expectation, g_2 yields better results than g_1 in the case of the weakest perturbation.

4.2.3 Conclusion

Even though a very similar system in Ref. [34] serves as an example that the TPT yields good results, it is evident, even without numerical investigation, that at least one condition of the TPT is not satisfied. Thus, the DOS is not constant in the range relevant for the dynamics, which violates condition i). Condition ii) is well fulfilled in most cases, only at the maximum perturbation strength the DOS is changed. Since even in small energy windows larger deviations between random matrices and the perturbation can be detected, condition iv) is never fulfilled. Even though the TPT yields good results, it can be seen that the perturbation is particularly favorable to the TPT in this system. For the case studied here, this can be understood by the prethermalization of the unperturbed system, while in the integrable case it can be explained by a change in the long-term value.

4.3 Spin lattice

The last system investigated by TPT is a lattice of spin-1/2 particles with open boundary conditions (see Fig. 33). The corresponding Hamiltonian and perturbation are given by

$$\hat{H}_0 = 0.16\hat{s}^z_{1,2} + 4 \cdot \sum_{i,j=1}^{L-1} \overrightarrow{\hat{s}}_{i,j} \overrightarrow{\hat{s}}_{i,j+1} + \overrightarrow{\hat{s}}_{i,j} \overrightarrow{\hat{s}}_{i+1,j} \tag{4.3.1}$$

$$\hat{V} = 4 \sum_{\alpha=x,y} \sum_{i,j=1}^{L-1} \left(\hat{s}^\alpha_{i,j} \hat{s}^\alpha_{i+1,j+1} + \hat{s}^\alpha_{i+1,j} \hat{s}^\alpha_{i,j+1} \right). \tag{4.3.2}$$

The dynamics considered is the expectation value of the observable

$$\hat{O} = 4\hat{s}^z_{2,2}\hat{s}^z_{3,3}, \tag{4.3.3}$$

which corresponds to the correlation of the z-magnetization between the spins marked in green in Fig. 33. At the beginning, the initial state

$$\hat{\rho} \propto \mathrm{e}^{-\frac{\hat{H}^2}{2\sigma_E^2}} \mathcal{P}^+_{2,2} \mathcal{P}^+_{3,3} \mathrm{e}^{-\frac{\hat{H}^2}{2\sigma_E^2}} \tag{4.3.4}$$

is assumed,

$$\mathcal{P}^+_{i,j} = \hat{s}^z_{i,j} + 0.5 \cdot \hat{1} \tag{4.3.5}$$

is a projection operator which ensures that the corresponding spin is up. Moreover, this state is energetically bounded by the Gaussian filters on the sides. For the filters $\sigma_E = 2$ was chosen. It should be mentioned that those filters are less sharp compared to the filters used before.
This results in

$$C_{\hat{O}}(t) = \mathrm{Tr}\left\{ \hat{\rho} \hat{O}(t) \right\} \tag{4.3.6}$$

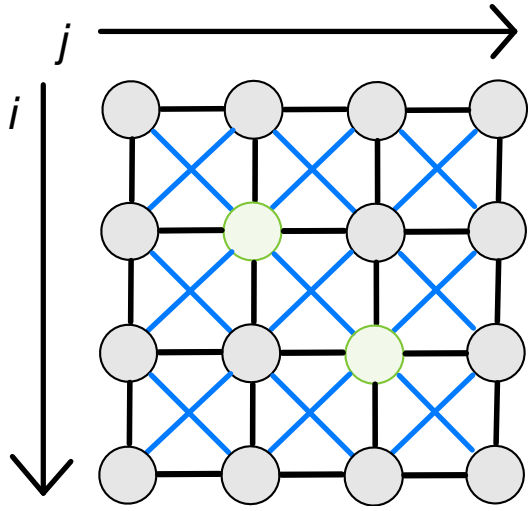

Fig. 33: Sketch of the model from Subsection 4.3: The gray circles symbolize the spin sites, the black lines represent the Heisenberg interaction of the unperturbed Hamiltonian, the blue lines represent the perturbation. The dashed lines indicate the periodic boundaries of this system. The green circles indicate the spins which are important for the observable.

for the dynamics. Apart from the symmetry breaking term of the Hamiltonian, that system has already been studied in Refs. [32, 34]. It was shown that the predictions of the TPT agree with the numerical results. It should be mentioned that in this study, however, the dynamics of the density operator $\hat{\rho}$ from Eq. (4.3.4) was not investigated directly, but was treated by means of typicality, so that pure states of the form

$$|\psi\rangle \propto e^{-\frac{\hat{H}^2}{2\sigma_E^2}} \mathcal{P}^+_{2,2}\mathcal{P}^+_{3,3} |\phi\rangle \tag{4.3.7}$$

were used there as initial states. $|\phi\rangle$ is a Haar-distributed random vector. Thereafter, the time evolution of the individual states is averaged. With the use of the typicality (see Subsection 2.3), however, it can be seen that the differences between these two cases are negligible.
In Ref. [32], it was shown that the predictions of the TPT using $g_{1,2}$ agree well with the numerical data. In addition, the transition between g_1 and g_2 was also clear as the perturbation strength increased. The system was investigated in the magnetization subspace and with a size of $L = 4$, which allowed the ED to be applied. Therefore, in contrast to the systems discussed so far, a determination of the parameters is possible. Further investigations of the system in Ref. [34] showed that g_3 also yields good results.

4.3.1 Conditions

The system size is $L = 4$, which is the same as in the previous work [32, 34]. Thus, all investigations can be performed using the ED.
Fig. 34 a) shows the DOS for different perturbation strengths. It can be seen that with the exception of $\lambda = 1.6$, the DOS hardly changes, so that condition i) is fulfilled in most cases.
The LDOS for the initial state $\hat{\rho}$ given in Eq. (4.3.4) is shown in Fig. 34 b). It can be seen that even for $\lambda = 0.8$ the LDOS is not negligible in the range of nonconstant DOS. As a consequence, condition ii) is not always fulfilled. To investigate condition iv), the sign-random method is again used. Three energy windows with different widths $\Delta E = 2, 4, 6$ are chosen. Thus, both energetic ranges are investigated, which are smaller, larger and equal to the standard deviation of the Gaussian filters. The resulting spectra can be seen in Fig. 35, where it is clear that even within those energy ranges there are deviations between sign-random and the original spectrum. This indicates that

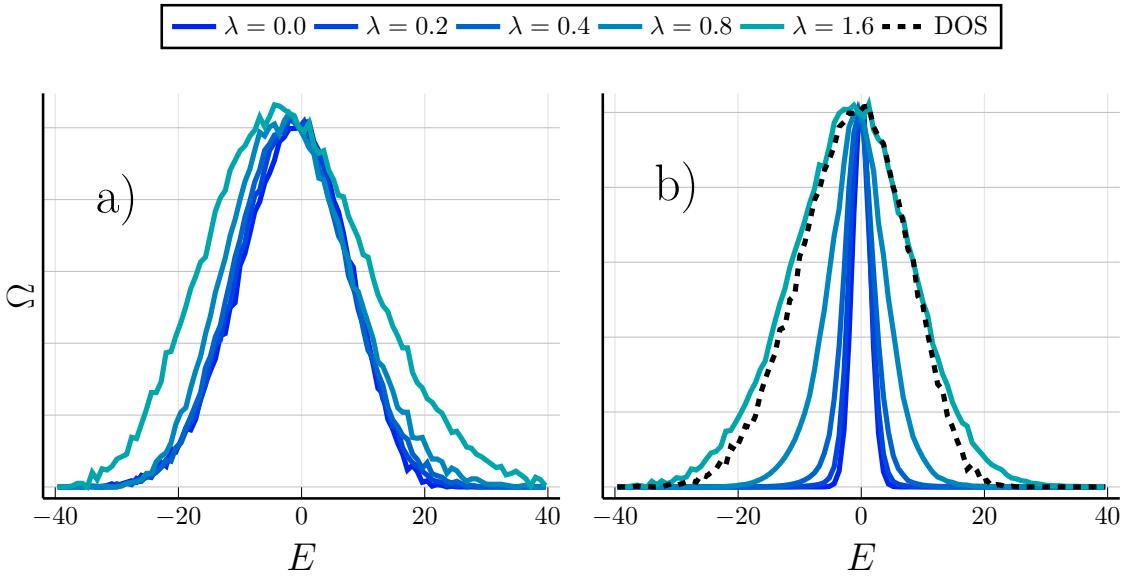

Fig. 34: DOS a) or LDOS b) at different perturbation strengths λ from the spin lattice. Scaled for better comparability.

correlations exist between the matrix elements. Thus, condition iv) is not fulfilled. In contrast to the systems considered above, the parameters of the TPT are not used for fitting. Instead, the values of the parameters determined in Ref. [33] are used. For this $\sigma^2(\omega)$ was calculated for 7722 central states (60% of the spectrum) and then fitted with

$$f_{\text{exp}}(\omega) = \sigma^2(0) \cdot e^{-\frac{\omega}{\Delta_v}}. \tag{4.3.8}$$

Fig. 36 shows both the data for σ and the fitting, with good agreement between the two. A coarse grained version of the data is also shown.
It should be noted that although the results for g_3 in Ref. [34] yielded good results, $\sigma^2(\omega)$ is better described as an exponential function than by a Lorentzian curve. This is in contradiction with the fact that a Lorentzian curve was assumed to derive g_3. For comparison, a Lorentzian curve

$$f_{\text{Lor}}(\omega) = \frac{\sigma^2(0)}{1 + \left(\frac{\pi\omega}{2\Delta_v}\right)^2} \tag{4.3.9}$$

was also used in Fig. 36, which leads to the same parameters as the exponential function. Both fittings show deviations close to $\omega = 0$. This is to be emphasized, since this value has a central role in the TPT. From this fitting in Ref. [33] the parameters

$$\sigma^2(0) = 0.00502 \qquad \Delta_v = 7.32 \tag{4.3.10}$$

were obtained.

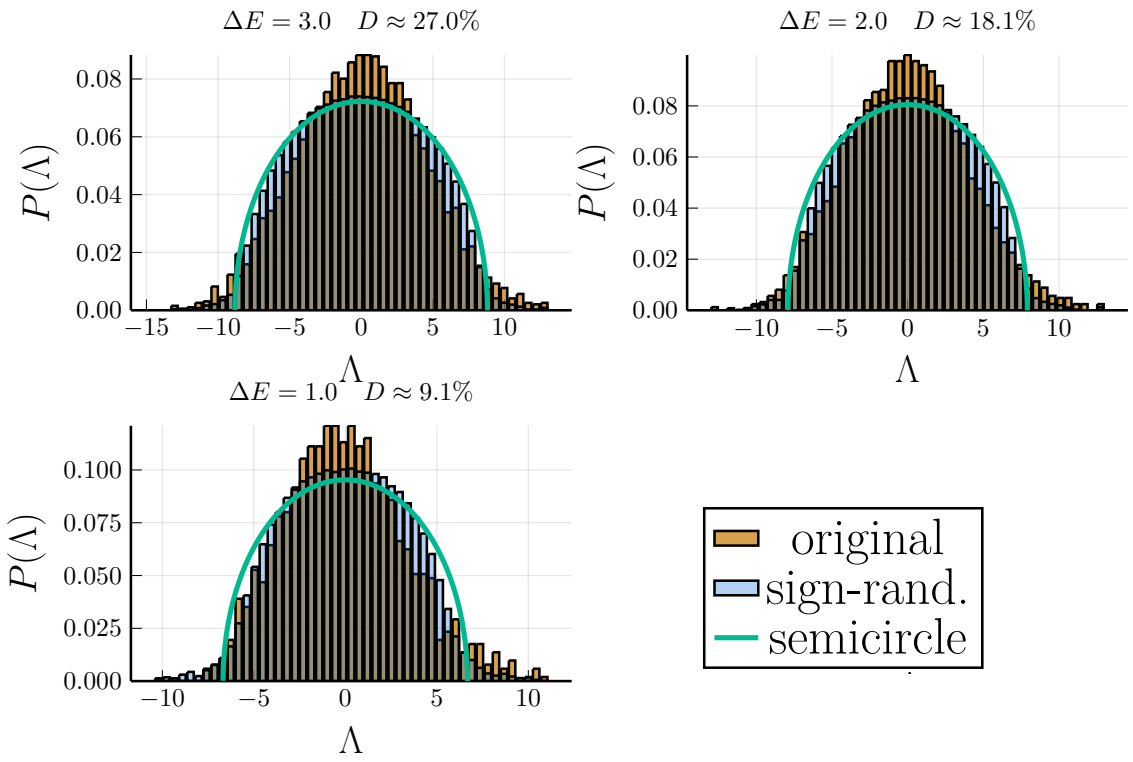

Fig. 35: Spectra of the (trace free) perturbation $\hat{V}_{\Delta E}$ and the sign-randomized version $\tilde{V}$ for different energy windows ΔE. In addition, the results are compared with the Wigner-semicircle law, which gives the distribution for a random matrix. D indicates what percentage of the total system is in the chosen energy window.

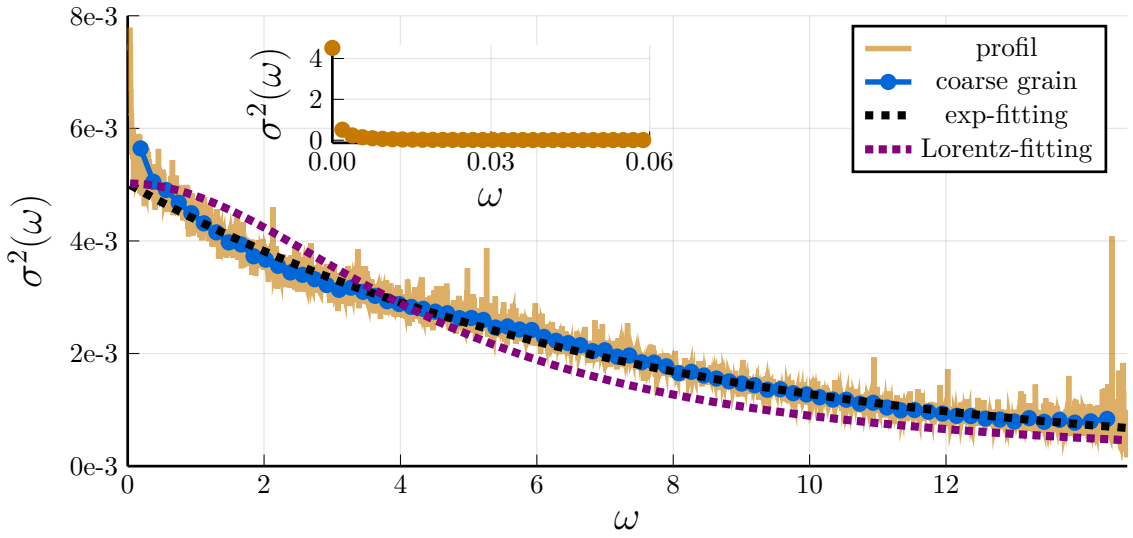

Fig. 36: The perturbation-profile $\sigma^2(\omega)$ for the perturbation in Eq. (4.3.2), with a coarse grained version. In addition, two fits can be seen, with parameters taken from Ref. [33]. The inset shows the variance of the low frequency elements, which are much larger than the other elements.

4.3.2 Comparison

In addition to the two parameters mentioned above, the application of TPT without free parameters (outside the long-term value) also requires the mean level spacing, which is also taken from Ref. [33] with

$$\epsilon = 0.0019. \tag{4.3.11}$$

The (un)perturbed dynamics can be seen in Fig. 37. The deviations between the dynamics and the predictions of the TPT can be seen in Fig. 38. Here, a comparison with the functions without theoretical basis (Eq. (4.1.14) and (4.1.15)) was omitted, since those would exhibit a free parameter due to their arbitrary nature. Moreover, since the parameters of the perturbation are known, the transition perturbation strength λ_c (Eq. 2.7.13) can be determined, above which g_2 should provide better results than g_1. This transition can also be seen in Fig. 38. Of all the variants of TPT studied, g_3 yields the best results. Moreover, g_1 and g_2 show the expected behavior that the former is more suitable for weak perturbations. This expectation has not been fulfilled by the previous schemes. Since for those the investigations were done by fitting, a possible explanation could be that it is an artifact of the fitting.

4.3.3 Conclusion

Conditions i) and ii) are not fulfilled for the larger perturbation strengths. In addition, correlations between matrix elements can be seen for different energy windows, so that condition iv) is not fulfilled. Nevertheless, all variants of the TPT yield good results even without free parameters. Moreover, it can be seen that the profile of the perturbation does not fulfill the additional condition for g_3. Whether this is an indication that the TPT yields merely randomly proper results or should be interpreted as a sign of the robustness of the TPT (as in Ref. [34]) remains open.

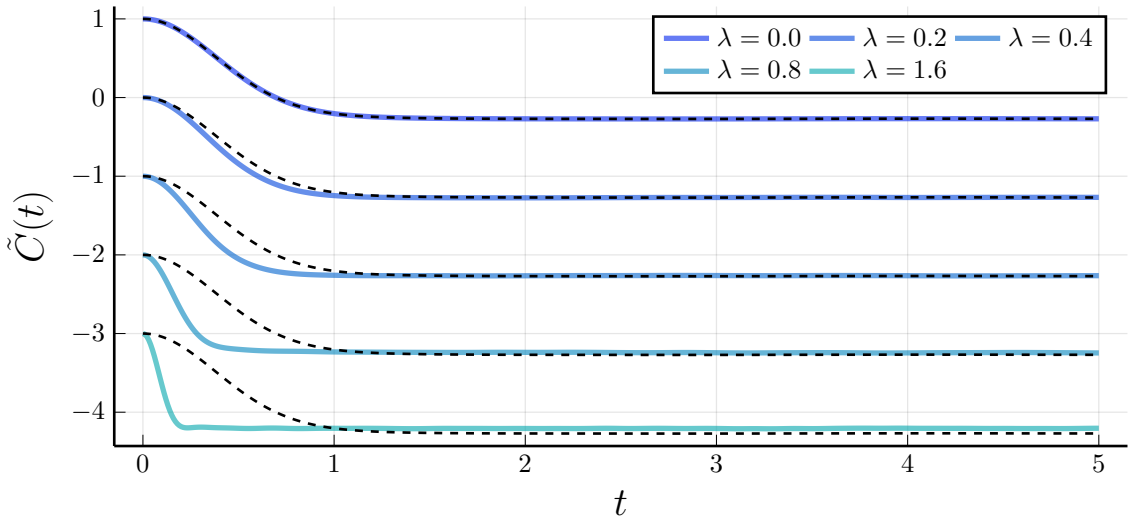

Fig. 37: Dynamics for various perturbation strengths λ of the spin lattice. The dashed lines denote the unperturbed dynamic. The curves are normalized and shifted by 1.

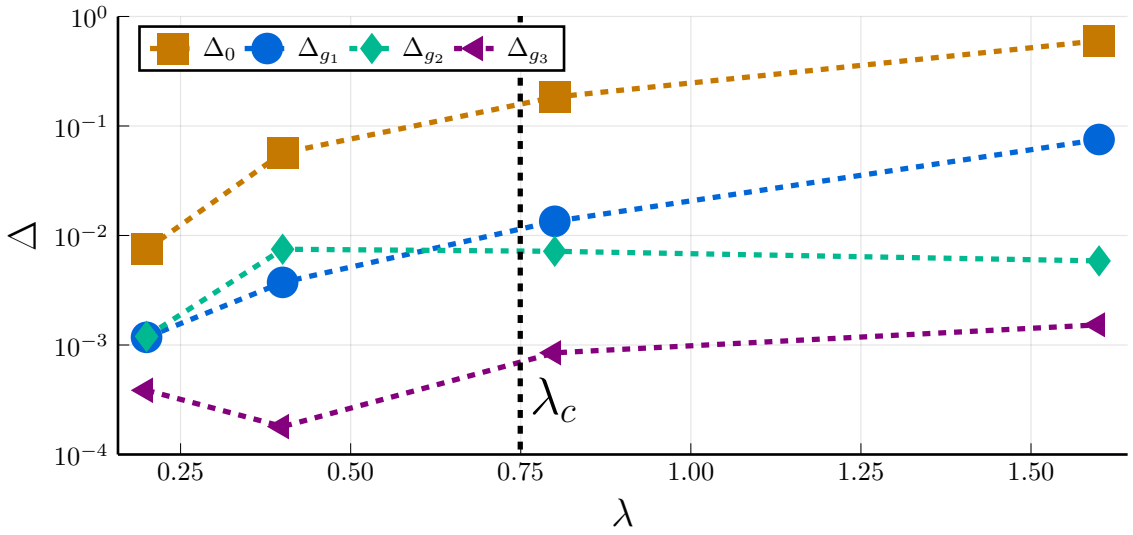

Fig. 38: Deviation between the prediction of the perturbation theory and perturbed dynamics as well as the deviation between the perturbed and unperturbed dynamics in spin lattice. λ_c denotes the theoretical crossover from weak perturbation (g_1,g_3) to large perturbation (g_2).

4.4 Comparison of the energy windows with a mesoscopic case

Since the fulfillment of the conditions strongly depends on the considered energy window and in the first system the TPT only fulfilled good results in the smallest energy window, the question arises to what extent these energy windows are relevant. For this purpose, the previously used energy windows shall be compared with a simple mesoscopic case.
For this purpose, imagine two iron blocks, each with a mass of 0.5g and different temperatures at the beginning. If both blocks are now brought into contact, an average temperature is reached after a few seconds, which in this case shall be $T = 273.15\text{K}$.
The variance of the energy then takes the form [67]

$$\sigma_E^2 = k_B C_v \cdot T^2. \tag{4.4.1}$$

$C_v \approx 0.45\,\text{J}\,\text{K}^{-1}$ is the heat capacity of the iron blocks[68] and $k_b = 1.380649 \cdot 10^{-23}\,\text{J}\,\text{K}^{-1}$ is the Boltzmann constant. Such an energy range results in a corresponding relevant frequency of

$$\omega_{\text{rel.}} = 2 \cdot \frac{\sqrt{k_B C_v} T}{\hbar}. \tag{4.4.2}$$

Since this estimation considers a real case, $\hbar = 1$ cannot be used here. The literature value of $\hbar \approx 1.05 \cdot 10^{-34}\,\text{J}\,\text{s}^{-1}$ must be used. Consequently, for the frequency $\omega_{\text{rel.}} = 1.30 \cdot 10^{25}\text{s}^{-1}$. If this is related to the relaxation time τ, which is estimated here to be a few seconds, it is shown that

$$\omega_{\text{rel.}} \cdot \tau \gg 1 \tag{4.4.3}$$

is valid.
For the system in Subsection 4.1, a relaxation time[55] of $\tau = 26.7$ was determined in the unperturbed and unfiltered case. Using the relation $\Delta E = \omega_{\text{rel.}}$, it can be concluded for the ratios of the different energy windows

$$\Delta E \cdot \tau = 26.7 \cdot \left\{ \pi, \frac{2\pi}{5}, \frac{\pi}{5} \right\} \tag{4.4.4}$$

$$\approx \{83.88, 33.55, 16.78\}\,. \tag{4.4.5}$$

It is readily apparent that these results differ greatly from the mesoscopic estimate. Moreover, it can be seen that the case in which the TPT yields the best results ($\Delta E = \frac{\pi}{5}$) deviates the most from the mesoscopic case. Therefore, it is questionable whether those results are relevant for everyday situations.
Since the system in Subsection 4.2 is not energy filtered, the standard deviation of the Hamiltonian $\sigma_{\hat{H}} \approx 2.24$ is taken as the relevant energy window. Thus, the associated frequency is given by $\omega_{\text{rel.}} \approx 4.48$.
The determination of the product on relevant frequency and relaxation time in this system is more difficult due to the phenomenon of prethermalization. As explained above, this phenomenon is shown by the fact that a large part of the relaxation takes place quickly, but is followed by a phase in which the system approaches the long-term value very slowly. Therefore, both timescales will be used for the investigation here. For the definition of the relaxation time used so far, $\tau = 186.4$ is obtained. However, if the dynamics shown in Fig. 31 are considered, it becomes apparent that the main part of the relaxation has already occurred at time $t = 30$. This time shall be used as a typical

[55] For the definition of the relaxation time, see Eq. (4.1.11).

timescale of the prethermalization $\tau_{\text{pre.}} = 30$.
These two timescales then yield the products

$$\omega_{\text{rel.}} \cdot \tau \approx 835.0 \tag{4.4.6}$$

$$\omega_{\text{rel.}} \cdot \tau_{pre.} \approx 134.4. \tag{4.4.7}$$

Both cases are closer to the mesoscopic value than the previous system, but still far from the estimation of the iron blocks.
The last system studied, shown in Subsection 4.3, has a relaxation time of $\tau = 1.34$. The relevant frequency can be given by means of the standard deviation $\sigma_E = 2$ in the Gaussian filter with $\omega_{\text{rel.}} = 4$. From this follows for the product $\omega_{\text{rel.}} \cdot \tau = 5.36$. Thus, this system shows both the largest deviation from the mesoscopic estimation and the best results for the TPT.

4.5 Conclusion for the TPT results

In summary, none of the investigated systems fulfills all conditions of the TPT. For instance, discrepancies between sign-random and original spectra of the perturbation were always found, indicating correlations between matrix elements and thus violating condition iv). However, the effect of those correlations are difficult to grasp.
In the first system, good results could be generated only for small energy windows. In that case, conditions i) and ii) were well fulfilled. However, the good results can be interpreted without the TPT by means of a softening of the energy window. A comparison with a mesoscopic case also shows that it is at least questionable whether the results can be transferred to mesoscopic systems.
The TPT also yielded good results in the second system, although it does not fulfill condition i) nor iv). Due to the fact that the long term value, which is a free parameter within the theory, changes, this system is, however, also well suited to obtain good results. Moreover, relatively arbitrary functions could also obtain equally good results.
In addition, these results were produced using fitting, so there is a possibility that the real parameters would still yield poor results.
Since for the last system the parameters were determined numerically, this source of error is excluded.
Even if the system shows correlations between matrix elements of the perturbation, the TPT yields good results. The conditions i) and ii) are mostly fulfilled. Also the variant with g_3 shows good results, although the additional condition for the application is not strictly fulfilled, since the profile of the perturbation is more exponential than Lorentzian. Moreover, a comparison with the mesoscopic case shows that this system has the largest deviations from this case of all systems treated.
In summary, a correlation between fulfilling the conditions and the validity of the TPT cannot be revealed. Only the tendency emerges, that smaller energy windows improve the results, but this behavior can also be understood without the TPT.

5 Lanczos Coefficient

In the following part of the thesis several results and approaches are explained, which are based on the perspective in the spirit of the Mori chain (see Subsection 2.8). At the time of writing, these results have not yet been published and are still part of active and intensive research.
Even though the Lanczos coefficients have been known for a long time, there has been an increased interest in this method in the last years, which is motivated on the one hand by the fact that these coefficients can be determined much more efficiently through better software and hardware (even so the number of determinable coefficients is still very limited). On the other hand, the OGH yields an expectation of how these coefficients behave, so that a justifiable continuation of the known coefficients is possible. In the following, that linear continuation is used for the numerical calculations, as long as not otherwise mentioned.
In Subsection 5.1, a model is introduced on which the research of this thesis is tested as an example. The results are presented in three parts: In Subsection 5.2 a method for breaking the semi-infinite chain is motivated. Moreover, it is shown that this truncation always yields superpositions of damped oscillations.
A particular case of the termination will be given special attention in Subsection 5.3, since it allows an estimation of the time integral of the AC.

5.1 Test system

For a better illustration and verification of the results, a test system will be introduced first. For this purpose, a mixed-field Ising model (see Subsection 2.9) is used, whose Hamiltonian can be described by

$$\hat{H} = \sum_{l=1}^{L=24} \hat{h}_l \tag{5.1.1}$$

with

$$\hat{h}_l = \frac{1}{2}\hat{\sigma}_l^x \hat{\sigma}_{l+1}^x - 1.05\hat{\sigma}_l^z + B_x \hat{\sigma}_l^x. \tag{5.1.2}$$

Periodic boundaries conditions are considered. For $B_x = 0$ this system is integrable [42]. By changing that parameter, this integrability can be broken gradually. Since for the determination of the Lanczos coefficients besides the Hamiltonian also an observable is necessary, consider

$$\hat{\mathcal{E}}_{12} \propto \sum_{l=1}^{L=24} \cos(\pi \cdot l)\hat{h}_l. \tag{5.1.3}$$

This observable corresponds to the fastest mode of energy transport for the chosen system size of $L = 24$. The proportionality sign here indicates that the prefactors are not relevant to the results within this section and are always chosen so that the associated autocorrelation function is normalized to $C(t = 0) = 1$.
Using the procedure explained in Subsubsection 2.10.4, the first 30 coefficients can be determined in this system. The results for different B_x can be seen in Fig. 39. It can be seen that, with the exception of the integrable case, there is always a linear increase within the coefficients. Motivated by the OGH (see Subsubsection 2.8.1), the last 15 coefficients are used for a linear continuation.

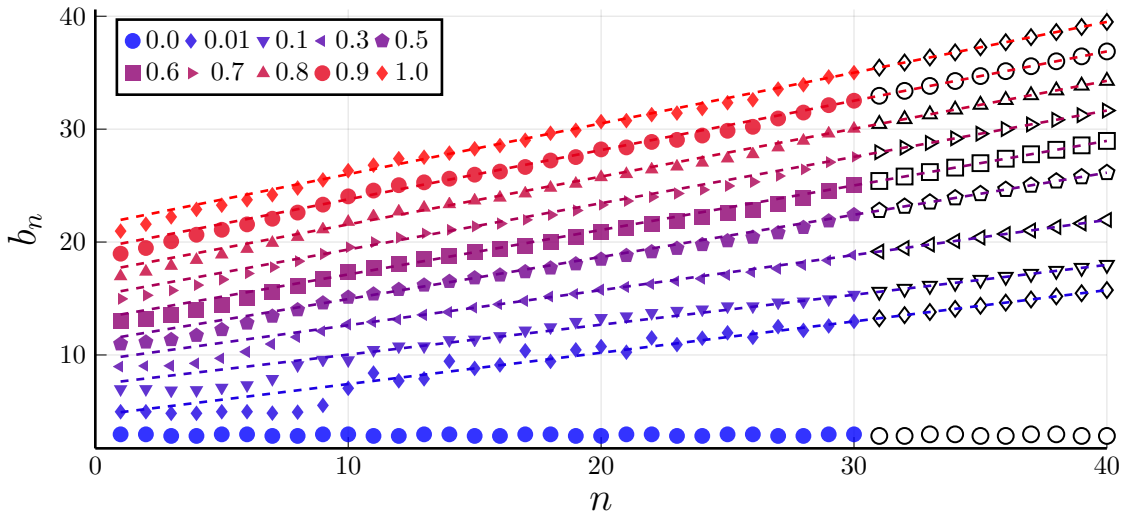

Fig. 39: Lanczos coefficients of the mixed-field Ising model for different values of B_x. The colored symbols are the numerically determined values while the others correspond to the linear continuation. The dotted lines illustrate the linear behavior. For $B_x = 0$ a linear continuation was omitted, instead the pattern found up to $n = 30$ was extended. For a better overview, the curves have been shifted upwards by 2.0.

The exception of the integrable case is taken into account by continuing the existing pattern. This pattern can be continued as

$$b_n^{\text{Int}} = \begin{cases} b_1 & \text{for} \quad \text{mod}\,(n,4)+1 > 2 \\ b_3 & \text{else} \end{cases} . \tag{5.1.4}$$

Using those continuations the systems are extended to a dimension $\mathcal{D} = 1000$[56]. It should be mentioned that this is far from the size of the real system in Liouville space, which, however, would also be too large to perform the following investigations. Nevertheless, this size allows simulations on reasonable timescales before the end of the chain has a greater influence on the course of the autocorrelation function[57]. To avoid the influence of such boundary effects, simulations are terminated if $|x_{\mathcal{D}}(t)| > 10^{-2}$ holds. This time shall be denoted here as τ_b, which can be approximated by

[56] This corresponds to 999 coefficients.
[57] This manifests itself mostly by recurrent dynamics.

considering the local current operator[58]

$$\mathscr{J}_R = \begin{pmatrix} 0 & 0 & 0 & \cdots & & \\ 0 & 0 & \ddots & \ddots & & \\ 0 & \ddots & \ddots & b_R & & \\ \vdots & \ddots & b_R & & 0 & \\ & & & 0 & & \ddots \\ & & & & \ddots & \end{pmatrix}. \tag{5.1.5}$$

The expectation value of the current operator is given by

$$J_R(t) = 2b_R x(t)_R x_{R+1}(t). \tag{5.1.6}$$

Using the interpretation of $x_R(t)^2$ as local density, the local velocity

$$v_R(t) = 2b_R \frac{x_R(t)x_{R+1}(t)}{x_R^2(t)} \tag{5.1.7}$$

is obtained. This results in a maximum velocity

$$v_R^{\max} = 2b_R \tag{5.1.8}$$

which can be reached if $x_R(t) = x_{R+1}(t)$. From that maximum speed results the time, which is needed at least to reach the end of the chain

$$\tau_a = \frac{1}{2}\sum_{n=1}^{\mathcal{D}} \frac{1}{b_n}. \tag{5.1.9}$$

A comparison of this approximated time limit with the numerical determinate boundary time τ_b for different B_x and dimensions $\mathcal{D}$ is shown in Fig. 40. It is clearly visible that the two values are nearly equivalent to each other. This equivalence especially becomes better for larger dimensions. Even though τ_a increases with larger dimensions $\mathcal{D}$, this increment decreases reciprocally for the cases of linear b_n. For large n, the boundary time exhibits a logarithmic behavior, which can be seen in the inset of Fig. 40. Thus, on the one hand, increasing the size of the chain (using linear continuation) ensures only a slightly larger simulated time, on the other hand, the numerical investigations in this section are done with ED, which scales with $\mathcal{O}(\mathcal{D}^3)$, so that the effort would increase substantially[59].

[58] This is the current of $|x_n(t)|^2$ within the Mori chain and should not be confused with the spin current operator in Heisenberg models.

[59] Also, the iterative methods introduced in Subsection 2.10 scale with $\mathcal{O}(\mathcal{D}^2)$, so that the numerical effort would increase substantially there as well.

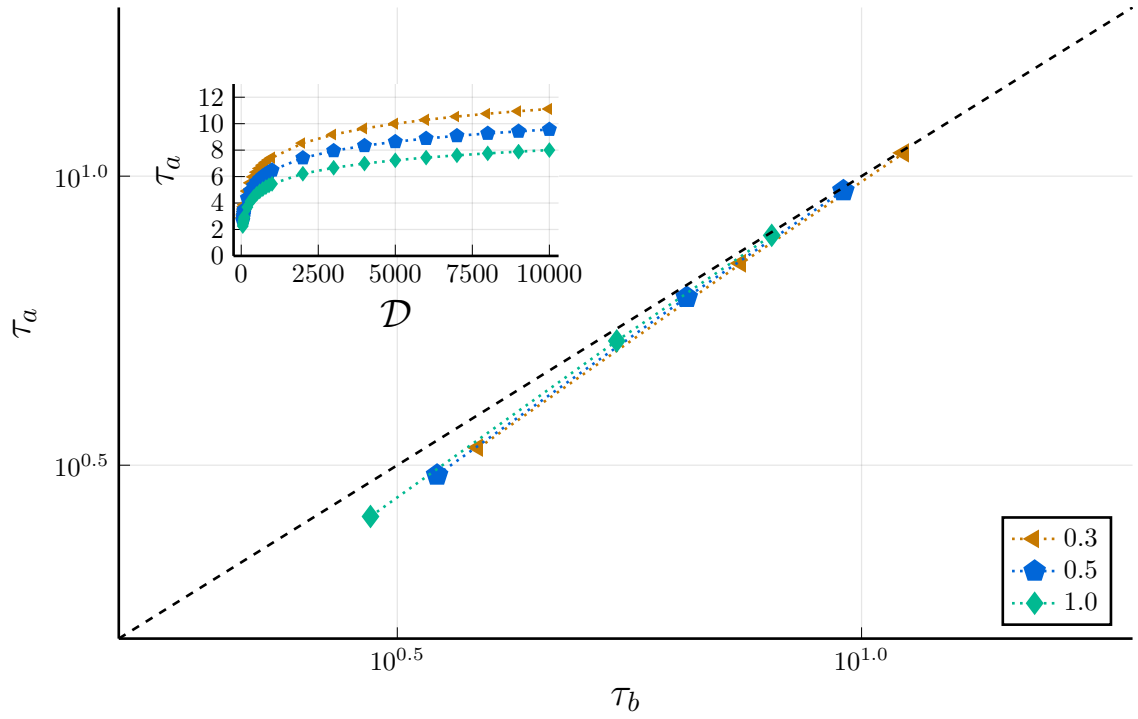

Fig. 40: Comparison of times τ_b and τ_a for different B_x $(0.3, 0.5, 1.0)$ and dimensions $\mathcal{D}$ $(10^2, 10^3, 10^4)$. The colors denote the magnetic field B_x while the dimension increases with τ_a (see Eq. (5.1.9)). The inset shows τ_a versus the dimension $\mathcal{D}$ and displays a logarithmic behavior.

Moreover, to check whether the linear continuation alters the dynamics strongly, the autocorrelation functions are determined in the common manner using Chebyshev method and DQT (see Subsections 2.10 and 2.3). In Fig. 41 these comparisons are shown. It can be seen that in some cases the boundary effects already come into play, although the dynamic itself is not yet fully relaxed. This happens for the smallest and the largest B_x. This can be caused by fast increasing b_n, such that the boundary of the chain will be reached more quickly (this can be seen for large B_x), or by long lasting dynamics, which is most likely the case for small B_x.
Even before the boundaries are reached, some deviation of the curves are clearly visible. A possible explanation for this is that the linear continuation neglects some small but important features of the coefficients. Since the focus here is on statements of the representation and the system is to serve here only as a test balloon, despite these deviations further with the linear continuation is used. It is assumed, however, that the determination of even more coefficients could allow more accurate continuation.

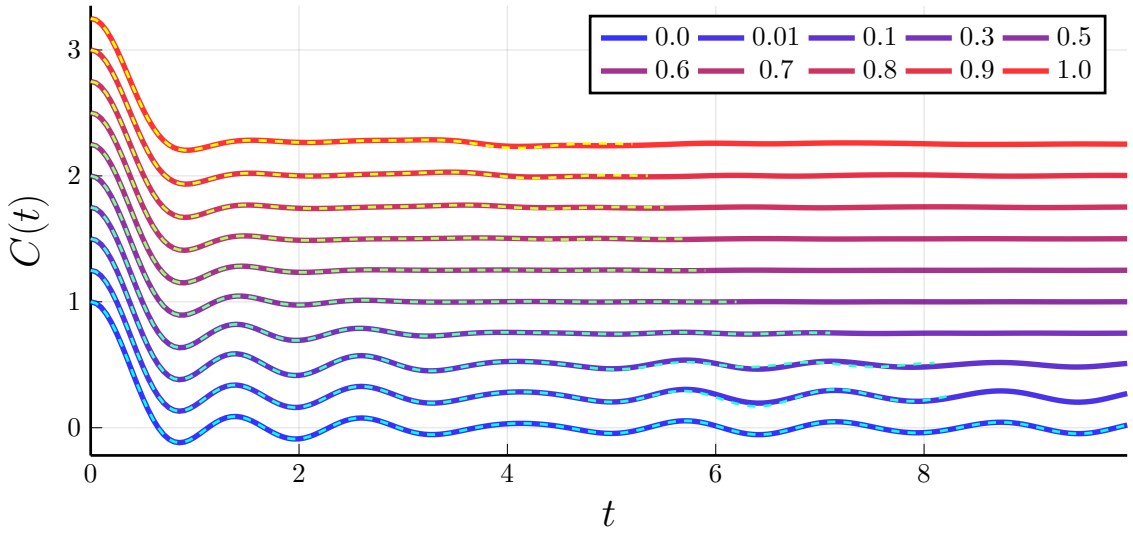

Fig. 41: Comparison of the autocorrelation function of $\hat{\mathcal{E}}_{12}$ by usual methods and the linear continuation of Lanczos coefficients. The dashed lines denote the data for the linear continuation and stop when the boundary is reached ($\mathcal{D} = 1000$). The solid lines are determined by the usual Chebyshev method. For a better overview, the curves have been shifted upwards by 0.25.

5.2 Reduction of the Mori chain from several points of view

Within this subsection a possible break of the semi-infinite Mori chain shall be motivated and furthermore investigated.
Since the Recursion Method is not new, it is not surprising that there are already numerous attempts for the rather early truncation of this representation [69, 70]. The focus was often on the spectral representation of the chain in the direct image of the Continued Fraction (see Eq. (2.8.24)). This points out the first difference to the investigations described here, since the truncations within this thesis are more focused on representing the dynamics of a chain and thus take place in the time domain rather than the frequency domain. In addition, different new equivalent views are to be emphasized here, allowing to interpret more easily the meaning of a break-off. In contrast to the references mentioned above, no concrete proposal for the exact type of truncation is made within this subsection, instead a numerical method for the determination of an optimized truncation is briefly explained.
Some equations already introduced in Subsection 2.8 will be repeated here for a better overview.
First, let consider the dynamics of that chain, which can be described by

$$\vec{x}(t) = \mathrm{e}^{\hat{\mathscr{L}}t}\vec{e}_0. \tag{5.2.1}$$

Here $\vec{e}_0$ is the 0-th unit vector[60] and $\hat{\mathscr{L}}$ is the Liouvillian[61], which can be expressed by

$$\hat{\mathscr{L}} = \begin{pmatrix} 0 & -b_1 & 0 & \cdots \\ b_1 & 0 & -b_2 & \ddots \\ 0 & b_2 & \ddots & \ddots \\ \vdots & \ddots & \ddots & \end{pmatrix}. \tag{5.2.2}$$

b_n denotes the Lanczos coefficients and $x_n = \vec{x} \cdot \vec{e}_n$ corresponds to the value of the n-th chain link. In this case, the dynamics fulfill the differential equation

$$\dot{x}_n(t) = b_n x_{n-1}(t) - b_{n+1} x_{n+1}(t), \tag{5.2.3}$$

where $b_0 = 0$ applies.
These equations reveal a simple method for determining the derivatives of those dynamics

$$\frac{d^j}{dt^j}\vec{x}(t) = \hat{\mathscr{L}}^j \vec{x}(t). \tag{5.2.4}$$

Various numerical investigations showed that the x_n seemed to exhibit a certain smoothness (in the context of n). This behavior shall be considered here as an assumption, since there are known cases in which this smoothness is not present, for example if the b_n exhibits strong even-odd effects. However, these structures occurred only sporadically in the coefficients of the models examined here, so that it is at least reasonable that this assumption is fulfilled in some cases. For better illustration, two cases are considered here, one where the smoothness is well fulfilled and one where it is not. For this purpose, instantaneous images of the x_n at two different times are shown in Fig. 42.
Motivated by that finding of smoothness, it seems reasonable to consider x_R as a function of the preceding chain links,

$$x_R(t) \approx \sum_{n=0}^{R-1} \gamma_n x_n(t). \tag{5.2.5}$$

Thereby the γ_n are time-independent. For the differential equation Eq. (5.2.3) follows thus

$$\dot{x}_n(t) = \begin{cases} b_n x_{n-1}(t) - b_{n+1} x_{n+1}(t) & \text{for } n < (R-1) \\ b_n x_{n-1}(t) - \sum_{n=0}^{R-1} \gamma_n x_n(t) & \text{for } n = (R-1) \\ 0 & \text{else} \end{cases}. \tag{5.2.6}$$

That differential equation can be represented as a $R \times R$ matrix. For the case $R = 3$ the matrix then has the form

$$\hat{\mathscr{L}}_3 = \begin{pmatrix} 0 & -b_1 & 0 \\ b_1 & 0 & -b_2 \\ -b_3\gamma_0 & b_2 - b_3\gamma_1 & -b_3\gamma_2 \end{pmatrix}. \tag{5.2.7}$$

[60] The nomenclature within this subject area is generally far from clear, however it is common to refer to the chain link at the edge as 0.

[61] It should be noted that this expression does not correspond to the usual Liouvillian, but an additional one has been multiplied by the complex number i. Nevertheless, for the sake of simplicity, this expression shall be called Liouvillian here.

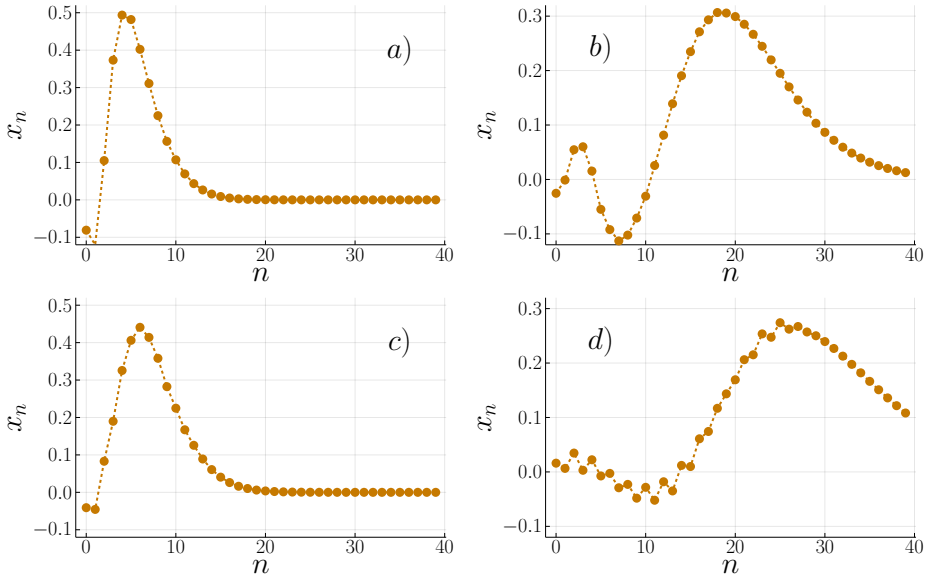

Fig. 42: Values of the first 40-chain links for dynamics of the system explained in Subsection 5.1 with $B_x = 0.5$ ($B_x = 1.0$) for a and b (c and d). Here, in a and c (b and d) are snapshots for $t = 1.0$ ($t = 2.0$).

In the further remainder of the thesis $\hat{\mathscr{L}}_R$ shall always denote a $R \times R$ matrix, which was created by means of the smoothness argument.
Another consideration of the derivation from Eq. (5.2.5), is the interpretation over vector $\vec{s}$, which should be avoided as far as possible. For this, let be the scalar product

$$\vec{s} \cdot \vec{x}(t) = \sum_{n=0}^{R} s_n x_n(t) \tag{5.2.8}$$

$$\tag{5.2.9}$$

with $\vec{s} \cdot \vec{e}_n = 0$ for $n > (R+1)$. Using the above approximation, it follows that

$$\vec{s} \cdot \vec{x}(t) \approx \sum_{n=0}^{R-1} s_n x_n(t) + s_R \sum_{n=0}^{R-1} \gamma_n x_n(t) \tag{5.2.10}$$

$$= \sum_{n=0}^{R-1} (s_n + s_R \gamma_n) x_n(t). \tag{5.2.11}$$

From this consideration, it is evident that to any good approximation in the form of Eq. (5.2.5), there is a vector $\vec{s}$ with

$$s_n = \vec{s} \cdot \vec{e}_n = \begin{cases} -\gamma_n & \text{for } n < R \\ 1 & \text{for } n = R \\ 0 & \text{for } n > R \end{cases} \tag{5.2.12}$$

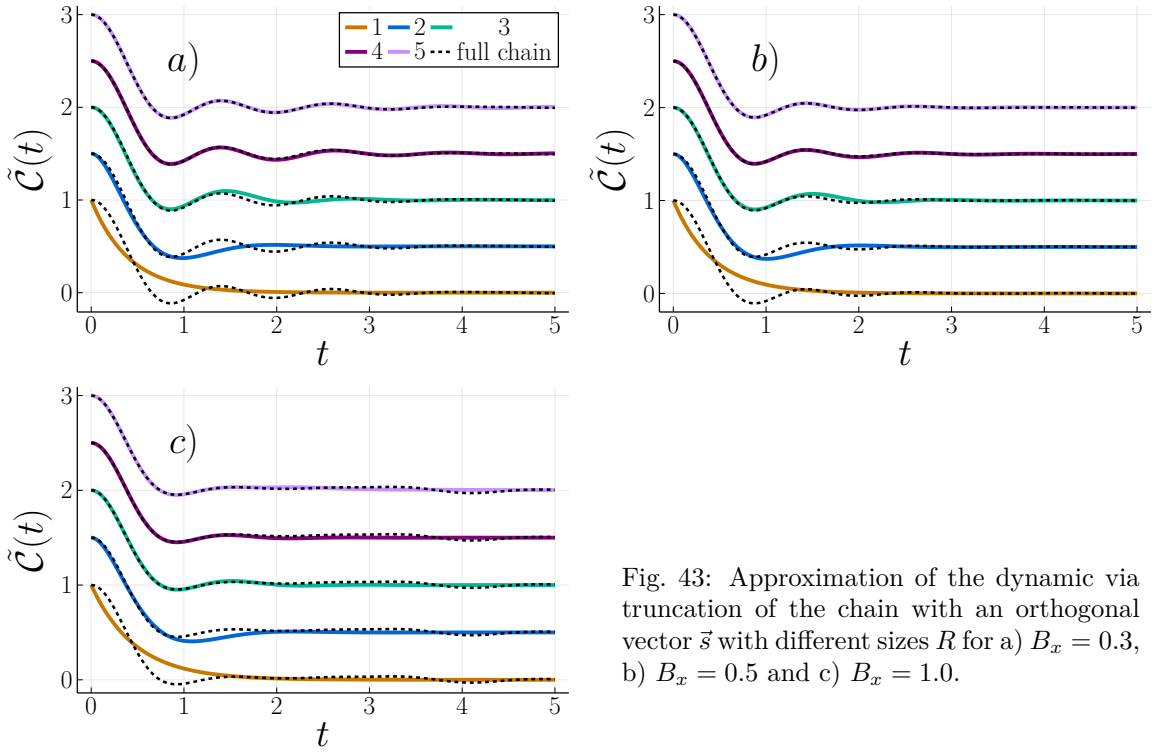

Fig. 43: Approximation of the dynamic via truncation of the chain with an orthogonal vector $\vec{s}$ with different sizes R for a) $B_x = 0.3$, b) $B_x = 0.5$ and c) $B_x = 1.0$.

which is at any time (approximately) orthogonal to $\vec{x}$, thus fulfilling $\vec{s} \cdot \vec{x}(t) \approx 0$[62]. This approach is numerically useful, since it results in an optimization problem: If the dynamics $\vec{x}(t)$ in single time steps are known (by previous simulations using ED or iterative methods), an optimized $\vec{s}$ can be found for each R by determining a $R \times \mathtt{T}$ matrix $\hat{X}$ from the first R chain links at $\mathtt{T}$ different times and multiplying that matrix by its transpose $\hat{X} \cdot \hat{X}^T$. The eigenvector with the smallest eigenvalue of that matrix corresponds to the vector which is most orthogonal to $\vec{x}$ over all times. Such an optimized $\vec{s}$ does not necessarily yield good results, since there are cases where no such an orthogonal vector exists at all. Whether good $\vec{s}$ exist for each system is a question of ongoing research.

To demonstrate that at some cases good orthogonal vectors can be found (where "good" is to be understood in the sense of the description of the dynamics by means of a reduced chain), Fig. 43 shows the resulting dynamics in comparison to the dynamics of the chains with $\mathcal{D} = 1000$. The orthogonal vectors, which are displayed in Fig. 44, were determined by the method described above. This was done for the test system for different magnetic field strengths as well as for different break-off points. It can be seen that by means of the truncation the dynamics were hit relatively precisely, although a maximum of 5 chain links were effectively available. Moreover, at least for very early truncations, the exponential or damped harmonic nature of the resulting curves can be seen. It also shows that the result works differently well for different magnetic field strengths.

Besides the approach via orthogonal vectors or continuation from previous components, there is another equivalent view by means of approximations of the dynamics by damped oscillations. In order to recognize this, let first recall that every unit vector $\vec{e}_n$ can be expressed by superposition

[62] Note that for complete orthogonality $\vec{s}$ is indeterminate on a prefactor.

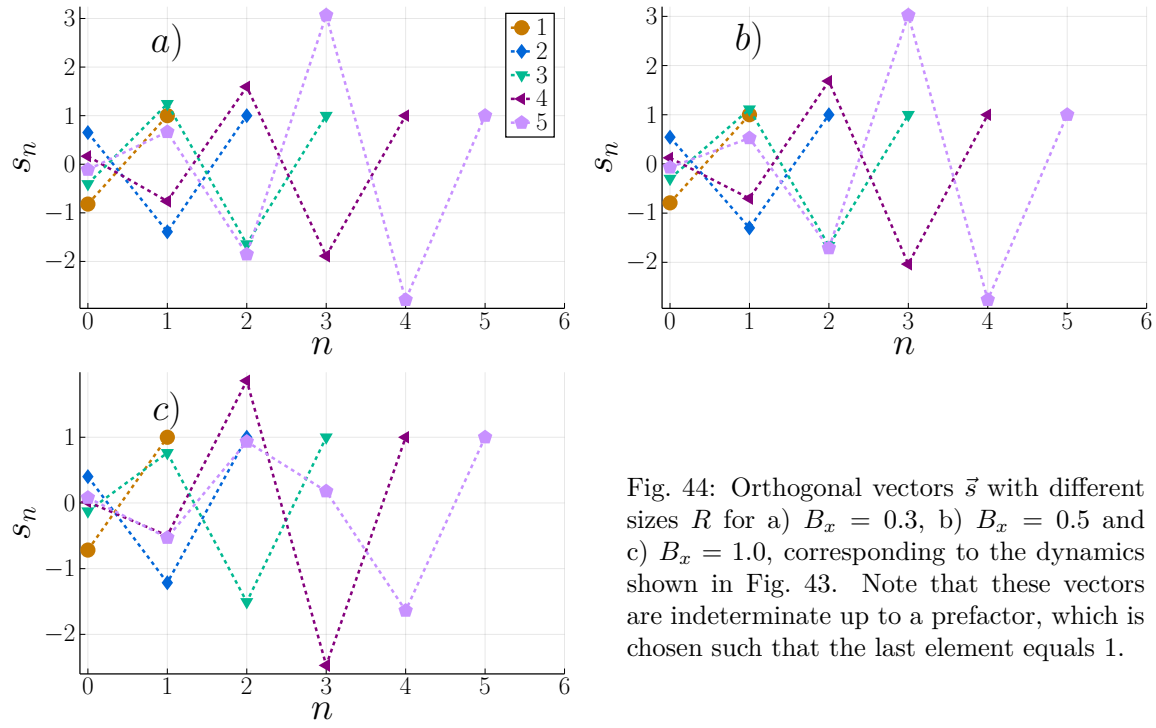

Fig. 44: Orthogonal vectors $\vec{s}$ with different sizes R for a) $B_x = 0.3$, b) $B_x = 0.5$ and c) $B_x = 1.0$, corresponding to the dynamics shown in Fig. 43. Note that these vectors are indeterminate up to a prefactor, which is chosen such that the last element equals 1.

via

$$\vec{e}_n = \sum_{j=0}^{n} c_{j,n} \hat{\mathscr{L}}^j \vec{e}_0. \tag{5.2.13}$$

This is given by the structure of the Liouvillian: Since that application of the operator corresponds to hopping (back and forth), the j-fold application to $\vec{e}_0$ is to be described by the first j unit vectors. Thus, conversely, these first j basis vectors are also to be constructed by the j-fold application of $\hat{\mathscr{L}}$. The calculation of this $c_{n,j}$ is explained in the Appendix A. Now let scalar product

$$\vec{s} \cdot \vec{x}(t) = \sum_{n=0}^{R} \vec{s} \cdot \vec{e}_n \vec{e}_n \cdot \vec{x}(t) \tag{5.2.14}$$

$$= \sum_{n=0}^{R} s_n \sum_{j=0}^{n} c_{j,n} \left(\hat{\mathscr{L}}^j \vec{e}_0 \right) \vec{x}(t) \tag{5.2.15}$$

be considered again. From the representation of the Liouvillian in Eq. (5.2.2), it can be seen that

$$\hat{\mathscr{L}}^\dagger = -\hat{\mathscr{L}}. \tag{5.2.16}$$

From this follows

$$\vec{s} \cdot \vec{x}(t) = \sum_{n=0}^{R} s_n \sum_{j=0}^{n} c_{j,n} \vec{e}_0 (-\hat{\mathscr{L}})^j \vec{x}(t). \tag{5.2.17}$$

Using Eq. (5.2.4), it further follows that

$$\vec{s}\cdot\vec{x}(t) = \sum_{n=0}^{R} s_n \sum_{j=0}^{n} c_{j,n}(-1)^j \vec{e}_0 \frac{d^j}{dt^j}\vec{x}(t) \tag{5.2.18}$$

$$= \underbrace{\sum_{n=0}^{R} s_n \sum_{j=0}^{n} c_{j,n}(-1)^j \frac{d^j}{dt^j}}_{\mathrm{D}} x_0(t) \tag{5.2.19}$$

$$= \mathrm{D}x_0(t) \tag{5.2.20}$$

is equivalent, where D is a linear differential operator of R-th order. Now, if $\vec{s}$ is orthogonal to $\vec{x}(t)$, then

$$\mathrm{D}x_0(t) = 0 \tag{5.2.21}$$

is valid, where the solution takes the form $\sum_{n=1}^{R} \alpha_n \mathrm{e}^{\lambda_n t}$.
Since the corresponding matrix $\hat{\mathscr{L}}_R$ is real, the solution must be real too, so for every $\lambda_n \in \mathrm{C}$ there must be another λ_m with $\lambda_n = \lambda_m^\star$. Thus, the solution corresponds to a superposition of damped oscillations (exponential decay also belongs to that group of functions as a special case $R = 1$). Moreover, this is also possible in the opposite way: If the dynamic corresponds to a superposition of damped oscillations, then there must also be an orthogonal $\vec{s}$.
The determination of $\vec{s}$ from already known λ_n is significantly easier than the reverse conclusion. This is due to the fact that for the conversion in one direction the zeros of a polynomial of order R have to be determined, while in the reverse case only a coefficient comparison of such a polynomial is necessary.
Since many relaxation dynamics have the form of damped oscillations (or even exponential decays), it can be assumed that the Lanczos coefficients of those dynamics have a structure which allows very short orthogonal vectors. A possible link for further research is to investigate which coefficients allow short orthogonal vectors. The goal of this further research could be, stability investigations on such coefficients, which could be used as a justification for the frequent finding of those curves in everyday systems (see Ref. [2]). Should a criterion for the coefficients be found which favors such a truncation, one could infer the dynamics directly from the coefficients, which is not possible in the general case.
Thus, it was found that all three perspectives described here are equivalent to each other: A smooth behavior of the chain links x_n are equivalent to an orthogonal vector $\vec{s}$ and a good fitting using damped oscillations.

5.3 Approximation of the integral via truncation of the chain

Another advantage of the previously described truncation is that it allows the expression

$$A = \lim_{\tau\to\infty} \int_0^\tau \tilde{C}(t)dt \tag{5.3.1}$$

to be estimated. Note that although τ should approach ∞, for finite systems the part of the echo should be neglected in the sense of the Poincare return [12]. This quantity plays a significant role in particular in transport theory, provided that $\tilde{C}(t)$ is the autocorrelation function of currents [4]. If that quantity diverges for larger times, then non-vanishing currents corresponding to ballistic transport are evident. That quantity is thus closely related to the concept of Drude weight [71, 72]. If and when such a Drude weight is non-vanishing in the thermodynamic limit is still part of ongoing research. Thus, an estimation of that quantity could be proof of use. For estimation, the special case

$$\gamma_n = \delta_{(R-1)n} \tag{5.3.2}$$

is used, where δ_{ij} is the Kronecker delta. This corresponds to the approximation

$$x_R(t) \approx x_{R-1}(t). \tag{5.3.3}$$

This results in a $R \times R$ matrix

$$\hat{\mathscr{L}}_R = \begin{pmatrix} 0 & -b_1 & 0 & \cdots & 0 \\ b_1 & 0 & -b_2 & \ddots & \vdots \\ 0 & b_2 & \ddots & \ddots & 0 \\ \vdots & \ddots & \ddots & \ddots & -b_{R-1} \\ 0 & \cdots & 0 & b_{R-1} & -b_R \end{pmatrix}. \tag{5.3.4}$$

Thus, for those new replacement dynamics, it follows

$$\vec{\chi}(t) = e^{\hat{\mathscr{L}}_R t}\vec{e_0} \tag{5.3.5}$$

which satisfies the differential equation

$$\dot{\vec{\chi}}(t) = \hat{\mathscr{L}}_R\vec{\chi}(t). \tag{5.3.6}$$

By using Laplace transformation it can be seen that

$$s\mathcal{L}\left\{\vec{\chi}(t)\right\}(s) - \vec{\chi}(t=0) = \hat{\mathscr{L}}_R\mathcal{L}\left\{\vec{\chi}\right\}(s) \tag{5.3.7}$$

with

$$\mathcal{L}\left\{f(t)\right\}(s) = \int_0^\infty f(t)e^{st}dt \tag{5.3.8}$$

holds. Since the above expression yields the desired integration for $s = 0$, this is substituted into Eq. (5.3.7). It follows

$$-\vec{e}_0\hat{\mathscr{L}}_R^{-1}\vec{e}_0 = \mathcal{L}\left\{\chi_0\right\}(s=0) \tag{5.3.9}$$

where the right-hand side corresponds to the wanted integration. Thus, the determination of the integration of the substitute dynamics is rather simple with the negative first element of the inverted substitute matrix. This procedure is generally possible for other choices of γ_n[63] as well, but the simple choice from Eq. (5.3.2) allows the expression for the inverted element to be given explicitly:

$$-\vec{e}_0\hat{\mathscr{L}}_R^{-1}\vec{e}_0 = \frac{1}{b_1}\prod_{n=1}^{R-1}\left(\frac{b_n}{b_{n+1}}\right)^{(-1)^n} := A_R. \tag{5.3.10}$$

Two different derivations of this expression are shown in Appendix B. Note that A_R is always finite for an arbitrary but fixed R[64]. Since this kind of truncation results in substitute dynamics, which are superpositions of damped oscillations, one can conclude that all damping coefficients are non-negative. Thus, there is no exponential increase. From the Mori chain model, it is also apparent that divergences between the replacement dynamics and the original can only occur when the chain termination is reached. The larger R is, the latter is that point in time. It follows that for arbitrarily long time periods, one can create good substitute dynamics by letting $R \to \infty$ go. Applying the logarithm to the above expression, yields the equation

$$\ln(A_R) = -\ln(b_1) + \sum_{n=1}^{R-1}\ln\left(\left(\frac{b_n}{b_{n+1}}\right)^{(-1)^n}\right) \tag{5.3.11}$$

$$= -\ln(b_1) + \sum_{n=1}^{R-1}(-1)^n\ln\left(\frac{b_n}{b_{n+1}}\right) \tag{5.3.12}$$

As long as $b_n > 0$ holds for all n [65], $\ln(A_R)$ is a finite value. In this form, the alternating sign shows that the Leibniz criterion is suitable for an investigation of convergence. That criterion states that series of the form

$$\sum_{n=0}^{\infty}(-1)^n\alpha_n \tag{5.3.13}$$

converge if α_n is monotonically increasing (or decreasing) towards zero. Considering Eq. (5.3.12), it is to prove that $\ln\left(\frac{b_n}{b_{n+1}}\right)$ is such a sequence. Since $\ln(x)$ is monotonically increasing, this holds when $\frac{b_n}{b_{n+1}}$ is a monotone function with $\lim_{n\to\infty}\frac{b_n}{b_{n+1}} = 1$. This is the case, for example, for $b_n = \alpha n^\gamma$ as long as $\alpha > 0$ holds (since for finite R the values are always convergent, it suffices if above a certain R^*). For these cases, it follows that $\lim_{R\to\infty}\ln(A_R) = \ln(A_\infty)$ converges to a finite value. Moreover, the Leibniz criterion also yields convergence bounds; it holds

$$\ln(A_R) < \ln(A_\infty) < \ln(A_{R+1}) \qquad \text{for } \ln(A_R) < \ln(A_{R+1}) \tag{5.3.14}$$

$$\ln(A_{R+1}) < \ln(A_\infty) < \ln(A_R) \qquad \text{for } \ln(A_{R+1}) < \ln(A_R), \tag{5.3.15}$$

that is, the convergence value lies between two following partial sums. Since the exponential function does not have a definition gap and is monotone increasing, convergence also follows for the integral and the above estimations can be transferred, too, from which follows

$$A_R < A_\infty < A_{R+1} \text{ for } A_R < A_{R+1} \tag{5.3.16}$$

$$A_{R+1} < A_\infty < A_R \text{ for } A_{R+1} < A_R. \tag{5.3.17}$$

[63] As long as the substitute matrix is invertible.
[64] There exists an exception at $b_n = 0$, but in that case the chain is broken anyway.
[65] This is assumed throughout the following, since this corresponds to a natural termination of the chain anyway.

Since, as argued above, the substitute dynamics and the real dynamics yield equivalent results for $R \to \infty$ of arbitrary length, the logical conclusion is that $A_\infty = A$ holds. Thus, it is shown that a monotone continuation of the coefficients always suppresses ballistic transport.
Since A_∞ is always between two neighboring A_R, the averaging of two such values seems reasonable. Here, the geometric mean is used, which is hereby introduced as

$$A_R^{\mathrm{GM}} = \sqrt{A_R \cdot A_{R-1}}. \tag{5.3.18}$$

If one now inserts Eq. (5.3.10), one obtains

$$A_R^{\mathrm{GM}} = \sqrt{\frac{1}{b_1}\prod_{n=1}^{R-1}\left(\frac{b_n}{b_{n+1}}\right)^{(-1)^n} \cdot \frac{1}{b_1}\prod_{n=1}^{R-2}\left(\frac{b_n}{b_{n+1}}\right)^{(-1)^n}} \tag{5.3.19}$$

$$= \sqrt{\frac{b_2}{b_1^3}\prod_{n=1}^{R-2}\left(\frac{b_n b_{n+2}}{b_{n+1}^2}\right)^{(-1)^n}}. \tag{5.3.20}$$

To determine the convergence of that expression, consider the logarithm in a similar way as above;

$$2 \cdot \ln\left(A_R^{\mathrm{GM}}\right) = \ln\left(\frac{b_2}{b_1^3}\right) + \sum_{n=1}^{R-1}(-1)^n \ln\left(\frac{b_n b_{n+2}}{b_{n+1}^2}\right) \tag{5.3.21}$$

which again shows a possible application of the Leibniz criterion. Thus, this geometric mean converges if $\frac{b_n b_{n+2}}{b_{n+1}^2}$ is a sequence which is monotonically approaching 1.
The geometric mean in Eq. (5.3.18) was already used in Ref. [73]. There, no statement could be made about the individual A_R, because it contains an unknown prefactor k_R depending on R[66]. However, it was assumed that $\lim_{R\to\infty} \frac{k_R}{k_{R+1}} = 1$ should hold[67]. Moreover, the convergence has been checked for various systems which can be studied analytically and yields good results.
However, no proof of convergence was shown in that paper, moreover, there is also a strict distinction between even and odd R within the notation, while the notation within this thesis is uniform for both cases.
By the similarity of the convergence conditions of A_R as well as its geometric mean, the question arises whether a repeated geometric mean also allows a form which is to be examined again by means of Leibniz. Indeed, such an averaging is always possible, resulting in the averaged area of

$$A_R^F = \sqrt[2^{(F-1)}]{\mathtt{c}_F \cdot \prod_{n=1}^{R-F} \mathtt{b}_{n,F}^{(-1)^n}} \tag{5.3.22}$$

with

$$\mathtt{c}_F = \prod_{j=1}^{F} b_j^{(-1)^j \cdot (2^F - \sum_{l=0}^{j-1}\binom{F}{l})} \tag{5.3.23}$$

$$\mathtt{b}_{n,F} = \prod_{j=n}^{F+n} b_j^{\left((-1)^{(j-n)} \cdot \binom{F}{j-n}\right)}. \tag{5.3.24}$$

[66] The approximation in this thesis results in $k_R = b_R$.
[67] Remark that this is also a necessary requirement for the usage of the Leibniz criterion.

Here F is the order of the averaging ($F = 1$ is for example without geometric averaging, $F = 2$ corresponds to the above case of simple geometric averaging etc.). $\binom{n}{k}$ corresponds to the binomial coefficient.
The derivation is done by complete induction and can be taken from Appendix C.
$\mathtt{c}_F$ is not relevant for the convergence itself, because this only leads to a constant prefactor[68]. By means of logarithm and Leibniz criterion, it can be seen that the surface converges if $\mathtt{b}_{n,F}$ approaches monotonically towards 1.
In the following, a few cases are discussed, in which the resulting area and the coefficients are known. The exact derivations can be found in Ref. [73] and the sources therein. The cases can be seen in Tab. 2.
It is easy to see that every possible estimation of the area of the kind mentioned above always yields

Nr.	Coefficient	Dynamic	Analytical integral
1	$b_n = 1$	$C(t) = \frac{J_1(2t)}{t}$	$A_\infty = 1$
2	$b_n = n$	$C(t) = \operatorname{sech}(t)$	$A_\infty = \frac{\pi}{2}$
3	$b_n = \sqrt{n}$	$C(t) = e^{-\frac{t^2}{2}}$	$A_\infty = \sqrt{\frac{\pi}{2}}$
4	$b_n = \begin{cases} \sqrt{\frac{n+2}{3}} & \text{n odd} \\ \sqrt{\frac{n}{3}} & \text{n even} \end{cases}$	$C(t) = (1 - \frac{1}{3}t^2) \cdot e^{-\frac{t^2}{6}}$	$A_\infty = 0$

Table 2: Analytically known cases of Mori chains and the resulting integration of the autocorrelation function.

a perfect estimation for the first case, since these estimations always consist only of products of the coefficients. In the case that those are all 1, every result is 1 and thus exactly equal to the analytical result.
Since the other cases are not trivial, the investigations here will be numerical, where a symbolic treatment provides very high accuracy. For this reason the quantity

$$\Delta A_R = \frac{|A_R - A_\infty|}{A_\infty} \tag{5.3.25}$$

is introduced, whereby A_∞ is the exact value of the integral[69]. For the case 4 in Tab. 2, $|A_R - A_\infty|$ is considered as an indicator, since $A_\infty = 0$ makes the usage of ΔA_R impossible.
Now consider the second case, $b_n = n$. Firstly, it shall be shown that

$$\lim_{n\to\infty} \mathtt{b}_{n,F} = 1 \tag{5.3.26}$$

holds. A useful property of the binomial coefficients for this reason is

$$\sum_{j=1} \binom{F}{2j-1} = 2^{F-1} = \sum_{j=1} \binom{F}{2j}. \tag{5.3.27}$$

[68] In the logarithmic representation this corresponds to an offset.
[69] If the exact value is not known, a common numerical integration is chosen for comparison.

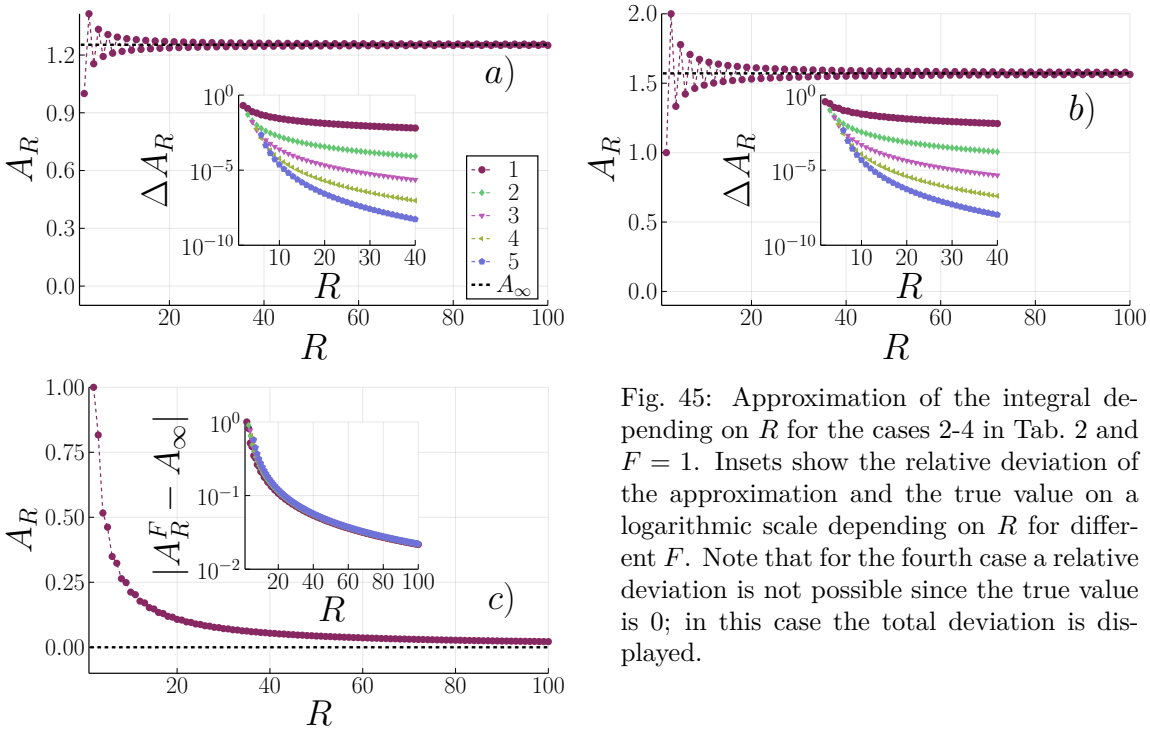

Fig. 45: Approximation of the integral depending on R for the cases 2-4 in Tab. 2 and $F = 1$. Insets show the relative deviation of the approximation and the true value on a logarithmic scale depending on R for different F. Note that for the fourth case a relative deviation is not possible since the true value is 0; in this case the total deviation is displayed.

With this knowledge, it is easy to see that in Eq. (5.3.24) the denominator and the nominator contain the same number of Lanczos coefficients. For the considered special case, all coefficients have the form of $(n + j)$, such that the resulting fraction is a fraction of two polynomials of order 2^{F-1} without any prefactor. Since for large n the highest order dominates the fraction, the fraction approaches 1.

In addition to this limit, it is also necessary that the series is monotone, which is shown in Appendix D. This is also displayed for the $F \leq 5$ in Fig. 45 a). Thereby it can be seen that repeatedly averaging yields better results as long R is a bit larger than F. However, a very high precision is already reached after a few averages, so that large F are not necessary in this case.

The convergence of the third case is equivalent to the convergence of the second case, since the coefficients differ only by an exponent, which in the logarithmic representation corresponds only to a prefactor, which is not relevant for the convergence[70]. Thus, the results in Fig. 45 c) are quite similar as in b). Note that the comparison is made with the same amount of b_n used. This shows that averaging often yields better results without having to determine more coefficients. Since the determination of those coefficients is very time-consuming for many models and the number of those is strongly limited by the numerics, this insight could be helpful to achieve nevertheless quite precise results.

The last case in Tab. 2 does not fulfill the conditions of the Leibniz criterion due to a strong even-odd effect, so that convergence is not necessarily present here. Nevertheless, it was shown in Ref. [73] that the one-time geometric mean ($F = 2$) converges to the analytically known value. This is also shown in Fig. 45, but this convergence is much slower than in the other cases. In addition, it can be seen that further geometric averaging slows down the convergence. This could indicate an increasing

[70] Note that if b_n are convergence that all $\alpha \cdot b_n^\gamma$ are also convergence, as long all parameters are positive.

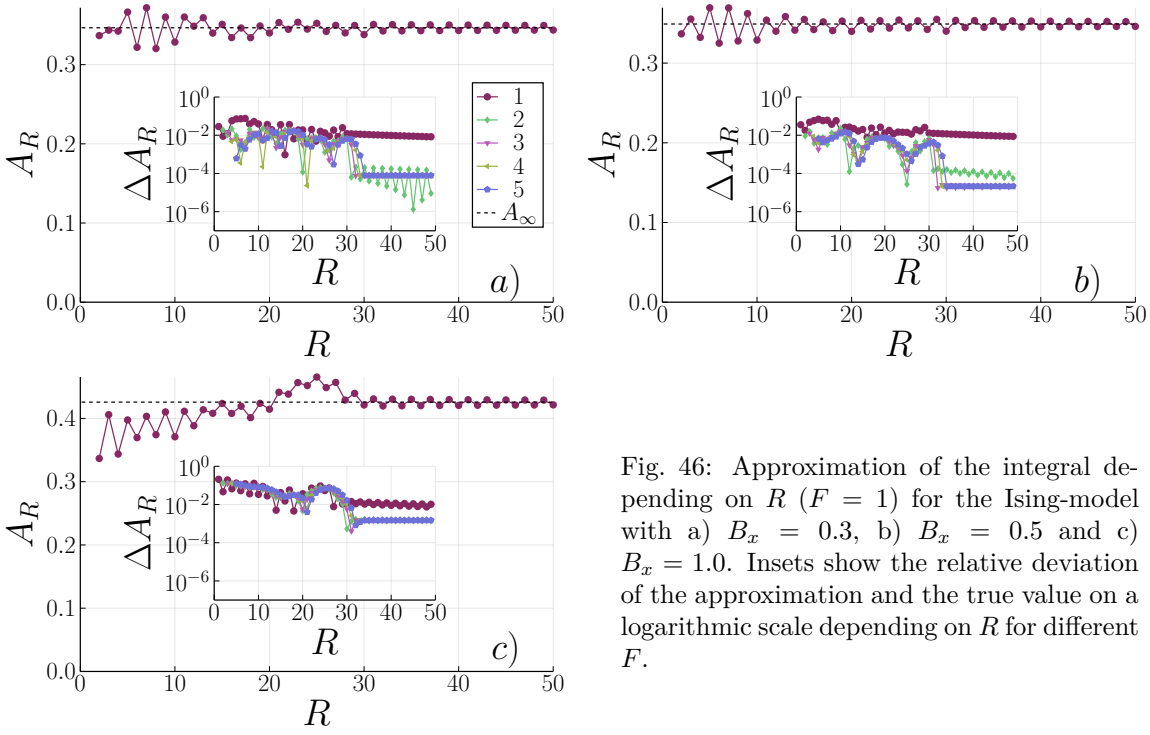

Fig. 46: Approximation of the integral depending on R ($F = 1$) for the Ising-model with a) $B_x = 0.3$, b) $B_x = 0.5$ and c) $B_x = 1.0$. Insets show the relative deviation of the approximation and the true value on a logarithmic scale depending on R for different F.

sensitivity to even-odd effects at higher F. Furthermore, the estimation of integrals without averaging yields the best results, so that the method introduced here allows an improved estimation. Furthermore, it can be seen that although the system appears to converge, A_∞ is not between two consecutive A_R. This is not surprising since that property follows from the Leibniz criterion, but it is still worth mentioning since that situation does not allow for an upper and lower bound of the limit.

Furthermore, the area estimation is to be examined also on the basis of the test system. Since no analytical expression of the integral is known in this case, the integral is determined numerically, so that the comparison value can already contain numerical uncertainties. Thereby in Fig. 46 the convergence for different B_x, R and F is displayed. In the latter, it can be seen that the approximation is close to the comparison value even before the range of linear continuation. In addition, it shows that the geometric mean improves the results strongly, but further averaging does not bring any further advantage. The cases with very weak magnetic fields ($B_x \leq 0.1$) are neglected, since the dynamics of these systems are still far from over by the time the end of the chain is reached. Thus, it is not possible to determine the integral by numerical means. This finding is purely numerical and is counterintuitive, since these systems actually have a larger time τ_b due to the smaller slope. Convergence seems to be approached much slower in all treated cases of the Ising model than in the analytical cases. Nevertheless, an estimate is possible, which deviates only a few percent from the comparison value. At this point, however, it should also be mentioned that the comparison value is also based on the linear continuation. An analysis of how sensitive this estimation reacts to perturbations is an interesting question for further research and represents a possible continuation of this work. Also the investigation under which conditions the individual $\mathfrak{b}_{n,F}$ satisfies the Leibniz criterion, as well as under which conditions the averaging represents an improvement of the results

could be further starting points.

5.4 Conclusion

Altogether, it is shown that the consideration of the Mori chain offers promising and manifold grounds for tackling unsolved problems of quantum thermodynamics, despite the age of that representation. In particular, although the OGH does not provide a way to exactly increase the strongly limited number of coefficients, it does provide a general way to justifiably continue the already known coefficients.
Especially since the investigations discussed here strongly show one of the core properties of thermodynamics, namely the reduction of the necessary parameters for the description of systems. However, it should not be concealed that the results shown here are far from being really understood. Thus, it is still questionable when the breaking of the chain is well possible and, moreover, whether such breaking follows general laws, so that knowledge of the dynamics would no longer be necessary to produce a well-behaved breaking of the chain. Also, a possible linkage of the stability of some types of dynamics is a promising continuation.
Although the estimation of the integral has shown excellent results for the analytic cases and has also given good results in the test system, there are still some open questions: Can better results possibly be obtained with other types of chain termination? How does the estimation react to perturbations? Can statements be made about an optimal number of averages?
Other ways of reducing the Mori chain are discussed in Ref. [74] where it was shown in some cases that already the first two Lanczos coefficients contain a lot of information about the form of the actual dynamics.

6 Conclusion and outlook

The results of this work can be summarized in two categories.
In the first category the results of Sections 3-4 can be placed. Specifically, in the former, a method has been developed which allows the detection of correlations between matrix elements in observables in the energy eigenbasis. Thus, it is shown that considering those observables as random matrices is inaccurate. In particular, since many previous studies of systems have failed to find deviations from random matrices even in energy/frequency windows, this result is relevant. This relevance is also shown in Section 5, where a theory based on the randomness of the matrix elements was tested. It was found that TPT either did not yield good results in the systems studied or that these results could be explained outside the theory.
The results of Section 3, in particular, are part of continuing research: Even if it has been shown that comparisons with pure random matrices are invalid, the question still arises as to why so many indicators have previously failed to distinguish between random matrices and observables. The exact nature of the correlations remains unexplained; the implications of those correlations also have yet to be determined. Especially in the context of TPT, the question arises whether that theory can be adapted to account for the existing correlations.
The second category is to be understood in the sense of the so far unpublished results in Section 5. In particular, it shows the potential of a benign truncation of the Mori chain. Should a general break-off be possible, statements could be made about the form of the dynamics itself. In addition, links to the investigation of stable dynamics can be found. Furthermore, it could be shown that statements about the integral of the curve can already be made under relatively mild assumptions. An extension of these statements and further softening of the conditions seems to be desirable for the investigation of transport properties of diverse systems.
In addition, a technical result of this work should be pointed out, which itself does not provide any new physical knowledge, but shows new possibilities of investigations: The method of filtering energy introduced in Subsection 3.1 offers the possibility to consider future investigations in energy windows, even outside the ED domain.

References

[P1] J. Wang, M. H. Lamann, J. Richter, R. Steinigeweg, A. Dymarsky, and J. Gemmer. "Eigenstate Thermalization Hypothesis and Its Deviations from Random-Matrix Theory beyond the Thermalization Time". In: *Phys. Rev. Lett.* 128 (18 May 2022), p. 180601. DOI: 10.1103/PhysRevLett.128.180601. URL: https://link.aps.org/doi/10.1103/PhysRevLett.128.180601.

[P2] M. H. Lamann and J. Gemmer. "Typical perturbation theory: Conditions, accuracy, and comparison with a mesoscopic case". In: *Phys. Rev. E* 106 (5 Nov. 2022), p. 054148. DOI: 10.1103/PhysRevE.106.054148. URL: https://link.aps.org/doi/10.1103/PhysRevE.106.054148.

[1] J. Gemmer, M. Michel, and G. Mahler. *Quantum Thermodynamics*. Springer Berlin Heidelberg, 2009. DOI: 10.1007/978-3-540-70510-9. URL: https://doi.org/10.1007/978-3-540-70510-9.

[2] R. Heveling, J. Wang, C. Bartsch, and J. Gemmer. "Stability of exponentially damped oscillations under perturbations of the Mori-Chain". In: *Journal of Physics Communications* 6.8 (Aug. 2022), p. 085009. DOI: 10.1088/2399-6528/ac863b. URL: https://dx.doi.org/10.1088/2399-6528/ac863b.

[3] W. Nolting. *Grundkurs Theoretische Physik 5/2*. Springer Berlin Heidelberg, 2015. DOI: 10.1007/978-3-662-44230-2. URL: https://doi.org/10.1007/978-3-662-44230-2.

[4] R. Kubo, M. Toda, and N. Hashitsume. *Statistical Physics II*. Springer Berlin Heidelberg, 1991. DOI: 10.1007/978-3-642-58244-8. URL: https://doi.org/10.1007/978-3-642-58244-8.

[5] C. Bartsch and J. Gemmer. "Dynamical Typicality of Quantum Expectation Values". In: *Phys. Rev. Lett.* 102 (11 Mar. 2009), p. 110403. DOI: 10.1103/PhysRevLett.102.110403. URL: https://link.aps.org/doi/10.1103/PhysRevLett.102.110403.

[6] P. Reimann and J. Gemmer. "Why are macroscopic experiments reproducible? Imitating the behavior of an ensemble by single pure states". In: *Physica A: Statistical Mechanics and its Applications* 552 (Aug. 2020), p. 121840. DOI: 10.1016/j.physa.2019.121840. URL: https://doi.org/10.1016/j.physa.2019.121840.

[7] T. Heitmann, J. Richter, D. Schubert, and R. Steinigeweg. "Selected applications of typicality to real-time dynamics of quantum many-body systems". In: *Zeitschrift für Naturforschung A* 75.5 (Apr. 2020), pp. 421–432. DOI: 10.1515/zna-2020-0010. URL: https://doi.org/10.1515/zna-2020-0010.

[8] B. N. Balz, J. Richter, J. Gemmer, R. Steinigeweg, and P. Reimann. "Dynamical typicality for initial states with a preset measurement statistics of several commuting observables". In: *Thermodynamics in the Quantum Regime*. Vol. 195. Fundamental Theories of Physics. Springer, 2019, p. 413. URL: http://dx.doi.org/10.1007/978-3-319-99046-0_17.

[9] A. Iwaki and C. Hotta. "Purity of thermal mixed quantum states". In: *Phys. Rev. B* 106 (9 Sept. 2022), p. 094409. DOI: 10.1103/PhysRevB.106.094409. URL: https://link.aps.org/doi/10.1103/PhysRevB.106.094409.

[10] J. Richter and R. Steinigeweg. "Combining dynamical quantum typicality and numerical linked cluster expansions". In: *Physical Review B* 99.9 (Mar. 2019). DOI: 10.1103/physrevb.99.094419. URL: https://doi.org/10.1103/physrevb.99.094419.

[11] R. Edgeworth, B. J. Dalton, and T. Parnell. "The pitch drop experiment". In: *European Journal of Physics* 5.4 (Oct. 1984), pp. 198–200. DOI: 10.1088/0143-0807/5/4/003. URL: https://doi.org/10.1088/0143-0807/5/4/003.

[12] H. Poincaré. "Sur le problème des trois corps et les équations de la dynamique". In: *Acta Mathematica* 13.1-2 (1890), pp. 5–7. DOI: 10.1007/bf02392506. URL: https://doi.org/10.1007/bf02392506.

[13] J. von Neumann. "Proof of the ergodic theorem and the H-theorem in quantum mechanics". In: *The European Physical Journal H* 35.2 (Sept. 2010), pp. 201–237. DOI: 10.1140/epjh/e2010-00008-5. URL: https://doi.org/10.1140/epjh/e2010-00008-5.

[14] L. D'Alessio, Y. Kafri, A. Polkovnikov, and M. Rigol. "From quantum chaos and eigenstate thermalization to statistical mechanics and thermodynamics". In: *Advances in Physics* 65.3 (May 2016), pp. 239–362. DOI: 10.1080/00018732.2016.1198134. URL: https://doi.org/10.1080/00018732.2016.1198134.

[15] R. Alicki and R. Kosloff. "Introduction to Quantum Thermodynamics: History and Prospects". In: *Fundamental Theories of Physics*. Springer International Publishing, 2018, pp. 1–33. DOI: 10.1007/978-3-319-99046-0_1. URL: https://doi.org/10.1007/978-3-319-99046-0_1.

[16] M. Srednicki. "Chaos and quantum thermalization". In: *Phys. Rev. E* 50 (2 Aug. 1994), pp. 888–901. DOI: 10.1103/PhysRevE.50.888. URL: https://link.aps.org/doi/10.1103/PhysRevE.50.888.

[17] J. M. Deutsch. "Quantum statistical mechanics in a closed system". In: *Phys. Rev. A* 43 (4 Feb. 1991), pp. 2046–2049. DOI: 10.1103/PhysRevA.43.2046. URL: https://link.aps.org/doi/10.1103/PhysRevA.43.2046.

[18] M. Srednicki. "The approach to thermal equilibrium in quantized chaotic systems". In: *Journal of Physics A: Mathematical and General* 32.7 (Feb. 1999), p. 1163. DOI: 10.1088/0305-4470/32/7/007. URL: https://dx.doi.org/10.1088/0305-4470/32/7/007.

[19] T. LeBlond, K. Mallayya, L. Vidmar, and M. Rigol. "Entanglement and matrix elements of observables in interacting integrable systems". In: *Phys. Rev. E* 100 (6 Dec. 2019), p. 062134. DOI: 10.1103/PhysRevE.100.062134. URL: https://link.aps.org/doi/10.1103/PhysRevE.100.062134.

[20] D. Jansen, J. Stolpp, L. Vidmar, and F. Heidrich-Meisner. "Eigenstate thermalization and quantum chaos in the Holstein polaron model". In: *Phys. Rev. B* 99 (15 Apr. 2019), p. 155130. DOI: 10.1103/PhysRevB.99.155130. URL: https://link.aps.org/doi/10.1103/PhysRevB.99.155130.

[21] R. Mondaini and M. Rigol. "Eigenstate thermalization in the two-dimensional transverse field Ising model. II. Off-diagonal matrix elements of observables". In: *Phys. Rev. E* 96 (1 July 2017), p. 012157. DOI: 10.1103/PhysRevE.96.012157. URL: https://link.aps.org/doi/10.1103/PhysRevE.96.012157.

[22] W. Beugeling, R. Moessner, and M. Haque. "Off-diagonal matrix elements of local operators in many-body quantum systems". In: *Phys. Rev. E* 91 (1 Jan. 2015), p. 012144. DOI: 10.1103/PhysRevE.91.012144. URL: https://link.aps.org/doi/10.1103/PhysRevE.91.012144.

[23] L. Foini and J. Kurchan. "Eigenstate thermalization hypothesis and out of time order correlators". In: *Phys. Rev. E* 99 (4 Apr. 2019), p. 042139. DOI: 10.1103/PhysRevE.99.042139. URL: https://link.aps.org/doi/10.1103/PhysRevE.99.042139.

[24] J. Richter, A. Dymarsky, R. Steinigeweg, and J. Gemmer. "Eigenstate thermalization hypothesis beyond standard indicators: Emergence of random-matrix behavior at small frequencies". In: *Phys. Rev. E* 102 (4 Oct. 2020), p. 042127. DOI: 10.1103/PhysRevE.102.042127. URL: https://link.aps.org/doi/10.1103/PhysRevE.102.042127.

[25] D. Thouless. "Electrons in disordered systems and the theory of localization". In: *Physics Reports* 13.3 (Oct. 1974), pp. 93–142. DOI: 10.1016/0370-1573(74)90029-5. URL: https://doi.org/10.1016/0370-1573(74)90029-5.

[26] M. Serbyn, Z. Papi, and D. A. Abanin. "Thouless energy and multifractality across the many-body localization transition". In: *Physical Review B* 96.10 (Sept. 2017). DOI: 10.1103/physrevb.96.104201. URL: https://doi.org/10.1103/physrevb.96.104201.

[27] Y. Y. Atas, E. Bogomolny, O. Giraud, and G. Roux. "Distribution of the Ratio of Consecutive Level Spacings in Random Matrix Ensembles". In: *Phys. Rev. Lett.* 110 (8 Feb. 2013), p. 084101. DOI: 10.1103/PhysRevLett.110.084101. URL: https://link.aps.org/doi/10.1103/PhysRevLett.110.084101.

[28] V. Oganesyan and D. A. Huse. "Localization of interacting fermions at high temperature". In: *Phys. Rev. B* 75 (15 Apr. 2007), p. 155111. DOI: 10.1103/PhysRevB.75.155111. URL: https://link.aps.org/doi/10.1103/PhysRevB.75.155111.

[29] C. E. Porter and R. G. Thomas. "Fluctuations of Nuclear Reaction Widths". In: *Phys. Rev.* 104 (2 Oct. 1956), pp. 483–491. DOI: 10.1103/PhysRev.104.483. URL: https://link.aps.org/doi/10.1103/PhysRev.104.483.

[30] D. Cohen and T. Kottos. "Parametric dependent Hamiltonians, wave functions, random matrix theory, and quantal-classical correspondence". In: *Phys. Rev. E* 63 (3 Feb. 2001), p. 036203. DOI: 10.1103/PhysRevE.63.036203. URL: https://link.aps.org/doi/10.1103/PhysRevE.63.036203.

[31] T. Kottos and D. Cohen. "Failure of random matrix theory to correctly describe quantum dynamics". In: *Phys. Rev. E* 64 (6 Nov. 2001), p. 065202. DOI: 10.1103/PhysRevE.64.065202. URL: https://link.aps.org/doi/10.1103/PhysRevE.64.065202.

[32] L. Dabelow and P. Reimann. "Relaxation Theory for Perturbed Many-Body Quantum Systems versus Numerics and Experiment". In: *Phys. Rev. Lett.* 124 (12 Mar. 2020), p. 120602. DOI: 10.1103/PhysRevLett.124.120602. URL: https://link.aps.org/doi/10.1103/PhysRevLett.124.120602.

[33] L. Dabelow, P. Vorndamme, and P. Reimann. "Modification of quantum many-body relaxation by perturbations exhibiting a banded matrix structure". In: *Phys. Rev. Research* 2 (3 Aug. 2020), p. 033210. DOI: 10.1103/PhysRevResearch.2.033210. URL: https://link.aps.org/doi/10.1103/PhysRevResearch.2.033210.

[34] L. Dabelow and P. Reimann. "Typical relaxation of perturbed quantum many-body systems". In: *Journal of Statistical Mechanics: Theory and Experiment* 2021.1 (Jan. 2021), p. 013106. DOI: 10.1088/1742-5468/abd026. URL: https://doi.org/10.1088/1742-5468/abd026.

[35] V. S. Viswanath and G. Müller. *The Recursion Method*. Springer Berlin Heidelberg, 1994. DOI: 10.1007/978-3-540-48651-0. URL: https://doi.org/10.1007/978-3-540-48651-0.

[36] T. J. Park and J. C. Light. "Unitary quantum time evolution by iterative Lanczos reduction". In: *The Journal of Chemical Physics* 85.10 (Nov. 1986), pp. 5870–5876. DOI: 10.1063/1.451548. URL: https://doi.org/10.1063/1.451548.

[37] E. Rabinovici, A. Sánchez-Garrido, R. Shir, and J. Sonner. "Operator complexity: a journey to the edge of Krylov space". In: *Journal of High Energy Physics* 2021.6 (June 2021). DOI: 10.1007/jhep06(2021)062. URL: https://doi.org/10.1007/jhep06(2021)062.

[38] B. N. Parlett. *The Symmetric Eigenvalue Problem*. Society for Industrial and Applied Mathematics, Jan. 1998. DOI: 10.1137/1.9781611971163. URL: https://doi.org/10.1137/1.9781611971163.

[39] D. E. Parker, X. Cao, A. Avdoshkin, T. Scaffidi, and E. Altman. "A Universal Operator Growth Hypothesis". In: *Phys. Rev. X* 9 (4 Oct. 2019), p. 041017. DOI: 10.1103/PhysRevX.9.041017. URL: https://link.aps.org/doi/10.1103/PhysRevX.9.041017.

[40] R. Heveling, J. Wang, and J. Gemmer. "Numerically probing the universal operator growth hypothesis". In: *Phys. Rev. E* 106 (1 July 2022), p. 014152. DOI: 10.1103/PhysRevE.106.014152. URL: https://link.aps.org/doi/10.1103/PhysRevE.106.014152.

[41] H. Bethe. "Zur Theorie der Metalle". In: *Zeitschrift für Physik* 71.3-4 (Mar. 1931), pp. 205–226. DOI: 10.1007/bf01341708. URL: https://doi.org/10.1007/bf01341708.

[42] F. Franchini. *An Introduction to Integrable Techniques for One-Dimensional Quantum Systems*. Springer International Publishing, 2017. DOI: 10.1007/978-3-319-48487-7. URL: https://doi.org/10.1007/978-3-319-48487-7.

[43] P. Jordan and E. Wigner. "Über das Paulische Äquivalenzverbot". In: *Zeitschrift für Physik* 47.9-10 (Sept. 1928), pp. 631–651. DOI: 10.1007/bf01331938. URL: https://doi.org/10.1007/bf01331938.

[44] T. Holstein and H. Primakoff. "Field Dependence of the Intrinsic Domain Magnetization of a Ferromagnet". In: *Phys. Rev.* 58 (12 Dec. 1940), pp. 1098–1113. DOI: 10.1103/PhysRev.58.1098. URL: https://link.aps.org/doi/10.1103/PhysRev.58.1098.

[45] I. S. Duff, A. M. Erisman, and J. K. Reid. *Direct Methods for Sparse Matrices*. Oxford University Press, Jan. 2017. DOI: 10.1093/acprof:oso/9780198508380.001.0001. URL: https://doi.org/10.1093/acprof:oso/9780198508380.001.0001.

[46] K. Kim, M.-S. Chang, S. Korenblit, R. Islam, E. E. Edwards, J. K. Freericks, G.-D. Lin, L.-M. Duan, and C. Monroe. "Quantum simulation of frustrated Ising spins with trapped ions". In: *Nature* 465.7298 (June 2010), pp. 590–593. DOI: 10.1038/nature09071. URL: https://doi.org/10.1038/nature09071.

[47] J. Simon, W. S. Bakr, R. Ma, M. E. Tai, P. M. Preiss, and M. Greiner. "Quantum simulation of antiferromagnetic spin chains in an optical lattice". In: *Nature* 472.7343 (Apr. 2011), pp. 307–312. DOI: 10.1038/nature09994. URL: https://doi.org/10.1038/nature09994.

[48] A. Friedenauer, H. Schmitz, J. T. Glueckert, D. Porras, and T. Schaetz. "Simulating a quantum magnet with trapped ions". In: *Nature Physics* 4.10 (July 2008), pp. 757–761. DOI: 10.1038/nphys1032. URL: https://doi.org/10.1038/nphys1032.

[49] O. Breunig, M. Garst, A. Klümper, J. Rohrkamp, M. M. Turnbull, and T. Lorenz. "Quantum criticality in the spin-1/2 Heisenberg chain system copper pyrazine dinitrate". In: *Science Advances* 3.12 (2017), eaao3773. DOI: 10.1126/sciadv.aao3773. eprint: https://www.science.org/doi/pdf/10.1126/sciadv.aao3773. URL: https://www.science.org/doi/abs/10.1126/sciadv.aao3773.

[50] E. Anderson, Z. Bai, C. Bischof, S. Blackford, J. Demmel, J. Dongarra, J. Du Croz, A. Greenbaum, S. Hammarling, A. McKenney, and D. Sorensen. *LAPACK Users' Guide*. Third. Philadelphia, PA: Society for Industrial and Applied Mathematics, 1999. ISBN: 0-89871-447-8 (paperback).

[51] H. Tal-Ezer and R. Kosloff. "An accurate and efficient scheme for propagating the time dependent Schrödinger equation". In: *The Journal of Chemical Physics* 81.9 (Nov. 1984), pp. 3967–3971. DOI: 10.1063/1.448136. URL: https://doi.org/10.1063/1.448136.

[52] H. Fehske, J. Schleede, G. Schubert, G. Wellein, V. S. Filinov, and A. R. Bishop. "Numerical approaches to time evolution of complex quantum systems". In: *Physics Letters A* 373.25 (2009), pp. 2182–2188. ISSN: 0375-9601. DOI: https://doi.org/10.1016/j.physleta.2009.04.022. URL: https://www.sciencedirect.com/science/article/pii/S0375960109004927.

[53] R. V. Mises and H. Pollaczek-Geiringer. "Praktische Verfahren der Gleichungsauflösung ." In: *ZAMM - Journal of Applied Mathematics and Mechanics / Zeitschrift für Angewandte Mathematik und Mechanik* 9.2 (1929), pp. 152–164. DOI: https://doi.org/10.1002/zamm.19290090206. eprint: https://onlinelibrary.wiley.com/doi/pdf/10.1002/zamm.19290090206. URL: https://onlinelibrary.wiley.com/doi/abs/10.1002/zamm.19290090206.

[54] C. Lanczos. "An iteration method for the solution of the eigenvalue problem of linear differential and integral operators". In: *Journal of Research of the National Bureau of Standards* 45.4 (Oct. 1950), p. 255. DOI: 10.6028/jres.045.026. URL: https://doi.org/10.6028/jres.045.026.

[55] A. Dymarsky. "Bound on Eigenstate Thermalization from Transport". In: *Phys. Rev. Lett.* 128 (19 May 2022), p. 190601. DOI: 10.1103/PhysRevLett.128.190601. URL: https://link.aps.org/doi/10.1103/PhysRevLett.128.190601.

[56] T. Yoshizawa, E. Iyoda, and T. Sagawa. "Numerical Large Deviation Analysis of the Eigenstate Thermalization Hypothesis". In: *Phys. Rev. Lett.* 120 (20 May 2018), p. 200604. DOI: 10.1103/PhysRevLett.120.200604. URL: https://link.aps.org/doi/10.1103/PhysRevLett.120.200604.

[57] M. Wilkinson. "Statistical aspects of dissipation by Landau-Zener transitions". In: *Journal of Physics A: Mathematical and General* 21.21 (Nov. 1988), pp. 4021–4037. DOI: 10.1088/0305-4470/21/21/011. URL: https://doi.org/10.1088/0305-4470/21/21/011.

[58] A. Larkin and Y. Ovchinnikov. "Quasiclassical method in the theory of superconductivity". In: *JETP* 28.6 (June 1969). URL: http://jetp.ras.ru/cgi-bin/e/index/e/28/6/p1200?a=list.

[59] J. Maldacena, S. H. Shenker, and D. Stanford. "A bound on chaos". In: *Journal of High Energy Physics* 2016.8 (Aug. 2016). DOI: 10.1007/jhep08(2016)106. URL: https://doi.org/10.1007/jhep08(2016)106.

[60] M. Brenes, S. Pappalardi, M. T. Mitchison, J. Goold, and A. Silva. "Out-of-time-order correlations and the fine structure of eigenstate thermalization". In: *Physical Review E* 104.3 (Sept. 2021). DOI: 10.1103/physreve.104.034120. URL: https://doi.org/10.1103/physreve.104.034120.

[61] S. Pappalardi, F. Fritzsch, and T. Prosen. *General Eigenstate Thermalization via Free Cumulants in Quantum Lattice Systems*. 2023. DOI: 10.48550/ARXIV.2303.00713. URL: https://arxiv.org/abs/2303.00713.

[62] S. Pappalardi, L. Foini, and J. Kurchan. "Eigenstate Thermalization Hypothesis and Free Probability". In: *Physical Review Letters* 129.17 (Oct. 2022). DOI: 10.1103/physrevlett.129.170603. URL: https://doi.org/10.1103/physrevlett.129.170603.

[63] R. Heveling, L. Knipschild, and J. Gemmer. In: *Zeitschrift für Naturforschung A* 75.5 (2020), pp. 475–481. DOI: doi:10.1515/zna-2020-0034. URL: https://doi.org/10.1515/zna-2020-0034.

[64] L. Knipschild and J. Gemmer. "Stability of quantum dynamics under constant Hamiltonian perturbations". In: *Phys. Rev. E* 98 (6 Dec. 2018), p. 062103. DOI: 10.1103/PhysRevE.98.062103. URL: https://link.aps.org/doi/10.1103/PhysRevE.98.062103.

[65] J. Richter, F. Jin, L. Knipschild, H. D. Raedt, K. Michielsen, J. Gemmer, and R. Steinigeweg. "Exponential damping induced by random and realistic perturbations". In: *Physical Review E* 101.6 (June 2020). DOI: 10.1103/physreve.101.062133. URL: https://doi.org/10.1103/physreve.101.062133.

[66] T. Mori, T. N. Ikeda, E. Kaminishi, and M. Ueda. "Thermalization and prethermalization in isolated quantum systems: a theoretical overview". In: *Journal of Physics B: Atomic, Molecular and Optical Physics* 51.11 (May 2018), p. 112001. DOI: 10.1088/1361-6455/aabcdf. URL: https://doi.org/10.1088/1361-6455/aabcdf.

[67] T. FlieSSbach. *Statistische Physik*. Springer Berlin Heidelberg, 2018. DOI: 10.1007/978-3-662-58033-2. URL: https://doi.org/10.1007/978-3-662-58033-2.

[68] H. Binder. *Lexikon der chemischen Elemente*. 1st ed. Stuttgart, Germany: Hirzel, S., Verlag, 1999.

[69] J. Oitmaa, M. Plischke, and T. A. Winchester. "High-temperature dynamics of the Ising model in a transverse field". In: *Phys. Rev. B* 29 (3 Feb. 1984), pp. 1321–1332. DOI: 10.1103/PhysRevB.29.1321. URL: https://link.aps.org/doi/10.1103/PhysRevB.29.1321.

[70] K. N. Pak. "On the Dynamics of Hydrogen-Bonded Ferroelectrics". In: *physica status solidi (b)* 74.2 (Apr. 1976), pp. 673–682. DOI: 10.1002/pssb.2220740228. URL: https://doi.org/10.1002/pssb.2220740228.

[71] B. Bertini, F. Heidrich-Meisner, C. Karrasch, T. Prosen, R. Steinigeweg, and M. nidari . "Finite-temperature transport in one-dimensional quantum lattice models". In: *Rev. Mod. Phys.* 93 (2 May 2021), p. 025003. DOI: 10.1103/RevModPhys.93.025003. URL: https://link.aps.org/doi/10.1103/RevModPhys.93.025003.

[72] F. Heidrich-Meisner, A. Honecker, and W. Brenig. "Transport in quasi one-dimensional spin-1/2 systems". In: *The European Physical Journal Special Topics* 151.1 (Dec. 2007), pp. 135–145. DOI: 10.1140/epjst/e2007-00369-2. URL: https://doi.org/10.1140/epjst/e2007-00369-2.

[73] C. Joslin and C. Gray. "Calculation of transport coefficients using a modified Mori formalism". In: *Molecular Physics* 58.4 (July 1986), pp. 789–797. DOI: 10.1080/00268978600101571. URL: https://doi.org/10.1080/00268978600101571.

[74] R. Zhang and H. Zhai. *Universal Hypothesis of Autocorrelation Function from Krylov Complexity*. 2023. DOI: 10.48550/ARXIV.2305.02356. URL: https://arxiv.org/abs/2305.02356.

[75] H. Jeffreys and B. Jeffreys. *Cambridge mathematical library: Methods of mathematical physics*. en. 3rd ed. Cambridge, England: Cambridge University Press, Nov. 1999.

A Calculation of the coefficients for the developing the basisstates via usage of the Liouvillian

To determine the coefficients in Eq. (5.2.13), firstly multiply $\vec{e}_m$ from left on the equation;

$$\delta_{nm} = \sum_{j=0}^{n} c_{j,n} \vec{e}_m \hat{\mathscr{L}}^j \vec{e}_0. \tag{A.1}$$

Since the Liouvillian only connects neighboring states, it follows consequently that

$$\vec{e}_m \hat{\mathscr{L}}^j \vec{e}_0 = 0 \qquad \text{for } m > j \tag{A.2}$$

holds. Thus, the equation can be simplified to

$$\delta_{nm} = \sum_{j=m}^{n} c_{j,n} \vec{e}_m \hat{\mathscr{L}}^j \vec{e}_0, \tag{A.3}$$

which reduces even more for the case $m = n$. Then

$$1 = c_{n,n} \vec{e}_n \hat{\mathscr{L}}^n \vec{e}_0 \tag{A.4}$$

$$\Rightarrow c_{n,n} = \frac{1}{\vec{e}_n \hat{\mathscr{L}}^n \vec{e}_0} \tag{A.5}$$

holds. All other coefficients can be calculated iterative, since for $m < n$

$$0 = \sum_{j=m}^{n} c_{j,n} \vec{e}_m \hat{\mathscr{L}}^j \vec{e}_0 \tag{A.6}$$

$$\Rightarrow c_{m,n} = -\sum_{j=m+1}^{n} c_{j,n} \frac{\vec{e}_m \hat{\mathscr{L}}^j \vec{e}_0}{\vec{e}_m \hat{\mathscr{L}}^m \vec{e}_0} \tag{A.7}$$

holds. Thus, one can determine all coefficients in an iterative way.

B Derivation of the area approximation via Continued Fraction and inversion of the reduced Liouvillian

Two derivations of Eq. (5.3.10) shall be shown in this section.
The first derivation is based on the matrix notation. Hereby

$$\hat{\mathscr{L}}_R^{-1} = \frac{1}{\det(\hat{\mathscr{L}}_R)}\mathrm{adj}(\hat{\mathscr{L}}_R) \tag{B.1}$$

shall be used as a starting point. adj(•) denotes the adjunct of the matrix and det(•) is the determinant. Since only the 0-th element on the diagonal[71] is needed, one obtains

$$\vec{e}_0\hat{\mathscr{L}}_R^{-1}\vec{e}_0 = \frac{1}{\det(\hat{\mathscr{L}}_R)}\vec{e}_0\mathrm{adj}(\hat{\mathscr{L}}_R)\vec{e}_0. \tag{B.2}$$

Focus on the determinant

$$\det(\hat{\mathscr{L}}_R) = \begin{vmatrix} 0 & -b_1 & 0 & \cdots & 0 \\ b_1 & 0 & -b_2 & \ddots & \vdots \\ 0 & b_2 & \ddots & \ddots & 0 \\ \vdots & \ddots & \ddots & \ddots & -b_{R-1} \\ 0 & \cdots & 0 & b_{R-1} & -b_R \end{vmatrix} \tag{B.3}$$

$$= b_1 \cdot \begin{vmatrix} -b_1 & 0 & 0 & \cdots & 0 \\ b_2 & 0 & -b_3 & \ddots & \vdots \\ 0 & b_3 & 0 & \ddots & 0 \\ \vdots & \ddots & \ddots & \ddots & b_{R-1} \\ 0 & \cdots & 0 & b_{R-1} & -b_R \end{vmatrix} = b_1^2 \begin{vmatrix} 0 & -b_3 & 0 & \cdots & 0 \\ b_3 & 0 & -b_4 & \ddots & \vdots \\ 0 & b_4 & \ddots & \ddots & 0 \\ \vdots & \ddots & \ddots & \ddots & -b_{R-1} \\ 0 & \cdots & 0 & b_{R-1} & -b_R \end{vmatrix}. \tag{B.4}$$

[71] Note that in the Lanczos notation all indices started with 0.

It is easy to see that now this method can be repeatedly used until either the determinant of a 3×3 or a 2×2 matrix is the only thing left to calculate. This two cases results in

$$\left|\begin{pmatrix} 0 & -b_R \\ b_r & -b_R \end{pmatrix}\right| = b_R^2 \qquad \left|\begin{pmatrix} 0 & -b_{R-1} & 0 \\ b_{R-1} & 0 & -b_R \\ 0 & b_R & -b_R \end{pmatrix}\right| = -b_{R-1}^2 \cdot b_R. \tag{B.5}$$

Thus in total one obtains

$$\det(\hat{\mathscr{L}}_R) = \prod_{n=1}^{\lceil R/2\rceil} b_{2n-1}^2 \cdot \begin{cases} 1 & \text{for } R \text{ odd} \\ -b_R & \text{for } R \text{ even} \end{cases} \tag{B.6}$$

$$= (-b_R)^{\frac{1+(-1)^R}{2}} \cdot \prod_{n=1}^{R} (b_n)^{1-(-1)^n} \tag{B.7}$$

where the exponents ensure the even-odd effect.
The knowledge of these kinds of determinants are helpful, also for calculating the 0-th element of the adjunct, since this is equivalent to the determinant for the matrix just without the 0-th row and column. This new matrix has the same structure as the original one, thus one obtains via the same approach as before

$$\vec{e}_0 \mathrm{adj}(\hat{\mathscr{L}}_R)\vec{e}_0 = (-b_R)^{\frac{1-(-1)^R}{2}} \cdot \prod_{n=2}^{R} (b_n)^{1+(-1)^n}. \tag{B.8}$$

Note that the exponents, which cause an even-odd effect, are now shifted by 1. Thus, the 0-th diagonal element of the inverse reduced Liouvillian is given by

$$\hat{\mathscr{L}}_R^{-1} = \frac{(-b_R)^{\frac{1-(-1)^R}{2}}}{(-b_R)^{\frac{1+(-1)^R}{2}}} \frac{\prod_{n=2}^{R}(b_n)^{1+(-1)^n}}{\prod_{n=1}^{R}(b_n)^{1-(-1)^n}} \tag{B.9}$$

$$= -\frac{1}{b_R}^{(-1)^R} \prod_{n=2}^{R} \left(b_1^2\right)^{(-1)^n}. \tag{B.10}$$

By rearranging the elements of the product series one receives

$$\hat{\mathscr{L}}_R^{-1} = -\frac{1}{b_1} \prod_{n=1}^{R} \left(\frac{b_{n+1}}{b_n}\right)^{(-1)^n}. \tag{B.11}$$

In combination with Eq. (5.3.9) this results in

$$\mathcal{L}\left\{\chi_0\right\}(s=0) = \frac{1}{b_1} \prod_{n=1}^{R} \left(\frac{b_{n+1}}{b_n}\right)^{(-1)^n}. \tag{B.12}$$

$\chi_0(t)$ denotes the dynamic of the reduced system.
In addition to this matrix-based derivation, also a second derivation via the Laplace transform shall

be given. Starting by the Continued Fraction of the dynamic caused by the full Liouvillian (see Subsection 2.8)

$$x_0(s) = \cfrac{1}{s + \cfrac{b_1^2}{s + \cfrac{b_2^2}{s + \cfrac{b_3^2}{s + \ddots}}}}, \tag{B.13}$$

which was constructed by inserting the equations

$$x_0(s) = \frac{1}{s + b_1 \frac{x_1(s)}{x_0(s)}} \qquad \text{for } n = 0 \tag{B.14}$$

$$b_n \frac{x_{n-1}(s)}{x_n(s)} = s + b_{n+1} \frac{x_{n+1}(s)}{x_n(s)} \qquad \text{for } n \neq 0 \tag{B.15}$$

into each other recursively. Since the reduced Liouvillian was created based on the assumption $x_R(t) = x_{R-1}(t)$ for the Laplace transform

$$x_R(s) = x_{R-1}(s) \tag{B.16}$$

holds. Thus, one obtains three equations for the Laplace transform of the reduced dynamic (which is denoted by $\chi_n(s)$):

$$\chi_0(s) = \frac{1}{s + b_1 \frac{\chi_1(s)}{\chi_0(s)}} \qquad \text{for } n = 0 \tag{B.17}$$

$$b_n \frac{\chi_{n-1}(s)}{\chi_n(s)} = s + b_{n+1} \frac{\chi_{n+1}(s)}{\chi_n(s)} \qquad \text{for } 0 < n < R-1 \tag{B.18}$$

$$b_{R-1} \frac{\chi_{R-2}(s)}{\chi_{R-1}(s)} = s + b_R \qquad \text{for } n = R-1 \tag{B.19}$$

The last line causes an end of the otherwise infinite Continued Fraction, which can be expressed as

$$\chi_0(s) = \cfrac{1}{s + \cfrac{b_1^2}{s + \cfrac{b_2^2}{s + \cfrac{b_3^2}{\ddots \cfrac{b_{R-1}^2}{s + b_R}}}}}. \tag{B.20}$$

For the case $s = 0$ (which is the main interest here) this results in

$$\chi_0(s=0) = \left(\frac{1}{b_R}\right)^{(-1)^R} \prod_{n=1}^{R-1} \left(b_n^2\right)^{(-1)^n} \tag{B.21}$$

which is equivalent to the expression one obtains via the matrix-based derivation.

C Derivation of the area approximation via repeatedly geometric averaging

Within this Appendix the Eq. (5.3.22), (5.3.23) and (5.3.24) shall be derived. This derivation is done by means of complete induction. For a better clarity, the equations, which will be derived, will be presented again:

$$A_R^F = \sqrt[2^{(F-1)}]{\mathtt{c}_F \cdot \prod_{n=1}^{R-F} \mathtt{b}_{n,F}^{(-1)^n}} \tag{C.1}$$

$$\mathtt{c}_F = \prod_{j=1}^{F} b_j^{(-1)^j \cdot (2^F - \sum_{l=0}^{j-1} \binom{F}{l})} \tag{C.2}$$

$$\mathtt{b}_{n,F} = \prod_{j=n}^{F+n} b_j^{\left((-1)^{(j-n)} \cdot \binom{F}{j-n}\right)} \tag{C.3}$$

For the usage of induction, one considers a basic case, here $F = 1$[P1]

$$A_R = \mathtt{c}_1 \cdot \prod_{n=1}^{R-1} \mathtt{b}_{n,1}^{(-1)^n} \tag{C.4}$$

$$\mathtt{c}_1 = \frac{1}{b_1} \tag{C.5}$$

$$\mathtt{b}_{n,1} = \prod_{j=n}^{1+n} b_j^{\left((-1)^{(j-n)} \cdot \binom{1}{j-n}\right)} = \frac{b_n}{b_{n+1}} \tag{C.6}$$

which corresponds with the results of the case without averaging.
Since A_R^F are determined by repeatedly geometric averaging, one can determine all higher A_R^F (in the sense of larger F) approximation recursively by

$$A_R^{F+1} = \sqrt{A_R^F \cdot A_{R-1}^F}. \tag{C.7}$$

Through this recursive relation, the induction step can now be verified:

$$\sqrt{A_R^F \cdot A_{R-1}^F} = \sqrt{\sqrt[2^{(F-1)}]{\mathtt{c}_F \cdot \prod_{n=1}^{R-F} \mathtt{b}_{n,F}^{(-1)^n}} \cdot \sqrt[2^{(F-1)}]{\mathtt{c}_F \cdot \prod_{n=1}^{R-1-F} \mathtt{b}_{n,F}^{(-1)^n}}} \tag{C.8}$$

$$= \sqrt[2^F]{\mathtt{c}_F^2 \cdot \left[\prod_{n=1}^{R-F} \mathtt{b}_{n,F}^{(-1)^n}\right] \cdot \left[\prod_{n=1}^{R-1-F} \mathtt{b}_{n,F}^{(-1)^n}\right]} \tag{C.9}$$

$$= \sqrt[2^F]{\frac{\mathtt{c}_F^2}{\mathtt{b}_{1,F}} \cdot \left[\prod_{n=1}^{R-1-F} \mathtt{b}_{n+1,F}^{(-1)^{n+1}}\right] \cdot \left[\prod_{n=1}^{R-1-F} \mathtt{b}_{n,F}^{(-1)^n}\right]} \tag{C.10}$$

$$= \sqrt[2^F]{\frac{\mathtt{c}_F^2}{\mathtt{b}_{1,F}} \cdot \left[\prod_{n=1}^{R-(F+1)} \mathtt{b}_{n+1,F}^{(-1)^{n+1}} \mathtt{b}_{n,F}^{(-1)^n}\right]} \tag{C.11}$$

At this point a separation of the different parts of the equation is useful for clarity. Thus, one focus first on the product within the row of products:

$$\mathtt{b}_{n,F}^{(-1)^n} \cdot \mathtt{b}_{n+1,F}^{(-1)^{n+1}} = \left[\prod_{j=n}^{F+n} b_j^{(-1)^j \cdot \binom{F}{j-n}}\right] \cdot \left[\prod_{j=n+1}^{F+n+1} b_j^{(-1)^j \cdot \binom{F}{j-(n+1)}}\right] \tag{C.12}$$

$$= b_n^{(-1)^n} b_{F+n+1}^{(-1)^{F+n+1}} \left[\prod_{j=n+1}^{F+n} b_j^{(-1)^j \cdot \binom{F}{j-n}}\right] \cdot \left[\prod_{j=n+1}^{F+n} b_j^{(-1)^j \cdot \binom{F}{j-(n+1)}}\right] \tag{C.13}$$

$$= b_n^{(-1)^n} b_{F+n+1}^{(-1)^{F+n+1}} \left[\prod_{j=n+1}^{F+n} b_j^{(-1)^j \cdot \left(\binom{F}{j-n} + \binom{F}{j-(n+1)}\right)}\right] \tag{C.14}$$

$$= b_n^{(-1)^n} b_{F+n+1}^{(-1)^{F+n+1}} \left[\prod_{j=n+1}^{F+n} b_j^{(-1)^j \cdot \binom{F+1}{j-n}}\right] \tag{C.15}$$

$$= \prod_{j=n}^{F+1+n} b_j^{(-1)^j \cdot \binom{F+1}{j-n}} = \mathtt{b}_{n,F+1}^{(-1)^n}. \tag{C.16}$$

Within this derivation, the relation

$$\binom{n}{k} + \binom{n}{k+1} = \binom{n+1}{k+1} \tag{C.17}$$

was used.

Second, one considers the expression

$$\frac{\mathtt{c}_F^2}{\mathtt{b}_{1,F}} = \frac{\prod_{j=1}^{F} b_j^{2\cdot(-1)^j\cdot(2^F-\sum_{l=0}^{j-1}\binom{F}{l})}}{\prod_{j=1}^{F+1} b_j^{\left((-1)^{(j-1)}\cdot\binom{F}{j-1}\right)}} \tag{C.18}$$

$$= \frac{1}{b_{F+1}^{(-1)^F}} \prod_{j=1}^{F} \frac{b_j^{2\cdot(-1)^j\cdot(2^F-\sum_{l=0}^{j-1}\binom{F}{l})}}{b_j^{\left((-1)^{(j-1)}\cdot\binom{F}{j-1}\right)}} \tag{C.19}$$

$$= \frac{1}{b_{F+1}^{(-1)^F}} \prod_{j=1}^{F} b_j^{2\cdot(-1)^j\cdot(2^F-\sum_{l=0}^{j-1}\binom{F}{l})-\left((-1)^{(j-1)}\cdot\binom{F}{j-1}\right)} \tag{C.20}$$

$$= \frac{1}{b_{F+1}^{(-1)^F}} \prod_{j=1}^{F} b_j^{(-1)^j\cdot\left[2^{F+1}+\binom{F}{j-1}-2\sum_{l=0}^{j-1}\binom{F}{l}\right]} \tag{C.21}$$

$$= \frac{1}{b_{F+1}^{(-1)^F}} \prod_{j=1}^{F} b_j^{(-1)^j\cdot\left[2^{F+1}-\sum_{l=0}^{j-2}\binom{F}{l}-\sum_{l=0}^{j-1}\binom{F}{l}\right]} \tag{C.22}$$

$$= \frac{1}{b_{F+1}^{(-1)^F}} \prod_{j=1}^{F} b_j^{(-1)^j\cdot\left[2^{F+1}-\sum_{l=0}^{j-1}\binom{F}{l-1}-\sum_{l=0}^{j-1}\binom{F}{l}\right]} \tag{C.23}$$

$$= \frac{1}{b_{F+1}^{(-1)^F}} \prod_{j=1}^{F} b_j^{(-1)^j\cdot\left[2^{F+1}-\sum_{l=0}^{j-1}\left(\binom{F}{l-1}+\binom{F}{l}\right)\right]} \tag{C.24}$$

$$= \frac{1}{b_{F+1}^{(-1)^F}} \prod_{j=1}^{F} b_j^{(-1)^j\cdot\left[2^{F+1}-\sum_{l=0}^{j-1}\binom{F+1}{l}\right]} \tag{C.25}$$

$$= \prod_{j=1}^{F+1} b_j^{(-1)^j\cdot\left[2^{F+1}-\sum_{l=0}^{j-1}\binom{F+1}{l}\right]} = \mathtt{c}_{F+1}. \tag{C.26}$$

In addition to Eq. (C.17) also

$$\binom{n}{k} = 0 \text{ for } k < 0 \tag{C.27}$$

was used.
By substituting in Eq. (C.11)

$$A_R^{F+1} = \sqrt[2^F]{\mathtt{c}_{F+1}\cdot\prod_{n=1}^{R-(F+1)}\mathtt{b}_{n,F+1}^{(-1)^n}} \tag{C.28}$$

thus one can see that Eq. (5.3.22), (5.3.23) and (5.3.24) can be proven by induction and are valid.

D Monotonic behavior of linear growing coefficients for arbitrary averaging

To show that the coefficients in Eq. 5.3.24 are monotonic for the special case $b_n = n$, one applies first the logarithm on this equation

$$\ln\left(\mathfrak{b}_{n,F}\right) = \sum_{j=0}^{F}(-1)^j \binom{F}{j} \ln\left(b_{n+j}\right). \tag{D.1}$$

In the next step, the derivative of that expression is determined

$$\frac{\mathfrak{b}'_{n,F}}{\mathfrak{b}_{n,F}} = \sum_{j=0}^{F}(-1)^j \binom{F}{j} \frac{b'_{n+j}}{b_{n+j}} \tag{D.2}$$

$$\Rightarrow \mathfrak{b}'_{n,F} = \mathfrak{b}_{n,F} \cdot \sum_{j=0}^{F}(-1)^j \binom{F}{j} \frac{b'_{n+j}}{b_{n+j}} \tag{D.3}$$

where $\bullet'$ denotes the derivative.
By inserting the special case, one obtains

$$\mathfrak{b}'_{n,F} = \mathfrak{b}_{n,F} \cdot \sum_{j=0}^{F}(-1)^j \binom{F}{j} \frac{1}{n+j}. \tag{D.4}$$

It can be shown that for the sum

$$\sum_{j=0}^{F}(-1)^j \binom{F}{j} \cdot \frac{1}{j+n} = \int_0^1 \sum_{j=0}^{F}(-1)^j \binom{F}{j} x^{j+n-1} dx \tag{D.5}$$

$$= \int_0^1 x^{n-1} \sum_{j=0}^{F}(-1)^j \binom{F}{j} x^j dx \tag{D.6}$$

$$= \int_0^1 x^{n-1}(1-x)^F dx \tag{D.7}$$

$$= B(n, F+1) \tag{D.8}$$

holds, whereby $B(n,m)$ denotes the beta function (or Euler integral of the first kind) [75]. In the first line the integral

$$\int_0^1 x^{j+n-1} dx = \frac{1}{j+n} \tag{D.9}$$

was used. In addition, the identity

$$\sum_{j=0}^{F}(-1)^j \binom{F}{j} x^j = (1-x)^F \tag{D.10}$$

was used in the third line.
Furthermore, it follows that

$$B(n, F+1) = \frac{n+F+1}{n \cdot (F+1) \cdot \binom{F+n+1}{n}} \tag{D.11}$$

$$= \frac{n+F+1}{n \cdot (F+1)} \frac{n!(F+1)!}{(F+n+1)!} \tag{D.12}$$

$$= \frac{1}{n} \frac{n!F!}{(F+n)!} \tag{D.13}$$

$$= \frac{1}{n\binom{F+n}{n}} \tag{D.14}$$

holds. This results in

$$\mathtt{b}'_{n,F} = \frac{\mathtt{b}_{n,F}}{n\binom{F+n}{n}}. \tag{D.15}$$

Since F and n are natural numbers and $\mathtt{b}_{n,F} > 0$ if $b_j > 0$ for all j, it is easy to see that the derivative is always positive for all F and n. Thus, the Leibniz criterion is fulfilled since the series is monotonic increasing.

Acknowledgment

In my long time at the University of Osnabrück, there are many people who have supported me in my studies, doctoral studies and also outside of academic life.
First of all, I thank Prof. Jochen Gemmer, who supported me since my undergraduate studies and was always available for questions and discussions even in stressful times. I would also like to thank him for giving me the freedom in research without ever losing contact.
As another longtime supporter, I thank Prof. Robin Steinigeweg, who had also supervised me partly since the bachelor thesis and always had an eye for possible improvements and probably knows better about the strengths and weaknesses of my work than I do myself.
I also thank Dr. Christian Bartsch, who helped me during the bachelor thesis and with whom I was thankfully able to work again during the PhD period, for a lot of professional support, especially for the supervision necessary at the beginning.
For good cooperation and always good improvement suggestions, I thank Dr. Jonas Richter.
I would also like to thank Dr. Robin Heveling for very good initial support, who gave me a good start to my PhD period and ensured that I was not overwhelmed by the daily routine here.
I thank Dr. Jiaozi Wang for many interesting discussions as well as for an almost inhuman amount of data.
I thank Merlin Füllgraf, the newest member of the working group, for his willingness to build up my work. I can only hope that I could give him a decent starting point.
For enough computing power for the simulations presented in the thesis, I thank Dr. Lars Knipschild.
Furthermore, I thank Dr. Anatoly Dymarsky, who has always pushed the research with his tireless interest.
I also thank the “Fachschaft” and all its members, who I got to know during my time here, and also for the many “Feierabendbier” in the student council room after work.
Many thanks are going to my family for always supporting me on my own path.
Finally, I would like to thank Dani, who was probably the biggest support for me in many years, and just by the fact that she never took a vacation from it. Thank you for always being there for me when I need you and for giving me space when I need it.

Erklärung über die Eigenständigkeit der erbrachten wissenschaftlichen Leistung

Ich erkläre hiermit, dass ich die vorliegende Arbeit ohne unzulässige Hilfe Dritter und ohne Benutzung anderer als der angegebenen Hilfsmittel angefertigt habe. Die aus anderen Quellen direkt oder indirekt übernommenen Daten und Konzepte sind unter Angabe der Quelle gekennzeichnet. Bei der Auswahl und Auswertung folgenden Materials haben mir die nachstehend aufgeführten Personen in der jeweils beschriebenen Weise entgeltlich / unentgeltlich geholfen.

1. .....
2. .....
3. .....

Weitere Personen waren an der inhaltlichen materiellen Erstellung der vorliegenden Arbeit nicht beteiligt. Insbesondere habe ich hierfür nicht die entgeltliche Hilfe von Vermittlungs- bzw. Beratungsdiensten (Promotionsberater oder andere Personen) in Anspruch genommen. Niemand hat von mir unmittelbar oder mittelbar geldwerte Leistungen für Arbeiten erhalten, die im Zusammenhang mit dem Inhalt der vorgelegten Dissertation stehen. Die Arbeit wurde bisher weder im In- noch im Ausland in gleicher oder ähnlicher Form einer anderen Prüfungsbehörde vorgelegt.

....

Ort,Datum Unterschrift